UNIVERSIDAD DE SEVILLA

Departamento de Fisiología Médica y Biofísica

Evaluation of Volumetric Modulated Arc Therapy and Quality Assurance based on Monte Carlo Simulation
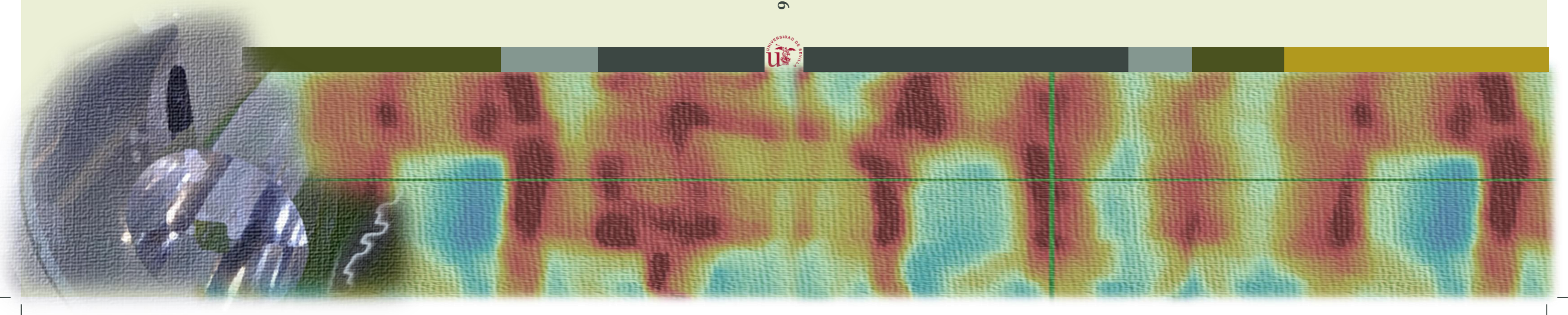
Doctoral Thesis

Ana Rita Pereira Barbeiro

2016

Complex intensity modulated fields delivered by means of rotational dynamic techniques, such as Volumetric Modulated Arc Therapy (VMAT), can provide demanding dose distributions in short irradiation times and fewer monitor units. However this dynamic implementation involves two main sources of uncertainty: one related to the dose calculation accuracy, and the other linked to the continuous delivery of a discrete calculation. Therefore, require new quality assurance (QA) protocols and detailed verification capable of predicting the actual delivered dose to the patient. This is especially critical when used with hypofractionated schemes and for stereotactic body radiotherapy (SBRT) treatments. In this scenario, Monte Carlo (MC) simulation presents an ideal tool to complete the linac commissioning required for VMAT, as well as the gold standard for dose distribution verification. The present thesis reflects the work carried out in order to implement a routine MC verification of VMAT treatments, and to develop a QA model able to control and potentially reduce the inherent uncertainties for a fair and reliable evaluation of current VMAT solutions, including further evaluation of VMAT QA systems. The developed model consists on a system composed by a specific phantom integrated with MC simulation of VMAT log files in a feedback procedure by implementing an optimization process able to adjust the Monitor Units and reconstruct the dose-volume histogram on the patient CT.

EVALUATION OF VOLUMETRIC MODULATED ARC THERAPY AND QUALITY ASSURANCE BASED ON MONTE CARLO SIMULATION

Ana Rita Pereira Barbeiro

Thesis submitted in partial fulfilment of the
requirements for the degree of
PhD

in the
Departamento de Fisiología Médica y Biofísica
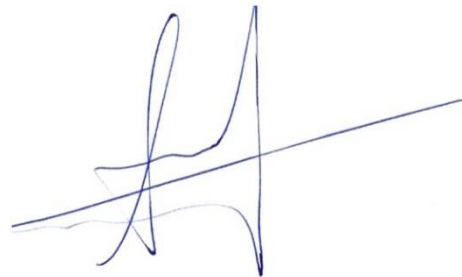UNIVERSIDAD DE SEVILLA

Supervisor
Prof. Dr. Antonio Leal Plaza

October 2016

Don Antonio Leal Plaza, Profesor Titular perteneciente al Departamento de Fisiología Médica y Biofísica de la Universidad de Sevilla

CERTIFICA:

Que Doña Ana Rita Pereira Barbeiro ha realizado bajo su dirección el trabajo de tesis titulado: *"Evaluation of Volumetric Modulated Arc Therapy and Quality Assurance based on Monte Carlo Simulation"*, que presenta para optar al grado de Doctor por la Universidad de Sevilla.

En Sevilla, a 11 de Octubre de 2016

Fdo. Antonio Leal Plaza

Agradecimientos

Deseo expresar mi más sincero agradecimiento a todas las personas que con su soporte científico y humano han colaborado en la realización de este trabajo de investigación.

Muy especialmente a mi director de tesis, Antonio, por su enorme paciencia a lo largo de estos años y, principalmente, por su valiosa orientación, consejos y discusión crítica, sin los que este trabajo no habría sido posible. Gracias por la oportunidad, por el esfuerzo invertido en mi formación, y por haberme transmitido una buena parte de tu conocimiento y gusto por la ciencia.

A Paco, igualmente por el profesor magnífico que es y por todos sus consejos y generosidad. A mis compañeros del grupo de investigación de Física Médica, Ana, Elisa, José Antonio, Sergio y Leticia y a los que me acompañaron desde mis primeros pasos por el departamento Maite, Isa y Bianey, que tanto me enseñaron, ¡no sólo de física médica sino de español! A todos los miembros de este departamento, por el ambiente de trabajo y momentos vividos a lo largo de estos años. Haber tenido la oportunidad de seguir formándome y creciendo como persona e investigadora, rodeada de gente tan brillante y humilde, ha sido tremendamente inspirador.

A todos los colaboradores del proyecto en el cual he participado, y los que directamente o indirectamente han contribuido a este trabajo. De modo general, agradecer a los servicios de radiofísica de los hospitales Universitarios Virgen Macarena y Virgen del Rocío y del hospital Infanta Luisa, por siempre abrirme sus puertas y por toda su ayuda y colaboración.

Por último, agradezco a mi familia y amigos por su comprensión y apoyo constate. De manera muy especial a mi madre por compartir mis alegrías y angustias. Obrigada mãe!

The results achieved and methodology developed in this work have led to the following publications and conference contributions:

A.R. Barbeiro, A. Ureba, J. A. Baeza, R. Linares, M. Perucha, E. Jiménez-Ortega, S. Velázquez, J. C. Mateos and A. Leal, '3D VMAT verification based on Monte Carlo log file simulation with experimental feedback from film dosimetry'. *PLOS ONE* **11**(11): e0166767 (2016).

A. Ureba, F. J. Salguero, A. R. Barbeiro, E. Jimenez-Ortega, J. A. Baeza, H. Miras, R. Linares, M. Perucha, and A. Leal. 'MCTP system model based on linear programming optimization of apertures obtained from sequencing patient image data maps'. *Medical Physics* **41**(8):1719-1-15 (2014).

———————————————————

Selected work as invited speaker at 1st workshop SFPM: Radiotherapy Modelling, Luz Saint-Sauveur, France, 2016:
A.R. Barbeiro, A. Ureba, J. A. Baeza, R. Linares, M. Perucha, E. Jiménez-Ortega and A. Leal. A model for assessing VMAT pre-treatment verification systems and VMAT optimization algorithms.

Poster communication. 57th AAPM Annual Meeting. Aneheim, CA, USA, 2015:
A.R. Barbeiro, A. Ureba, J.A. Baeza, R. Linares, E. Jimenez-Ortega, J.C. Mateos, S. Velazquez and A. Leal Plaza. SU-E-T-644: QuAArC: A 3D VMAT QA System Based On Radiochromic Film and Monte Carlo Simulation of Log Files. *Medical Physics* **42**:3484-3484 (2015).

Poster communication. 33rd ESTRO Annual Meeting. Vienna, Austria, 2014:
A.R. Barbeiro, A. Ureba, J.A. Baeza, J.C. Mateos, S. Velazquez, R. Linares, E. Jimenez-Ortega, M. Perucha and A. Leal. 'VMAT verification, commissioning and QA based on MC simulation'. *Radiotherapy and Oncology* **111**(S1):322-322 (2014).

Oral communication. III Congreso Conjunto SEFM-SEPR. Cáceres, Spain, 2013:
A.R. Pereira-Barbeiro, A. Ureba-Sanchez, J.A. Baeza-Ortega, J.C. Mateos Pérez, S. Velazquez-Miranda, E. Jiménez-Ortega, A. Leal-Plaza: 'Control de calidad de la arcoterapia volumétrica modulada (VMAT) basado en simulación Monte Carlo'.

Abstract

Complex intensity modulated fields delivered by means of rotational dynamic techniques, such as Volumetric Modulated Arc Therapy (VMAT), can be considered a step forward in comparison to conventional, static technique, providing demanding dose distributions in short irradiation times. However this dynamic implementation involves two main sources of uncertainty: one related to the dose calculation accuracy, and the other linked to the continuous delivery of a discrete calculation. Therefore, require new quality assurance (QA) protocols and detailed verification capable of predicting the actual delivered dose to the patient. This is especially critical when used with hypofractionated schemes and for stereotactic body radiotherapy (SBRT) treatments. In this scenario, Monte Carlo (MC) simulation presents an ideal tool to complete the linac commissioning required for VMAT, as well as the gold standard for dose distribution verification.

The present thesis reflects the work carried out in order to implement a routine MC verification of VMAT treatments, and to develop a QA model able to control and potentially reduce the inherent uncertainties for a fair and reliable evaluation of current VMAT solutions, including further evaluation of VMAT QA systems. The developed model consists on a system composed by a specific phantom integrated with MC simulation of VMAT log files in a feedback procedure by implementing an optimization process able to adjust the Monitor Units and reconstruct the dose-volume histogram on the patient CT.

Several clinical cases, previously planned with different treatment planning systems and verified with different commercial solutions were selected in order to test operational feasibility of the proposed model. The proper operation of the feedback procedure was proved through the achieved high agreement between reconstructed dose distributions and the film measurements. The proposed model showed to be valid for VMAT assessment, and also for linac commissioning and evaluation of other QA systems. Besides, the results also showed enough robustness and efficiency of the model to be considered as a pre-treatment VMAT verification system.

x

Resumen

Los tratamientos de radioterapia con intensidad modulada, impartidos por medio de técnicas dinámicas rotacionales, como es el caso de la arcoterapia volumétrica modulada (VMAT, del inglés *Volumetric Modulated Arc Therapy*), pueden ser considerados un avance en relación a la técnica estática convencional, proporcionando distribuciones de dosis complejas en tiempos de irradiación más cortos. Sin embargo, esta implementación dinámica involucra dos principales fuentes de incertidumbre: una relacionada a la precisión del cálculo de la dosis, y otra asociada a la impartición continua de un cálculo discreto. Esto requiere nuevos protocolos de control de calidad (QA del inglés *Quality Assurance*) y una verificación detallada, capaz de estimar la dosis que recibirá el paciente. Esto es especialmente importante cuando se emplea esta técnica en tratamientos bajo esquemas hipofraccionados o de radioterapia estereotáxica extracraneal (SBRT del inglés *Stereotactic Body Radiotherapy*). En este escenario, la simulación Monte Carlo (MC) se presenta como una herramienta ideal para completar la puesta a punto del acelerador lineal requerido para la VMAT, así como la referencia estándar para la verificación de la distribución de dosis.

El presente trabajo se ha llevado a cabo con el fin de implementar una verificación MC rutinaria de tratamientos de VMAT, y desarrollar un modelo de QA para controlar y, potencialmente, reducir las incertidumbres inherentes para una evaluación justa y fiable de las soluciones de VMAT actuales. El modelo desarrollado, consiste en un sistema compuesto por un maniquí específico integrado con la simulación MC de los ficheros log de VMAT, en un procedimiento de retroalimentación, a través de un método de optimización capaz de ajustar las unidades monitor para reconstruir, experimentalmente, el histograma dosis-volumen en la imagen del paciente.

Varios casos clínicos, previamente solucionados con diferentes sistemas de planificación y verificados con distintas soluciones comerciales, fueron seleccionados para poner a prueba la viabilidad operativa del modelo propuesto.

El funcionamiento correcto del procedimiento de retroalimentación se demostró a través del alto acuerdo alcanzado entre las distribuciones de dosis reconstruidas y las medidas en película. El modelo propuesto mostró ser válido para la evaluación de la VMAT, para llevar a cabo la puesta a punto del linac, e incluso para evaluar otros sistemas de QA. Además, los resultados obtenidos también mostraron que el modelo es suficientemente robusto y eficiente para su aplicación clínica, como sistema de verificación pre-tratamiento de VMAT.

Table of Contents

List of Figures & Tables

List of Abbreviations

AAPM	American Association of Physicists in Medicine
AMAT	Aperture Modulated Arc Therapy
AMRT	Arc-modulated radiation therapy
CBT	Cone Beam Therapy
CM	Component Module
CP	Control Point
CT	Computed Tomography
DAO	Direct Aperture Optimization
DICOM	Digital Imaging and Communication in Medicine
DNA	DeoxyriboNucleic Acid
DVH	Dose Volume Histogram
EPID	Electronic portal imaging device
ESTRO	European Society for Radiotherapy and Oncology
FMO	Fluence Map Optimization
FWHM	Full Width at Half Maximum
HT	Helical Tomotherapy
HIL	*Hospital Infanta Luisa*
HU	Hounsfield Units
HUVR	*Hospital Universitario Virgen del Rocío*
IAEA	International Atomic Energy Agency
ICRU	International Commission on Radiation Units and measurements
IGRT	Image-Guided Radiation Therapy
IMAT	Intensity Modulated Arc Therapy
IMRT	Intensity Modulated Radiation Therapy
Linac	Linear accelerator
MC	Monte Carlo
MLC	Multileaf Collimator
MU	Monitor Unit
NRCC	National Research Council of Canada
OMEGA	Ottawa Madison Electron Gamma Algorithm

PDD	Percentage Depth Dose
PET	Positron Emission Tomography
PMMA	PolyMethylMethAcrylate
PSD	Phase Space Data
PTV	Planning Tumor Volume
QA	Quality Assurance
SA	Simulated Annealing
SLAC	Stanford Linear Accelerator Centre
SSD	Source Surface Distance
TERMA	Total Energy Released per unit Mass
TPS	Treatment Planning System
VMAT	Volumetric Modulated Arc Therapy
SBRT	Stereotactic Body Radiation Therapy

Introduction

Nowadays, radiotherapy is a prominent and widely used modality of cancer treatment, often in combination with surgery and/or chemotherapy. In broad terms, radiotherapy exploits the fact that ionizing radiation produce damage to tumor cell's DNA (both directly and indirectly via free radical production) and can lead to cell death. Unfortunately, the same is true for healthy cells surrounding the tumor. The main goal of radiotherapy, therefore, is to increase cell kill in tumors while minimizing it in healthy tissues, such that acute and late side-effects can be reduced.

According to data provided by GLOBOCAN, about 14.1 million new cancer cases were estimated to have occurred in 2012 worldwide (Ferlay *et al.*, 2015), and about half of these cases were or will be undergo radiotherapy in some of the treatment phases (Delaney *et al.*, 2005). Although cancer is a leading cause of death worldwide, with 8.2 million deaths estimated for 2012 (Ferlay *et al.*, 2015), the 5-year survival rate for all diagnosed cancers has been improved over the years due to advances in early diagnosis and treatment.

In the past few decades, radiotherapy techniques have improved drastically along with important advances in technology and imaging techniques, increasing the accuracy, flexibility and efficiency of beam delivery. These developments have been mainly driven by the need to reduce the dose to normal tissue structures and thereby minimize the risk of toxicity and morbidity, which then allows dose escalation to the tumor volume potentially leading to improved loco-regional control. The culmination of these modern developments has been the intensity modulated radiotherapy (IMRT), which has widened the horizons of radiotherapy due to its ability to conform radiation dose distributions to complex tumor target volumes while sparing nearby critical structures as much as physically possible. This is reached by the delivery of an optimized non-uniform fluence (Webb, 2000). The radiation fields with high non-uniform intensities are sometimes needed to create the prescribed uniform dose to the

target volume. This is the case for obtaining homogeneous concave dose distributions, as it was first recognized and described by Brahme *et al.* in 1982 (1982).

The non-uniform fluence can be achieved either by intercepting the beam with physical filters of varying thickness (compensators) or by changing beam aperture, usually created by a multi-leaf collimator (MLC) (e.g. by dividing the field into segments of varying weights). The latter can be performed with static or rotating gantry. Techniques with fixed gantry are delivered in either dynamic mode, in which leaves move while the radiation is on (sliding window mode), or static mode (step-and-shoot mode), in which the beam is held off while the MLC leaves move ("step") and is turned on when they reach their pre-defined static positions ("shoot").

Although IMRT offers optimal dosimetric results, a few undesirable aspects of this technique have to be taken into account. These include increased treatment times, considerable rise in number of delivered monitor units (MUs) and the need for more extensive quality assurance (QA) checks than for conventional techniques (Mijnheer and Georg, 2008). Moreover, in the most usual techniques of IMRT a large volume of normal tissue can receive low doses of radiation, what increases the potential late effects of a big number of patients treated with IMRT and the risk of secondary cancers (Hall and Wuu, 2003; Palma *et al.*, 2010). This is of particular concern in the case of pediatric patients.

All these considerations have led to an increased interest in arc-based or rotational techniques for delivery the modulated intensity, such as volumetric modulated arc therapy (VMAT), in pursuit of delivery demanding dose distributions, in shorter treatment times and potentially fewer MUs compared to conventional static field IMRT. Moreover, it is expected to decrease the low dose radiation to surrounding normal tissue, which potentially would decrease the risk of secondary malignancy (Teoh *et al.*, 2011), although this could not be observed in all situations (Abo-Madyan *et al.*, 2014).

Throughout this first introductory section an overview of the rotational IMRT techniques including tomotherapy, on one hand, and intensity modulated arc therapy (IMAT), on the other hand will be included. A brief historical review of the works leading to the wide adoption of VMAT and comparisons with other IMRT delivery techniques will be discussed. Considerations for clinical implementation and VMAT quality assurance (QA) will be also included, in the context of this thesis, and finally the hypothesis and the aims will be described.

1.1   Intensity Modulated Arc Therapy

Among the rotational alternatives proposed for the delivery of IMRT, two dominant but different approaches have emerged, depending on the beam type delivered. Based on the original ideas of Brahme el al., Mackie *et al.* (1993) proposed a rotational approach called tomotherapy in which intensity modulated photon therapy is delivered using a rotating fan beam. Intensity modulation is achieved through the use of a dedicated system that incorporates a temporally modulated slit multileaf collimator revolving around the patient. Either the patient is moved between successive rotations (serial tomotherapy) or continuously during rotation called helical tomotherapy (HT). For the latter, the system looks like a conventional CT scanner and includes a megavoltage portal detector to provide the reconstruction of the CT images. Contrary to common belief, historically, clinical IMRT by tomotherapy preceded clinical IMRT by any MLC-based technique.

In 1995, Yu (1995) introduced an alternative approach to the delivery of rotational IMRT using a cone beam of radiation, called intensity modulated arc therapy (IMAT). A key difference from tomotherapy is that IMAT can be delivered using a conventional linear accelerator (linac) and a conventional (non-binary) MLC. IMAT is a multiple arc technique in which the aperture defined by multi-leaf collimator changes dynamically while gantry rotation speed and dose rate remain constant (Meyer, 2011). The degree of intensity modulation is related to the number of beam shapes per arc and the total number of arcs (Yu and Tang, 2011).

Several clinical studies were conducted to implement IMAT for different treatment sites (Duthoy *et al.*, 2004; Wong *et al.*, 2005; Yu *et al.*, 2002). Nevertheless, as a clinical tool, the IMAT technique did not mature into clinical application. The possible reasons could be found in the lack of an efficient planning method for IMAT and the lack of commercial interest at that time. The linac manufacturers did not offer delivery control systems that were capable of taking full advantage of the IMAT delivery technique.

The IMAT technique did evolve by increasing the number of variable parameters. By assuming that the machine dose rate can vary as needed, Otto (2008) developed a single-arc IMAT algorithm that he named as volumetric modulated arc therapy (VMAT). In addition to allowing dose rate and gantry speed variation, the VMAT algorithm used progressive beam angle sampling to optimize a large number (greater than 100) of apertures using direct aperture optimization.

The major conceptual advantage of VMAT over standard fixed-field IMRT techniques is that the rotational nature of the delivery can provide more flexibility in terms of shaping the dose distributions, and time is used efficiently because the radiation delivery does not stop in between different beam angles (Otto, 2008).

1.2   Commercial implementation of VMAT

In recent years, manufacturers of medical linacs and developers of treatment planning systems (TPS) have introduced products for rotational IMRT. The availability of more advanced delivery control systems and robust inverse planning solutions have made it possible to realize the full potential of IMAT as a delivery technique.

In 2008, both Elekta and Varian introduced new delivery control systems that were capable of delivering IMAT. The critical innovation was that the new control systems provided the ability to vary the dose rate and to move the MLC leaves with a relative velocity to the gantry during rotational beam delivery.

Varian first commercialized Otto´s VMAT algorithm (Otto, 2008) with the trade name RadipArc™, offering their complete IMAT solution including both their delivery control system and their RapidArc module implemented in the Eclipse TPS solution. Varian RapidArc has been marketed primarily as a single arc solution but more recently, in order to get better modulation effect, has added support for multi-arc IMAT deliveries. On the other hand, Elekta has adopted the generic term VMAT to describe its commercial implementation.

Bzdusek *et al.* (2009) introduced a rotational IMRT solution, which was marketed by Philips Medical Systems, Inc. with the trade name SmartArc™. Also a VMAT module has been introduced for Nucletron's Oncentra TPS, developed by RaySearch Laboratories (Stockholm, Sweden), which shares the same optimization engine used in the Philips SmartArc. Both SmartArc and Nucletron Oncentra IMAT planning tools can be used with either Elekta or Varian linacs.

Another IMAT solution called cone beam therapy (CBT) was presented by Siemens, in collaboration with Prowess Inc. for integration into Siemens' linear accelerators.

Other names, such as arc-modulated radiation therapy (AMRT) (Wang et al., 2008) and aperture modulated arc therapy (AMAT) (Crooks et al., 2003) were also used to describe other planning methods for single-arc IMAT.

Despite debate on its theoretical justifications (Bortfeld, 2010; Bortfeld and Webb, 2009; Otto, 2009; Verbakel *et al.*, 2009b), VMAT has experienced a rapid and widespread clinical application. Consequently, various planning studies have been conducted in order to evaluate its benefits, in terms of plan quality and delivery efficiency, over more conventional IMRT forms and HT (Oliver *et al.*, 2009; Palma *et al.*, 2008; Rao *et al.*, 2010; Verbakel *et al.*, 2009a; Kjaer-Kristoffersen *et al.*, 2009). Other studies have also investigated the clinical applications of VMAT for a number of cases that require a greater precision and dose conformity (Bertelsen et al., 2010; Matuszak et al., 2010; Zhang et al., 2010). In general, it is shown that the dosimetric results of VMAT give, at least, similar target coverage and preservation of organs at risk (OARs), while significantly reducing the number of required MUs and the overall treatment time.

Shorter treatment times obviously have advantages, including greater patient comfort, less susceptibility of intra-session motion and possibly less radio-induced secondary cancers. But this efficiency must not be detrimental to the relative dose distribution and the integral dose. Despite theoretically offering greater protection to the organs at risk and present a lower maximum dose than other techniques, the commercial algorithms working with VMAT present the tendency to spread a low-dose bath larger than for fixed-field IMRT, which on the other hand, deposit higher doses along the paths of the individual beams (Kjaer-Kristoffersen *et al.*, 2009; Mehta *et al.*, 2009; Meyer, 2011).

The intense commercial promotion and fast clinical adoption also caused much confusion and controversy. Nowadays, there is a lack of a general understanding of how such treatments are planned, and what delivery limitations are unavoidable. In order to clarify some concepts, a brief description of VMAT planning is included in the following sections.

1.2.1 VMAT treatment plan optimization

VMAT planning is complex and the potential benefits of its application compared to conventional IMRT are clearly dependent on the optimization algorithm incorporated into the TPS (Bortfeld and Webb, 2009; Otto, 2009; Verbakel et al., 2009b). The considerable number of dynamic delivery parameters need to be adequately considered by the planning system to take full advantage of VMAT possibilities. For example, not consider the capacity of changing the dose rate in the optimization algorithm will be detrimental to the planning. Moreover, the greater number of variables to optimize implies an

additional difficulty for current planning algorithms. As argued by Otto (2009) the challenge is in the design of optimization algorithms that fully utilize these degrees of freedom and generate plans that conform the dose distribution while being efficient in delivering the same.

In practice, the complexity of the VMAT plan optimization can mainly be attributed to the need to account for the connectivity of the MLC shapes within an arc, since the trajectories have to fulfill constraints imposed by the machine limitations. The main limitations include: maximum MLC leaf seep (typical values are in the range of 3-6 cm/s); gantry speed constraint (typically 6°/s); dose rate constraints; and additional restrictions on the leaf motion depending on the MLC and linac models (e.g. interdigitation constraints) (Unkelbach et al., 2015).

Constraints on the leaf motion help to ensure the accuracy of the predicted dose distribution. These constraints define the maximum distance a leaf can travel between adjacent control points (discrete segments considered in the optimization algorithm), which are expressed as a distance per degree of gantry rotation (mm/deg). Each control point (CP) is described with three major parameters: a gantry angle, a specific MLC shape, and a corresponding monitor unit value. If there are dramatic changes in the aperture shapes from one CP to the next, the accuracy can be compromised and the linac could execute a different configuration to the parameters combination planned by the TPS. Leaf motion constraints showed to generate a significant impact on VMAT plans in terms of plan quality and delivery accuracy (Chen *et al.*, 2011). A less restrictive leaf motion constraint (greater than 5 mm/deg) results in improved plan quality but can lead to less accuracy in dose distribution, as it was evidenced by increasing discrepancies between the planned and the measured doses.

As for conventional IMRT plan optimization, different methods for VMAT plan optimization can use either a two-step or one-step optimization process. Depending on the implemented method, the additional constraints on the shape of the apertures are enforced in different stages during the optimization process, resulting in different delivery efficiency.

Traditional IMRT approaches include two stages, which were similar developed for VMAT. During the first stage, optimal intensity patterns are generated for all beams used for approximating one arc. The number of fields and gantry angles are defined and each beam (open field) is divided into a number of segments (beamlets). A search of beamlet weights is performed to determine the optimal beamlet weights (fluence map) such as the sum of weighted beamlets provide dose distribution in optimal agreement with the objective dose distribution. This fluence map optimization (FMO) is then

followed by an arc sequencing, in the second stage, where these fluence maps are converted to apertures into machine deliverable plans using leaf sequencing algorithms. Any delivery constraints of the linac are enforced in the second stage. This process may produce inefficient treatments and increased collimator artifacts (Aju-e-Taqaddas, 2011).

One-step processes on the other hand, aim to reduce the complexity and overcome the problem of plan degradation. Direct aperture optimization (DAO) is a one-step process approach whereby all the machine delivery constraints are enforced directly into the plan optimization, thereby eliminating the need for a separate leaf sequencing step. DAO bypasses the traditional two-phase planning approaches by simultaneously optimizing the shapes and the weights corresponding to each aperture. The concept of DAO has been applied to both static gantry IMRT (Shepard *et al.*, 2002) as well as VMAT (Bzdusek *et al.*, 2009; Earl *et al.*, 2003; Otto, 2008). It aids in reducing number of segments and MU thereby making DAO suitable for VMAT inverse planning.

Most of the commercial VMAT planning algorithms use DAO methods in their optimization process. This includes RapidArc (Varian), which uses a global stochastic optimization approach (simulating annealing), avoiding FMO and sequencing methods. Contrarily of what is allowed in DAO, simulating annealing accepts changes in the configuration of the variables that increase the cost function and does not get 'trapped' in local minima. SmartArc (Philips) as well as Monaco (Elekta) implement a local gradient based optimization approach to DAO, and adopt FMO and arc sequencing methods to obtain a starting point for DAO (Unkelbach *et al.*, 2015).

Besides mechanical constraints, the result of VMAT optimization may also depend on the choice of other plan parameters (efficiency constraints), e.g. the number of arcs, the maximal delivery time or the gantry angle spacing between subsequent CPs, which defines how many CPs will be used for optimization and dose calculation. Thus, they should be set to achieve a good compromise between plan quality, dose verification agreement and treatment time.

A dependence of the quality of the final solution on the number of starting CPs has been observed (Pardo Montero and Fenwick, 2011). Furthermore, the closer they are, in the final solution, the better is the approximation to a continuous arc irradiation. Therefore, the agreement of measured and calculated dose is expected to increase when reducing the gantry angle spacing. Feygelman *et al.* (2010) have confirmed this behavior when comparing the calculated dose with a large spacing of 6° between control points to a smaller spacing of 4°, finding less dosimetric errors in the later.

Theoretical considerations of VMAT have focused on determining what level of modulation is achievable in a single arc compared to fixed field IMRT (Bortfeld and Webb, 2009). Bortfeld′s work (Bortfeld, 2010) extended the theory that only a finite number of intensity modulated beams are required to approximate an ideal dose distribution. It is believed that most VMAT planning algorithms work using a 'small-arc approximation' (Webb and McQuaid, 2009). This concept assumes that over a limited angular range (gantry angle spacing between CPs), and from the viewpoint of the target region, the source is effectively locally static and the ray paths can be approximated from a set of fixed angular orientations with small angular spacing. Otherwise, it would be too computer-time-consuming to trace the actual ray paths from continuously moving sources. The diagram represented in Figure 1.1 illustrates this concept. It can clearly be seen that from a set of unmodulated divergent VMAT fields, the equivalent parallel beams are spatially modulated.
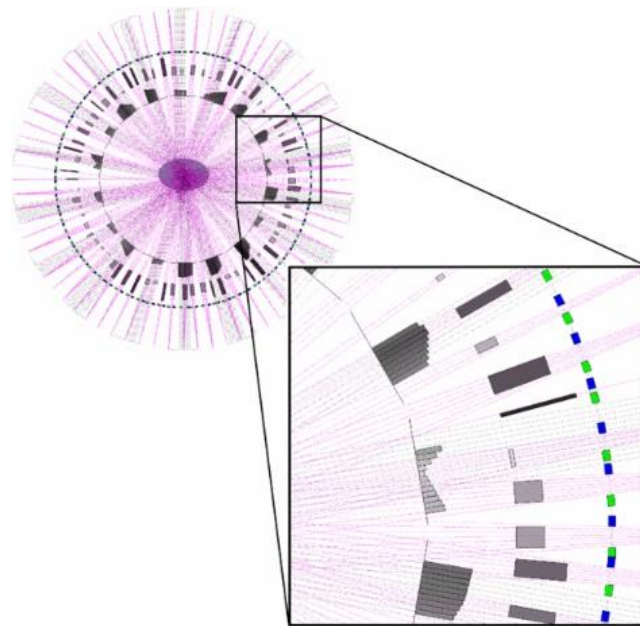
Figure 1.1. The divergent ray paths, leaf positions and segment weighting at each gantry angle. The reconstructed parallel rays and associated intensity-modulated beam are shown for every 4th angle (Webb and McQuaid, 2009).

Several studies have shown that single arc VMAT can achieve dose distributions comparable to IMRT for prostate cancer (Palma *et al.*, 2008; Tsai *et al.*, 2011), but for more complex geometries as head and neck tumors, reports are contradictory. Some publications state that two or more arcs are required

(Alvarez-Moret *et al.*, 2010; Guckenberger *et al.*, 2009; Verbakel *et al.*, 2009a), whereas Bertelsen *et al.* (2010) found that a single arc is sufficient to achieve plan quality comparable to IMRT. Beyond the theoretical discussion, in daily clinical practice, a balance must be made between plan quality and delivery efficiency that determines how many arcs should be used in VMAT planning to achieve the required modulation of fluence. Clearly, this task is more easily performed when a part of the problem is shared with another sweeping (Figure 1.2), providing additional flexibility in shaping the dose distribution. However, the delivery time increases significantly, and could even becoming larger than for conventional IMRT.

Unlike the technologies for optimizing conventional IMRT, this planning technology is not yet considered mature and completed. The current state of VMAT optimization was recently reviewed by some authors, who have also suggested some improvements (Unkelbach *et al.*, 2015).
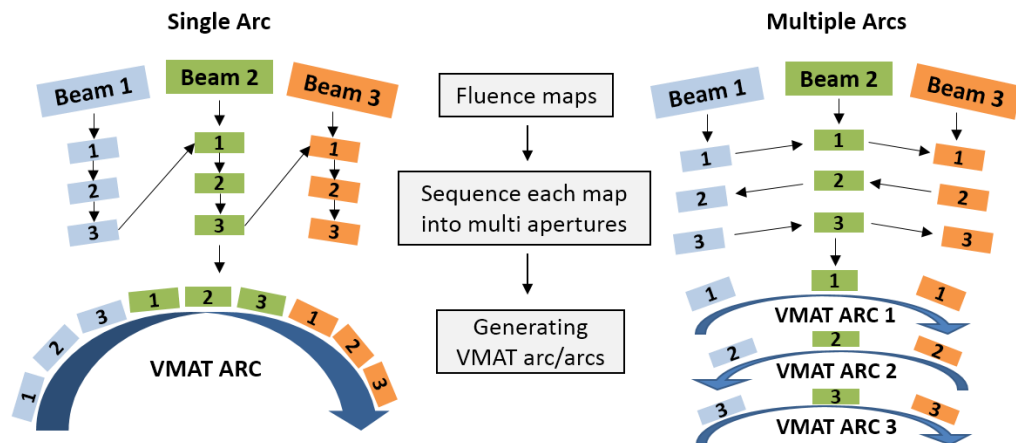
Figure 1.2. Single arc versus multiple arcs treatment optimization. Adapted from figure courtesy of Shepard.

1.2.2 VMAT dose calculation

The general concept and process for dose calculation in VMAT planning is basically the same as for IMRT planning. However, due to the many degrees of freedom in VMAT planning, the dose calculation involved in the VMAT optimization process is computationally more demanding, as exposed before.

Since most of the currently available VMAT optimization algorithms are based on a progressive sampling, dose calculation is performed using a combination of a fast dose calculation algorithm with limited accuracy, and a

slower but more accurate dose calculation engine for the final stage. Although the implementation of arc sampling and multiple dose calculation algorithms varies between vendors and software versions, a level of accuracy is mandatory in order to reach expected outcomes in tumor control and healthy tissues complications. It has been shown that dose differences up to 7% can be clinically detectable for different commercial software, while deviations from the prescribed dose of 5% or more can compromise tumor response and tissue morbidity (AAPM, 2004; Dische *et al.*, 1993; ICRU, 1976).

There are many considerations in the uncertainty estimation of the dose delivered to the patient, hence general recommendations of dose delivery accuracy such as, 5% (ICRU, 1976) and 3.5% (Mijnheer *et al.*, 1987), have been issued. To present an overall desired accuracy of 5% in the dose delivered to a volume (or point), the American Association of Physicists in Medicine (AAPM) recommends that the accuracy of computed dose distributions should be between 1% to 2% (AAPM, 2004). In fact, this accuracy has increased with the introduction into clinical practice of improved algorithms for patient dose calculation, in order to better account for complex geometries and tissue heterogeneities.

Most notably, the development of model-based convolution methods has significantly improved the accuracy of dose calculations for heterogeneous materials when compared to the conventional correction-based methods (Ahnesjo, 1989; Tillikainen *et al.*, 2008; Ulmer *et al.*, 2005). The limited accuracy of pencil beam algorithms has been thoroughly investigated. In particular, their ability to correctly model dose in the presence of tissue heterogeneities was examined, where miscalculations and significant differences with Monte Carlo dose calculation were reported (Cranmer-Sargison *et al.*, 2004; Knoos *et al.*, 1995; Ma *et al.*, 2000). The more accurate convolution/superposition methods use pre-calculated Monte Carlo dose (MC) "kernels" partly accounting for tissue density heterogeneities (Reynaert *et al.*, 2007).

The dose calculation is a problem linked to the local deposition of the energy of the particles in the beam and the energy associated to new particles generated from interactions with the linac head, the collimation system (MLC) and the patient. Thus, dose calculation algorithms have to take into account both primary and secondary radiation scatter to produce more accurate results in electronic disequilibrium circumstances. The high complexity of VMAT and other advanced techniques, based on small and irregular irradiation fields, and presenting regions of high dose gradients, require more accurate calculation than the one based on the experimental measurements concerning the standard

fields defined in dosimetry protocols. Moreover, density heterogeneities present inside the patient become critical for analytical calculation algorithms, which also lack precision under these dosimetric conditions (Leal *et al.*, 2003; Reynaert *et al.*, 2007; Sanchez-Doblado *et al.*, 2007; Spezi and Lewis, 2008).

Currently, the multiple commercial solutions for VMAT planning (e.g. Varian Eclipse RapidArc, Philips Pinnacle SmartArc, Elekta ERGO++, Elekta Monaco VMAT, Nucletron Oncentra MasterPlan VMAT, etc.) implement dose calculation engines with different level of robustness. With the development of computer hardware and variance reduction techniques for MC methods, the computation time was largely reduced, making MC approach feasible in some of the commercial TPSs (Hartman Siantar *et al.*, 2001; Kawrakow, 2000b; Ma *et al.*, 1999). On the theoretical definition of VMAT presented by Otto (2008), Monte Carlo was already proposed as an effective and necessary tool. MC treatment planning (MCTP) can provide a lower uncertainty in dose calculation well within the 3% required for accurate radiotherapy (Reynaert *et al.*, 2007).

Monte Carlo dose calculation algorithms are widely recognized as the gold standard for calculating dose distributions once the transport of particles through the accelerator head and the patient heterogeneous geometry may be explicitly modeled. The electromagnetic particle transport is well described by physics using probability distribution functions. Once the probabilities of possible events are well described as dependent on energy and the atomic number of the atoms, the most accurate dose distribution has to be obtained by a numerical method such as Monte Carlo simulation. Residual inaccuracies may nevertheless exist in MC dose calculation, which are inherent to the method i.e., statistical noise or approximations assumed in cross-section modeling, charge particle condensed history algorithms, and geometrical description of the regions.

Another important concern posed by the dose calculation algorithms in VMAT planning, is the calculation time due to the large number of beams used to approximate an arc. It was shown that the calculation time for MC-based algorithms is not so dependent of the number of beams used because the statistical uncertainty is linked to the total of events, while the calculation time using all the empirical methods linearly increases with the number of beams (Tang *et al.*, 2008).

Recently, a new version of a deterministic grid-based Boltzmann equation solver (GBBS or the discrete ordinates method) was integrated in the Eclipse TPS as the Acuros XB algorithm to improve the efficiency and accuracy of dose calculations. The GBBS directly discretizes the linear Boltzmann transport

equation (LBTE), which governs the macroscopic behavior of particle interactions with matter, in space, and in angle and energy domains. The GBBS then iteratively solve the radiation transport problem within specified volumes to compute radiation doses (Han *et al.*, 2011).

Both MC and LBTE methods can provide convergent results for specific situations. The achievable accuracy is equivalent for both approaches and is limited only by uncertainties in the particle interaction data (cross sections data) and uncertainties in the problem being analyzed.

In practice, neither Monte Carlo nor explicit LBTE solution methods are exact, and both methods produce errors. In MC, errors are random and result from simulating a finite number of particles and following each particle as it interacts with a medium. When MC methods employ techniques to accelerate solution times or reduce noise, statistic errors are assumed although systematic errors may be also introduced whether you abuse of an excessive recycle of particles from a phase space file. In the explicit LBTE solution methods, errors are primarily systematic and result from discretization of the variables in space, angle, and energy. Larger steps in the discretization process result in a faster solution, but less accuracy. In both methods, the efficiency is a trade-off between speed and accuracy (Vassiliev *et al.*, 2010). Nevertheless, the efficiency is better handled with MC by considering as a parameter directly linked to the number of events. Differences between the two methods may also result from the treatment of charged particle Coulomb interactions.

Nevertheless, it is important to remark that the MC calculation implemented in commercial algorithms is partial, since it does not include in a direct manner the simulation of the particle interactions with the linac head, in particular with the MLC, which plays a key role in VMAT. The accuracy of most commercial algorithms is limited by approximations used in the characterization of the radiation beam as well as approximations used to model the coupled electron-photon transport in complex heterogeneous media (Chetty *et al.*, 2007). For the LBTE solutions, it would be extremely complex, and even more inefficient, to solve the beam particle interactions with the linac head components, and therefore, these algorithms are only used to calculate the dose in the patient geometry.

1.3   Monte Carlo treatment planning in VMAT - CARMEN MCTP

As previously addressed, there is a fundamental disagreement between VMAT representation in most TPSs and the actual delivery: the discrete calculation of a dynamic process. In each TPS, the dynamic operation of the linac is modelled based on VMAT specific parameters which describe the mechanical and dosimetric limits of the treatment unit into a discrete process.

The connection between TPS and treatment unit is the DICOM treatment prescription, created by the TPS and interpreted by the linac. The standard for data transfer from the TPS to the treatment unit or R&V system is the DICOM RT plan format. In the DICOM RT plan prescription, a treatment beam (conventional, IMRT, or VMAT) is represented with a series of control points including the corresponding variables mentioned before, plus a set of properties, such as the treatment unit name and beam energy. In the case of static beam IMRT, all CPs for a specfic beam have an identical gantry angle, whereas for VMAT, all CPs usually have a different gantry angle. During beam delivery, the treatment unit will travel along all prescribed values in the CPs in the specified order. Therefore, the linac may need to adapt time-related parameters such as dose rate, leaf speed or gantry speed, in order to synchronize dose delivery at the control points. CP sequences have to be created to achieve a delivered dose distribution as close as possible to the calculated one.

In practice, VMAT treatment delivery is guided by a dedicated control loop feedback system. The machine monitors the actual values of all parameters many times in the time interval between CPs. One of the varying parameters is appointed as leading parameter to which all other parameters must be synchronized. This synchronicity will not be perfectly performed, so tolerances must be defined stating for each of the parameters to what extent it may deviate from ideal synchronicity.

The treatment unit will try to deliver the VMAT treatment as fast as possible, i.e., using that combination of speed and dose rate that will result in shortest delivery time. In between CPs, each varying parameter needs a certain amount of time to change from one prescribed value to the next. In a VMAT arc with a low number of MUs and little leaf motion, the gantry speed is likely to be the speed limiting factor. On the other hand, when the number of MUs is high, the dose rate is likely to be speed limiting. The actual delivery time of a VMAT prescription may differ between treatment machines, since maximum dose rate, gantry speed and MLC speed are machine dependent.

On Elekta machines, the delivered MU fraction is the leading parameter. Every 40 ms, the control system checks that all other dynamic parameters are within tolerance, for the actual number of delivered MUs. On Varian machines, the control system has been split into two parts: the machine control system and the MLC controller. The former monitors the delivered MUs and other parameters as a function of the gantry angle, while the latter monitors the MLC leaf positions as a function of gantry angle. The leaf positions are checked against the prescription every 50 ms for C-series machines and every 10 ms for TrueBeam machines (NCS, 2015).

The trade-off between complexity and treatment efficiency previously presented as the limiting factor inherent to the VMAT technique (Bortfeld and Webb, 2009), may not be such a limiting factor in the context of more modern linear accelerator design. More recently, new MLC designs have been commercially released, which allows for leaf speeds of up to 6.5 cm/s (Bedford *et al.*, 2013), and some upgraded control systems (e.g. Elekta Integrity) allowing for continuous variable dose rate (CVDR). Investigations have also been made into the delivery of VMAT plans using flattening filter-free linacs (Zhuang *et al.*, 2013), approaching the > 1000 MU/min, resulting in delivery systems with higher efficiency.

The benefit associated with the use of VMAT technique is argued by a higher efficiency, introducing new parameters in the planning. This efficiency is based on the reduction of radiation treatment times, but the clinical application results are very dependent on the planning algorithms used, and also on the linac itself. Therefore, treatment planning solutions, based on accurate dose calculation and optimization methods able to provide deliverable plans which can be executed and verified with more confidence, are desirable to justify the use of VMAT. In addition, one should have in mind that this confidence can be provided by reliable and accurate verification systems, in accordance to the high accuracy used to generate the treatment. This issue will be discussed later.

In order to objectively evaluate the feasibility and efficiency of VMAT technique, where situations of nonstandard radiation fields have a greater role, the calculation of the dose should be theoretically carried out, beyond the use of analytical algorithms. Full MC (fMC) simulations, in addition to the dose calculation based on the physical heterogeneities in the patient, make possible to consider MLC transmission, scattering and secondary particles contributions in order to take into account the physical characteristics of the beam reaching the heterogeneous patient structures (Reynaert *et al.*, 2007).

Monte Carlo methods are particularly well suited to calculate the dose from the complex MLC apertures commonly proposed during optimization process and finally used for the delivery of the VMAT treatments. The fundamental challenge of applying fMC as a MCTP system is to enable the consideration of all geometries implicated and perform the dose calculation in operating times for clinical practice. For VMAT solutions, the sequence of segments may be achieved from direct aperture optimization, since it results in more efficient solutions maintaining connectivity with the delivery, as aforementioned. As so, previous work developed in the Medical Physics group at the University of Seville was focused on developing and improving optimization algorithms in order to find the most efficient segments and beams in the planning process, to be integrated in a full MC treatment planning (CARMEN). As a result, a direct aperture-based optimization model applied to VMAT technique, exclusively based on patient image data was developed, to allow directly deliverable solutions and to perform a full MC dose calculation, resulting in a total treatment planning time within clinical routine times (Ureba *et al.*, 2014).

The CARMEN MCTP is based on the sequencing of a biophysical map, which is generated from enhanced image data of patients to achieve a set of segments actually deliverable. In order to reduce the required computation time, the conventional fluence map has been replaced by the biophysical map which is sequenced to provide direct apertures that will later be weighted by means of an optimization algorithm based on linear programming in order to impose restrictions at the voxel level (Ureba *et al.*, 2014).

This approach also enable the incorporation of dose painting by number, since the use of multimodality image providing morphological and functional data is easily implemented into the planning voxel by voxel. The information of the computed tomography (CT) necessary for planning can be complemented by magnetic resonance imaging (MRI), or positron, or single-photon emission tomography (PET and SPECT, respectively). This leads to even smaller and more complex segments, involving much sharper dose gradients from the planning target volume (PTV) to nearby OARs. In these conditions, MC simulation and an adequate verification, which constitutes part of the work presented in this thesis, can have a greater significance.

1.4 VMAT quality assurance

Quality assurance (QA) in radiotherapy comprises a series of processes designed to ensure consistency of the medical prescription within the clinical tolerance, and safe fulfilment of that prescription. Among the main objectives, it is also intended to minimize the dose deposited in healthy tissue and exposure of personnel, trying to ensure adequate patient monitoring aimed at determining the end result of treatment (WHO, 1988).

Overall, potential errors associated with advanced radiotherapy include dose calculation inaccuracies, plan transfer error, beam delivery errors, and target localization uncertainties due to patient setup errors and organ motion during the treatment. Considering the consequence of these errors, a comprehensive QA should be performed before and/or during the patient treatment (Kutcher *et al.*, 1994). This QA, thus aims the general reduction of uncertainties through the whole radiotherapy process, trying also to minimize and correct errors, in order to ensure an optimized treatment delivery with maximized tumor control probability and minimum injury to normal tissue.

VMAT commissioning and routine quality assurance builds upon the existing IMRT beam models and IMRT QA protocol. However, its completely dynamic implementation (combination of dynamic MLC with varying dose rate and gantry speed), and new method of operating the linac, demands additional QA measurements, as compared with IMRT and requires a rigorous QA program. The correct treatment delivery must be ensured by extensive dosimetric verifications which include both machine general specific performance and verification of treatment plans by measurements of delivered dose distributions. Focusing on the context of this work some of these steps are presented in the following subsections.

1.3.1 Commissioning and QA of treatment equipment

Before implementing VMAT, the acceptance testing and commissioning of the various aspects of the planning and delivery system should be performed, for which, extensive dosimetric measurements are needed. Periodic QA checks and audits can later ensure the maintenance of the original characteristics. Beam calibration, or the determination of dose at reference conditions, and its stability is a fundamental QA step, where the machine output is required to define the monitor unit. This is the charge collected in the machine's primary dosimetry

system, which corresponds to delivery of 1cGy under reference conditions, following formalisms specified by international codes of practice, such as IAEA report 398 (IAEA, 2001) and AAPM's Task Group 51 (Almond *et al.*, 1999). However, the use of nonstandard fields increases the uncertainty associated to the determination of absorbed dose to water and compromises the quality of treatment planning. This prompted the creation of a Working Group of reference dosimetry on nonstandard fields through the collaboration of IAEA and the AAPM, which published recommendations for the development of a new dosimetry protocol (Alfonso *et al.*, 2008).

In the TPS, thorough commissioning of the beam has to be performed in order to ensure that TPS calculated dose distributions reproduce the output of the treatment machine. The beam model should relate to the geometries in the resulting VMAT plans (e.g. small field sizes and elongated field shapes).

Additionally, a rigorous commissioning of the MLC is extremely important in order to obtain an adequate modeling by the current treatment planning systems. Appropriate leaf modelling is of great importance since, for a considerable part of the planning, only leaves are the beam modifiers blocking the radiation field. This effect may be slightly limited if collimator jaws are allowed to adapt to the MLC field shape and follow the most retracted leaf. Leaf transmission and inter-leaf leakage are often the most challenging part of the TPS commissioning. In addition, leaf positional accuracy, leaf-end penumbra modeling, the output of small segments defined by the MLC, small MU delivery stability, and communication lag between the MLC and linac controllers are some of the factors that potentially can significantly alter the prescribed dose. Entering the actual physical values in the TPS may nevertheless not always guarantee adequate correspondence between TPS and measurement, due to limited modelling in the TPS of the dynamic aspects of the treatment.

It is clear from the previous subsections that VMAT delivery is a complex process, requiring the linac to modulate various dynamic components simultaneously. As such, there is a strong requirement for routine machine QA regimes to ensure that the delivery system is working as expected. Typical recommendations on the tests, tolerance values and action levels for linac QA are presented in the AAPM Task Group 142 report (Klein *et al.*, 2009). Although QA regimes for fixed-field IMRT are already well established in the literature (IMRT Collaborative Working, 2001), the additional QA measures required for VMAT are not so clear. To date, several publications provide guidance on commissioning and QA for what concerns general machine performance by addressing issues such as accuracy in MLC positioning during rotation and

machine performance at variable dose rate. Ling *et al.* (2008) suggest tests examining the accuracy of MLC leaf positioning (e.g. picket fence pattern delivered with rotating gantry), the ability to vary and control dose rate and gantry speed for Varian RapidArc. In this study a direct relationship between MLC leaf position errors and leaf speed was observed. For Elekta VMAT, tests on beam flatness and symmetry, MLC leaf calibration, sliding window dose, as well as rotational accuracy were considered necessary (Bedford and Warrington, 2009). For dynamic MLC QA, log files have been used to detect leaf position errors (Agnew *et al.*, 2014; Kerns *et al.*, 2014), since it is assumed that actual leaf positions are recorded at a time point during treatment. However, some studies, which also used electronic portal imaging device (EPID) measurements, have observed that the leaf positions recorded in the log file cannot be considered to be the actual leaf positions during the delivery without an independent experimental verification for supporting it (Agnew *et al.*, 2014; Neal *et al.*, 2016).

An important aspect for VMAT is that, while the individual components of delivery can be checked independently, a set of tests need to be developed for checking the synchronization of these components. As mentioned before, during delivery time-related parameters such as dose rate, leaf speed or gantry speed, may need to be adapted in order to synchronize dose delivery at the control points. Therefore it is important that the limitations of these parameters of a treatment unit are realistically defined in the TPS (NCS, 2015).

1.3.2 Patient-specific quality assurance

The complexity of the IMRT delivery chain justifiably gave rise to a requirement of pre-treatment dosimetric QA for each patient plan (patient-specific QA). The purpose of patient-specific QA is to ensure that all plan parameters are properly transferred from the planning system to the treatment machine and that the measured plan closely matches the plan predicted by the treatment planning system.

Since VMAT is a form of IMRT, patient-specific QA is an integral part of the clinical practice. Furthermore, as the essential justification of this work, it is necessary to emphasize that the planning and delivery of IMAT should be more tightly integrated than IMRT due to the additional requirements on the linac control, as addressed before.

Most methods used for patient-specific QA of IMRT have been adapted for VMAT QA. These include applying a treatment plan to a phantom to allow the

calculated and the measured doses to be compared (Bedford *et al.*, 2009; Haga *et al.*, 2009; Letourneau *et al.*, 2009). A common strategy consists of per-beam analysis (measurement vs. TPS calculation) in a single plane in a flat phantom. This strategy was summarized in detail in the AAPM TG 119 report about the IMRT commissioning (Ezzell *et al.*, 2009), and also outlined in the ESTRO Booklet No.9 report (Mijnheer and Georg, 2008). However this approach is not so suitable for a rotating beam.

As rotational therapy grows in popularity, new QA strategies are emerging, one of which is the use of 3D dosimetry phantoms to allow the entire rotational plan to be delivered to the phantom and the corresponding measured dose values compared to the TPS calculations on the virtual model of the phantom (Bedford *et al.*, 2009; Letourneau *et al.*, 2009). More promising methods may be sensitive to important dosimetric inaccuracies, like recreating dose distributions using recorded delivery control files (Schreibmann *et al.*, 2009; Teke *et al.*, 2010; Tyagi *et al.*, 2012)

In considering a patient-specific QA solution, it is important to understand the performance of the QA device as a measurement system for rotational IMRT and know the limit of each system in order to obtain a high-quality VMAT plan QA.

Dosimetric QA systems for VMAT must be robust in measuring radiation emanating from any gantry angle. In addition, possible sharper dose gradients may require higher detector spatial resolution (smaller detection active volumes and more detectors per unit volume) compared to other forms of IMRT delivery. Important characteristics of radiation detectors and the majority of detector types used for dosimetry, and also implemented in current VMAT QA systems, were discussed in a recent review (Seco *et al.*, 2014).

Most of the current and emerging VMAT dosimetry systems and techniques are herein described, and their main advantages and drawbacks are also addressed. Among others, the following are highlighted:

- Film and ionization chamber;
- 2D diode array (MapCHECK in MapPhan phantom);
- 2D ion chamber array (MatriXX in MULTICube phantom and PTW 729 in Octavius);
- 3D diode arrays (Delta4 and ArcCHECK);
- Dose reconstruction (COMPASS, Delta4DVH, 3DVH, DVH4 Verisoft, MobiusFx).

This amount of different options also shows that VMAT verification is not a closed issue.

1.3.2.1 Two dimensional treatment verification

Ionization chamber and film dosimetry

Two dimensional (2D) spatial dose distributions are measured with relative dosimetry using passive and active methods, usually combined with one absolute dose measurement from which absolute dose values can be obtained (Figure 1.3).

The classical systems include ionization chambers typically used for absolute point dose verifications and radiographic or radiochromic films for 2D relative dose measurements. The ionization chamber is considered a good detector in regions of shallow dose gradients and for measuring low doses. In fact, the accuracy of the ionization chamber may be affected during IMRT as there are moments that the ionization chamber is outside the field or is partially irradiated. The role of volume effect is small compared to the effect of electron disequilibrium. The possible impact of this on absolute dosimetry has been investigated in terms of Monte Carlo simulation of stopping-power ratios (Sanchez-Doblado *et al.*, 2003) and ion chamber perturbation (Capote *et al.*, 2004). These studies indicated that the measuring error may amount to a considerable percent for individual segments, although the overall error could be compensated depending on the IMRT plan.

Film dosimetry can provide 2D dose distributions with high spatial resolution. Films are usually placed in water equivalent phantoms at planes of interest (Figure 1.3). The relative dose distributions obtained can be scaled to absolute values through cross calibration with a small ionization chamber measurement.

Figure 1.3. PTW Semiflex 0.125 cm3 and 0.3 cm3 ionization chambers (left) (PTW), and films placed in the Easy Cube phantom (right) (DonaldsonMarphil).

Radiochromic film is an alternative to radiographic film. The Gafchromic® EBT film was specially designed for IMRT QA purposes. It does not have to be

handled in a dark room thus can be easily cut and loaded under normal room lighting conditions. The lack of chemical processing not only reduces the post irradiation work load but also removes one of the more problematic aspects of traditional film dosimetry. The composition of radiochromic film is much closer to water or tissue and thus gives a more representative measure of dose in these materials compared with silver bromide radiographic film. A proper procedure for using this film as a dosimeter has to be established, because the performance also depends on how the film is scanned and analyzed.

Planar detector arrays

Different commercial detector arrays appeared through the last decade responding to the clinical demands and consisting usually in a number of detectors placed at fixed positions in a water equivalent phantom. Most detector arrays present a two dimensional, or planar, geometry, like MapCHECK (Sun Nuclear Corporation, Melbourne FL), PTW729 (PTW-Freiburg, Germany), or MatriXX (IBA Dosimetry, Louvain-La-Neuve, Belgium). These detectors employ different combination of detection technology, diode or ionization chamber, and spatial sampling. Most of them can perform absolute dosimetry measurements through the use of a calibration coefficients, generally measured for the central detector, and an array of correction factors that compensate for the inter-detector response variations through the device (Donetti *et al.*, 2006).

Planar diode or ion chamber arrays inserted into a solid water phantom are commonly used for IMRT and were also employed for VMAT treatment verifications (Figure 1.4).

(a)   **(b)**   **(c)**
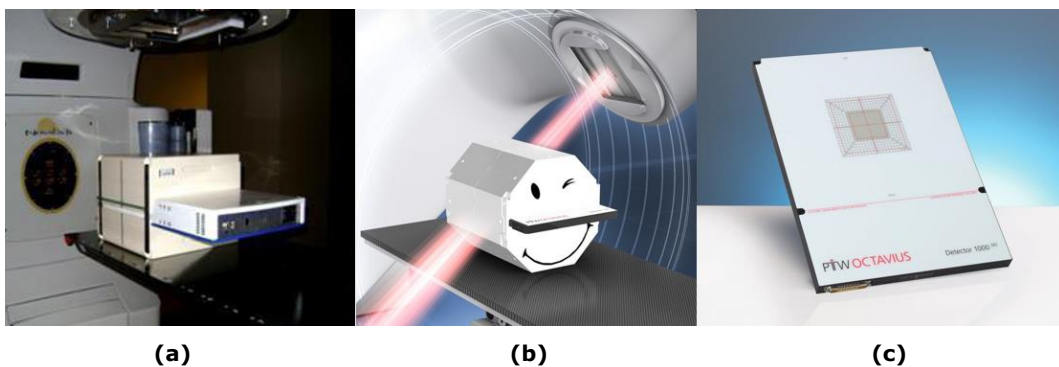
Figure 1.4. Example of different dosimetry systems commonly employed for 2D IMRT and VMAT treatment verification: (a) MultiCube phantom with IBA MatriXX ion chamber array (Chandraraj *et al.*, 2011); (b) Octavius phantom with PTW729 ion chamber array and (c) PTW Octavius 1000SRS liquid-filled ion chamber array (PTW).

In general, there are technical concerns over the use of both diode and ion chamber arrays for performing QA measurements. The small size (<1mm) and high signal of the semiconductor (silicon) diodes are attractive qualities for dosimetry arrays designed for IMRT verification measurements, allowing complex IMRT planar dose distributions measurements with minimal volume averaging effect (Feygelman and Nelms, 2011; Li *et al.*, 2009). However, diodes arranged in a matrix exhibit directional dependence of response, which is partly due to the intrinsic construction of the detectors, and partly to the way they are mounted and arranged in the phantom. The angular dependence consideration becomes critical when diode arrays are used to measure dose delivered by multiple beam geometries as those involved in VMAT plans. Planar arrays, were originally designed for field-by-field static gantry IMRT measurements analysis with the beam incidence perpendicular to the measurement plane. When used to measure dose distributions generated by VMAT, the angular response variation becomes a major concern. Angular dependence as large as 20%, was found for the original MapCHECK diode array (Jursinic *et al.*, 2010). This is due to the intrinsic properties of the diodes, as well as to the phantom design and to the way they are mounted on the circuit boards. Dose rate dependence is also of particular concern with VMAT treatments. It was shown that the variation of dose response with the dose rate for the same detector can reach up to 2.5% (Poppe *et al.*, 2006).

Diodes also present an energy dependent response (Boggula *et al.*, 2011). The silicon itself has the average atomic number, mass absorption coefficient, and stopping power different from water. In megavoltage (MV) photon dosimetry, this issue manifests itself as field-size and depth dependencies of the response, once the relative number of low energy photons in a megavoltage beam increases with field size and depth.

Ion chamber-based detector arrays are known to have insignificant energy and dose-rate dependence for MV photon beams, but require a larger sensitive volume, once the active volume of an ionization chamber inherently has to be substantially larger than that of a semiconductor detector to obtain an acceptable signal to noise ratio, and therefore will exhibit a volume averaging effect in steep dose gradient regions (Li *et al.*, 2009). Thus, the effect of volume averaging needs to be carefully characterized and considered in the interpretation of verification results. Although an angular variation of dose response also exists for ion chamber arrays, the magnitude is smaller compared with that of MapCHECK diode system. Dose response variations up to 8% (Poppe *et al.*, 2006; Van Esch *et al.*, 2007) and 10% (Li *et al.*, 2009) can be found

when the photon beam is parallel to the detector plane for PTW Seven29 and for MatriXX detector, respectively.

Although instantaneous data analysis provided by these arrays, when using these devices for VMAT patient specific QA, the angular dose response and dose rate dependence has to be considered during data collection and corrections are mandatory.

Lately, due to the increased use of smaller field sizes, some 2D detector arrays based on liquid-filled ionization chamber technology have been developed (Figure 1.4(c)). These provide higher spatial resolution measurements, due to smaller detector sizes (e.g. 2.3 mm x 2.3 mm x 0.5 mm), and minimal energy dependence, although ion recombination effects should be specially considered (Knill *et al.*, 2016).

1.3.2.2 Three dimensional treatment verification

Even the best planar dosimeter suffers a substantial drawback when used with multiple gantry angles or arcs. The amount of modulation information collected by the device is dependent on the beam incidence angle.

Ideally, a 3D dose measurement method would be the most comprehensive test, however, currently there is no such 3D measurement technique that can meet the requirements of both spatial resolution and accuracy. A gel dosimeter and an accurate tomography technique may be a solution but gel dosimeters are not routinely used due to the big number of practical issues.

Several QA strategies have been later developed for VMAT verification purposes, including 3D arrays, designed with their detectors distributed in several planes.

The use of film dosimetry in a 3D spatial distribution was also proposed (Park *et al.*, 2011; Richardson *et al.*, 2003), but the measurements were not managed to reconstruct the 3D dose distribution in the patient anatomy. One of these proposals consisted in a novel QA system, based on a cylindrical phantom with rolled-up radiochromic films (Park *et al.*, 2011), as an alternative tool to detect the pitfalls of planar dose verification and to detect dose discrepancies along the arc trajectory. Nonetheless, a 3D distribution from the dose actually delivered on rolled-up films was not included, which can be considered for the reconstruction of dose-volume histograms (DVHs) in order to allow direct comparison with the TPS calculations on the patients' anatomy.

3D detector arrays and phantom-less systems

Some systems include the use of diode arrays with different geometries, capable to provide 3D dose verifications, such as Delta4 (Scandidos, Uppsala, Sweden) (Bedford *et al.*, 2009), or ArcCHECK (Sun Nuclear Corporation) (Letourneau *et al.*, 2009; Fakir *et al.*, 2012) (Figure 1.5). Delta4 phantom includes a biplanar diode array, where the dose is recorded in two orthogonal planes of point detectors with an "X" axial cross section, a 3D dose distribution can be reconstructed for comparison with the QA plan. The 3D dosimetry system ArcCHECK has a cylindrical detector arrangement cross section.
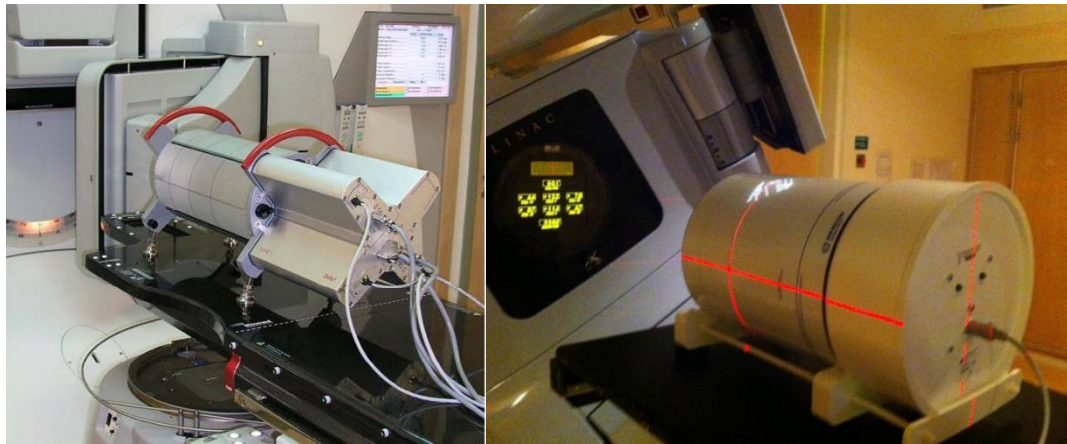
Figure 1.5. Delta 4 detector array (Scandidos, Sweden) at left, and ArcCHECK (Sun Nuclear Corporation) at right (Hammond *et al.*, 2011).

The most commonly employed technique for comparing measurements obtained with calculations is the gamma comparison which combines distance-to-agreement (DTA) and percent dose difference (%Diff) into only one parameter, called gamma index (Low *et al.*, 1998). However, the gamma index can be misleading and insensitive to clinically relevant dosimetric errors. Several studies have stated poor correlation between conventional QA and dose errors in the patient anatomy (Nelms *et al.*, 2011; Zhen *et al.*, 2011). Therefore, DVH-based metrics should also be examined, especially in regions with high-dose gradients (Song *et al.*, 2015). Apart from singular solutions for own use (Oldham *et al.*, 2012), only a limited number of 3D measurement-based anatomy dose QA devices are commercially available: 3DVH (Sun Nuclear Corporation), COMPASS (IBA Dosimetry) and Delta4DVH Anatomy (ScandiDos). These are associated with the previous described diode arrays, capable of provide 3D dose verifications, as Delta4 or ArcCHECK, or with planar measurements obtained

by an ion chamber array mounted on the gantry, as MatriXX (Figure 1.6) (Boggula *et al.*, 2010). Recently, an optional algorithm, called 'DVH 4D', can be used with the OCTAVIUS 4D version, which allows DVH in patient to be calculated. The basic version of OCTAVIUS 4D only reconstructs dose grids in the phantom.
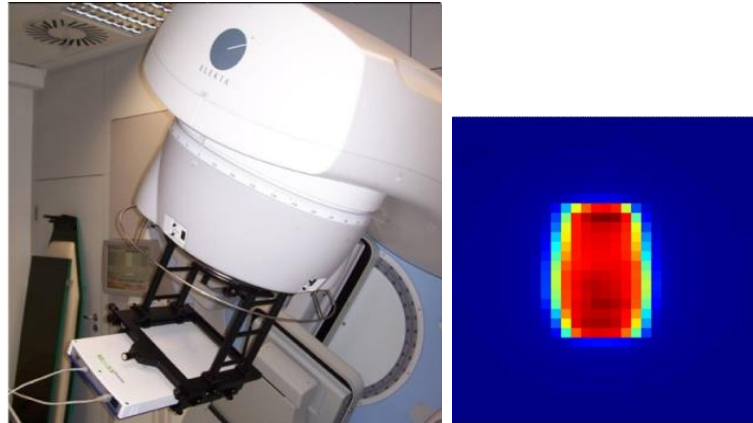
Figure 1.6. MatriXXEvolution (IBA Dosimetry) mounted on gantry (left) and example of the fluence obtained from measurements for a treatment plan verification (right) (Boggula *et al.*, 2011).

The Delta4DVH Anatomy and COMPASS use independent dose calculation algorithms, which calculate the dose to the patient using the energy fluence. The 3DVH does not recalculate the dose, but only perturbs the TPS patient planned dose to account for known errors measured in the conventional QA (Hauri *et al.*, 2014). In this case, the limitations related to the dose calculation engine are still present.

The field size dependence of the systems based on detector arrays, limited by their spatial resolution, may affect the verification results due to under-sampling effects (Hussein *et al.*, 2013), and requires careful attention, so DVH-based metrics should also be examined, especially in regions with high-dose gradients (Song *et al.*, 2015). In these cases, a DVH reconstruction based on measurements with sparse detection not as dense as the planned dose calculation grids requires an interpolation process, which can introduce uncertainties. In the best case, this QA approaches could be verifying the dose corresponding to a discrete set of CPs proposed by the planning system, but this could be not exactly the dose delivered to the patient.

Because of inherent limitations in the measurement resolution, precision, energy and angular dependences (Jin *et al.*, 2014; Bedford and Warrington, 2009), distinct detectors can provide different results for the same treatment plan, as it has been reported in several studies (Li *et al.*, 2009; Chandraraj *et al.*, 2011; Zhu *et al.*, 2013).

Methods based on detectors mounted on the gantry, or even on the EPID already installed on the linac (Woodruff *et al.*, 2015), have the advantage of avoiding the angular dependence but they do not provide a direct dose measurement, requiring the use of algorithms with different levels of approximation to reconstruct the dose in the patient geometry.

Transmission detectors

There are other 3D verification methods that not involve direct in-phantom dose measurements. These methods vary in their level of reliance on experimental data versus dose calculations.

Some transmission detectors can be mounted on the gantry to monitor fluence entering the patient. The measured 2D fluence is then used to recalculate the dose distribution on the patient CT dataset by the associated software. Two transmission detectors were described: the DAVID multi-wire ionization chamber array (PTW, Freiburg, Germany) consisting of a flat, vented multi-wire transmission-type ionization chamber, and COMPASS (IBA Dosimetry, Germany), which is a transmission 2D array detector of air-vented plane parallel chambers. For the latter, photon beam attenuation and secondary electron production were reported (Venkataraman *et al.*, 2009).

Electronic portal imaging dosimetry

Another alternative is based on the EPID which detect the radiation transmitted through the patient and treatment couch. While the devices described above are placed upstream of the isocenter, an EPID naturally records the fluence measurements downstream (patient exit fluence).

With the introduction of the amorphous-silicon detectors, the interest in EPID dosimetry has been increased due to the favorable characteristics such as fast image acquisition, high resolution, digital format, and potential for in vivo measurements. Measurements at different gantry angles are easily accomplished. Portal dosimetry can provide an easy and robust way for patient specific QA. However its use for quantitative dosimetry is currently a challenge.

Different configurations of using the EPID are possible (Iori *et al.*, 2010; Mans *et al.*, 2010). The fluence can be acquired without a patient and the dose can be reconstructed to mimic a flat phantom dataset or may also be estimated via EPID and used to independently calculate on the patient CT dataset. Alternatively, output EPID images can be acquired with the patient/phantom in the beam and the corresponding dose again can be estimated on the patient.

Linac log files

Linac log files (e.g. MLC DynaLog files in Varian RapidArc) registered during the irradiation can be considered to compute the delivered dose distribution on the patient CT images (Schreibmann *et al.*, 2009; Teke *et al.*, 2010; Tyagi *et al.*, 2012). It is assumed that the actual delivery process is truly represented in the log files, in which the MLC leaf and jaws positions, fractional MUs, and gantry angle are recorded. In fact, it is essential to know what has actually being performed by the linac at the time of treatment delivery.

Patient-specific QA has been implemented using logged leaf positions to perform safety checks (Agnew *et al.*, 2012), and recently commercial vendors have released log-file based patient QA products (MobiusFX, Mobius Medical, TX; Compass QuickCheck, IBA Dosimetry, Germany). Nevertheless, its implementation as a patient-specific QA method is controversial. Some authors point that the major disadvantage of this method is that log files need to be validated against an independent system (Manikandan *et al.*, 2012; Neal *et al.*, 2016). Moreover, some systems do not directly provide this information, as in Elekta linacs, forcing the access through the linac controller tools, such as service graphing module, not available in treatment mode (Pasler *et al.*, 2015). Thereby, these studies are scarce for Elekta systems, facing to better known works for Varian systems.

1.5 VMAT uncertainties – definition of the problem

It has been shown that VMAT can actually provide demanding dose distributions in short irradiation times and fewer monitor units. Nonetheless, it is clear these possibilities came in exchange for a high increase in treatment complexity that can compromise treatment delivery. The completely dynamic implementation involves an added complexity to the planning, and rise new concerns about the continuous delivery requiring more extensive QA, to ensure its consistency with the planned discrete calculation. Therefore, new QA

systems are continuously becoming available, while also there exist no clear guidelines and criteria for the accuracy required. The understanding of the different uncertainty sources and their relative dosimetric impacts is fundamental to design and established comprehensive QA procedures, to effectively ensure patient safety and accuracy.

It could be stated that, unlike static field IMRT, all systems implemented for VMAT QA have to face two main sources of uncertainty: one related to the dose calculation accuracy common to any modulated technique, and other linked to the continuous delivery of a discrete calculation.

On one hand, the dose calculation accuracy is a double problem concerning the consideration of patient heterogeneities and also the beam modifiers contribution to the final dose. MC particle transport simulation is recognized for its higher accuracy to model linac heads, especially in non-standard dosimetric conditions, like the ones involved in VMAT treatments. In particular, MC method can accurately model small radiation field apertures potentially present, not only in the solution proposed by the TPS after the optimization process, but also as typical control points from the discretization process of the log files. In this way, it is possible to know the final dose contribution of the scattered and transmitted radiation through the beam modifiers which, as expected, are playing a relevant role in a dynamic modulated technique, such as VMAT. Still considering the challenge of achieving operating times for clinical practice, the explicit and accurate calculation provided by MC method is suitable for assessing the real VMAT capabilities. With increasing complexity in treatment planning, posed by this modulated intensity techniques, and also biological optimization and evaluation, the knowledge of the low dose levels to organs at risk becomes more important, as well as the heterogeneous density considerations in dose calculation for lung SBRT techniques. In these situations, inaccuracies (e.g. fluence underestimation in the head scatter), in TPS dose model could be of significance.

On the other hand, the accuracy of the dose distribution can also be compromised by potential differences between the discrete apertures and corresponding MUs proposed by the TPS, and those continuously delivered by the linac. As discussed throughout this introduction chapter, detailed knowledge of plan deliverability is not necessarily available in conventional planning systems or secondary dose calculations used for verification. In spite of some TPS correctly model the dynamic behavior, even using Monte Carlo dose

calculation as Monaco®, most planning systems make an approximation by summing doses calculated at the discrete CP and not in between (Manikandan *et al.*, 2012). This means that the MUs optimized for a fixed aperture shape are actually delivered with different shapes at different angles (Yu and Tang, 2011). For this reason, the linac log files registered during the irradiation are usually considered to compute the delivered dose distribution. The considerable data recorded in log file requires a reduction of the actual dynamic event for the subsequent calculation. This reduction imposes a level of discretization that can be equivalent to the considered in the planning system (Schreibmann *et al.*, 2009; Tyagi *et al.*, 2012) but it seems reasonable to think the larger the number of CPs calculated from the log file, the better this approximation is. This issue was also studied in this thesis.

In order to cover both type of uncertainties commented above, some works proposed MC simulation of log files recorded during treatment delivery (Asuni *et al.*, 2013; Boylan *et al.*, 2013; Teke *et al.*, 2010). The dose distribution discrepancy introduced between the discretized plan and the continuous delivery was assessed by incorporating DynaLog files into MC simulations for RapidArc QA (Teke *et al.*, 2010). For that work, a new DOSXYZnrc source (Lobo and Popescu, 2010) was used to compute the dose distribution, by considering a continuous variable beam configuration, through sampling-based methods. This approach reached simulation times for routine clinical applications, although the required statistical uncertainty was only ensured in the high dose voxels. It could be efficient for treatment verification but not suitable to assess one of the expected VMAT benefits associated to the decrease of low dose radiation to surrounding normal tissue. Furthermore, this approach may over-simplify VMAT delivery in certain parts of the arc where changes in gantry speed are larger than in others and the variable dose rate could not be considered with the same accuracy. This could be important to assess the potential radiobiological influence of different dose rates during VMAT delivery. Because of these considerations, other works incorporate different methods to represent the linac motion with a VMAT delivery emulator (Boylan *et al.*, 2013) where important differences were found between static and continuous dose calculation, as it was differently reported by Teke *et al.* (2010). It is important to remark that different results could be also linked to the type of verification systems implemented to assess the impact of VMAT delivery efficiency, since dose experimental measurements should be used to support the dose calculation from log files, or even from an emulator. Actually, these approaches showed only an accurate second check of dose calculation based on MC by considering the

delivered geometrical parameters, since no experimental measurements were directly included to estimate the actual dose dynamically delivered to the patient. For this purpose, the discretization degree and the accuracy used in dose calculation would be sensible to the efficiency of detectors and their locations inside VMAT systems.

For an accurate 3D VMAT verification with high calculation resolution, based on the information provided by the log file, it would also be desirable the implementation of an experimental validation with high resolution detection in order to minimize the potential mismatching. Although the data analysis process makes film dosimetry a less popular method for QA compared to previously mentioned verification systems, the high spatial resolution, minor energy dependence, and near tissue-equivalence provided by the radiochromic films, are well suited for VMAT QA purposes.

1.6 Hypothesis and Objectives

Hypothesis

The high accuracy provided by the MC explicit radiation transport simulation, and the high spatial resolution from film dosimetry can control and potentially reduce the uncertainties involved in complex dynamic techniques, such as VMAT, and are suitable to complete the required commissioning and develop adequate QA strategies.

Objectives

1. Monte Carlo modelling of linac heads and characterization of the 6 MV photon beam used for VMAT treatments.

2. VMAT verification by means of an automated Monte Carlo simulation of TPS plan parameters.

3. Implementation of Monte Carlo simulation of log files under a flexible sampling model in order to consider the dynamic irradiation by using the actual parameters recorded during the treatment delivery.

4. Design of a specific phantom to allow 3D radiochromic film measurements, and experimental support to be integrated in a MC-based QA model.

5. Development of specific software to process and implement the dosimetric measurements from the phantom into the MC simulation in order to provide experimentally reconstructed DVHs.

6. Application of the proposed model to clinical cases in order to test the operational feasibility to address potential limitations in VMAT optimization algorithms and commercial verification systems.

Materials and Methods

The interplay of the many variables being used over a broad range of magnitudes in VMAT optimization and delivery, implies demanding QA methods. During the introduction chapter different methods and systems have been mentioned and described for that purposes, which present different level of robustness. It was also pointed out that solutions where errors in QA can be meaningfully correlated to patient specific geometry and structures, using measurements to recalculate DVHs can detect clinically relevant dose errors better than the widely used gamma criteria. Solutions to reconstruct the dose in the patient anatomy have therefore been integrated in commercial available systems, which are based on measurements in a phantom or others, which can use some type of 'phantom-less' measurement to reconstruct the 3D dose in the patient anatomy. Although these software systems claim the capability to estimate patient dose based on QA measurement, the confidence on using such products to perform patient DVH-based QA requires further investigation, as already pointed by some authors (Zhen *et al.*, 2011), in the case of IMRT QA. For VMAT QA this could be even more important, since the approximation level used in these software to estimate the continuous delivery can introduce discrepancies and the result can also be compromised by detection density implemented in the 3D dose reconstruction.

For the work developed in this thesis, two commercial systems, one based on phantom and the other on phantom-less measurements, were used for the verification of clinical VMAT treatments, in order to evaluate them and to compare with MC verifications and, finally, to check with the QA model developed as part of this thesis. Therefore, a technical description of these commercial QA systems is included in a first section, for further discussion. Since we support the hypothesis that a highly accurate QA system suitable for the complexity of such technique require the most accurate calculation provided by MC, the second section will describe the application of MC simulation carried

out for this work, as a tool for routine VMAT treatment verification. Furthermore, some related experimental support carried out with basic film dosimetry and also employing these commercial devices is outlined. In the third section of this chapter, the proposed self-developed model to complete the MC based QA with experimental measurements for an effective VMAT evaluation will be described.

2.1 Commercial systems used for VMAT treatment verification

COMPASS and Delta4 systems were used for verification of VMAT treatment plans at Hospital Universitario Virgen del Rocío (HUVR) and Hospital Infanta Luisa (HIL) in Seville, respectively. The implemented COMPASS at HUVR is commonly used to verify VMAT plans previously calculated by the Philips Pinnacle TPS and delivered with an Elekta Synergy linac. On the other side, the Delta4 system implemented at HIL is used to verify Monaco TPS solutions delivered with an Elekta Axesse linac.

2.1.1 COMPASS QA system

The COMPASS QA system (IBA Dosimetry) consists of a software package (also called COMPASS) for dose calculation as well as visualization and analysis of measured data that is acquired using a gantry-mounted MatriXX$^{\text{Evolution}}$ detector array and a gantry angle sensor.

MatriXX$^{\text{Evolution}}$, which is an upgraded version of I'mRT MatriXX, has been developed for composite dose verification of rotational techniques such as VMAT and consists of 1020 vented pixel ionization chambers arranged in an active area of 24.4 cm × 24.4 cm with a pixel-to-pixel distance of 7.62 mm arranged in a 32 × 32 matrix (there are no chambers in the corners of the array). Each ion chamber has a volume of 0.08 cm^3, a diameter of 4.5 mm and 5 mm height.

The purpose of the dose computation in COMPASS is to provide an independent dose calculation engine in order to cross-check the dose calculated by the TPS. The dose engine (including a beam model of the linac head) implemented in the COMPASS software uses a collapsed cone convolution/superposition algorithm for calculating the 3D dose distribution. Dose calculation is a two-step procedure: first, the TERMA (total energy released per unit mass) distribution is calculated; second, this energy (TERMA)

is convolved with the energy deposition point kernels in directions which represent the whole surrounding cone in space.

The beam data required for the beam model in COMPASS is equivalent to the one required in the TPS, and usually the data from TPS commissioning can be used (profiles, depth dose curves, output factors, absolute calibration). In addition, the detector commissioning is also a necessary step when using COMPASS, in order to incorporate the detector model.

2.1.1.1   Fluence acquisition and COMPASS dose reconstruction

Before the patient-specific dose verification can be carried out, the patient plan data have to be exported from the TPS to the COMPASS software. For each treatment, COMPASS requires four data sets, all exported via DICOM (Digital Imaging and Communications in Medicine): the RT Plan, the RT Structures, the dose calculated by the TPS (RT dose) and planning CT images. To perform the measurements, MatriXX^{Evolution} is inserted in a dedicated holder and mounted directly on the gantry. In this configuration, the dose is delivered with original gantry angles identical to the patient plan. The delivered fluence measurements of the treatment plan acquired with the MatriXX^{Evolution} are recorded together with the measured gantry angle, by the external gantry angle sensor, directly in the COMPASS software. The sampling time for the measurements taken for the evaluated cases was set to 300 ms. COMPASS workflow is represented by the schematic diagram in Figure 2.1.

Primarily, COMPASS determines the fluence for all segments in a beam. As this quantity cannot be directly measured, COMPASS does first a calculation of the expected response (electrical signal) for each segment and detector pixel, based on linac and detector models (previously commissioned). This is called the predicted or expected response. After the measurement, the predicted and measured responses are compared. The residual response (response difference) is then used for a computation of the really delivered fluence, considered in the final dose reconstruction. Therefore, the algorithm implemented in COMPASS uses a combination of 'ideal' and measured fluences to determine the 'real' delivered fluence.
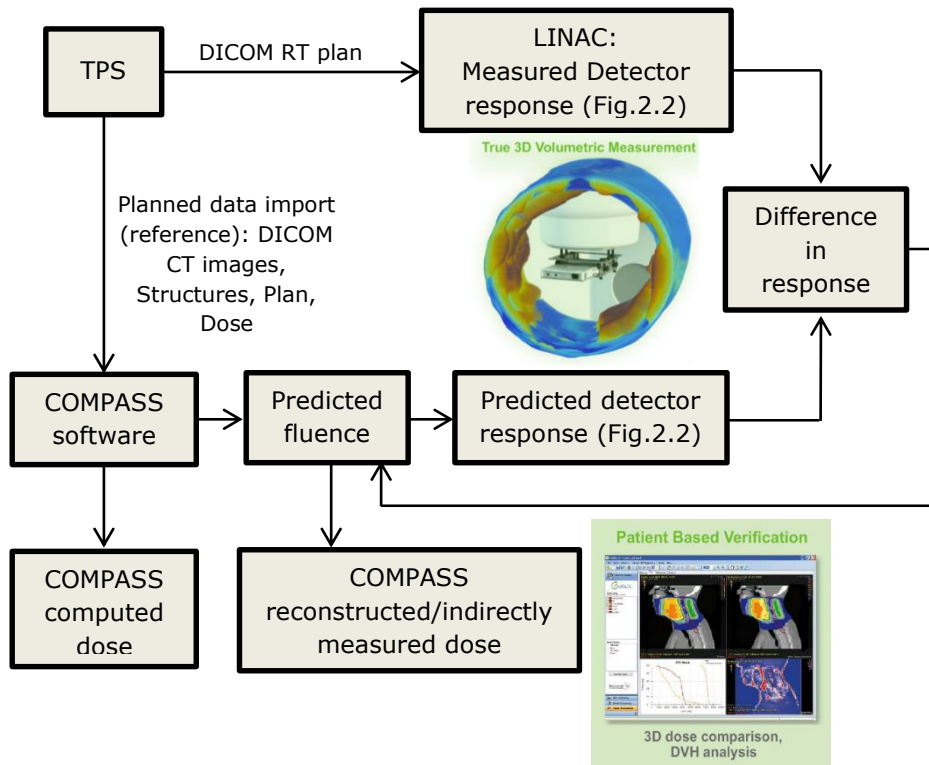
Figure 2.1. Schematic diagram of COMPASS workflow for 3D treatment verification and patient dose reconstruction from MatriXX^Evolution detector mounted on gantry for full 360° fluence acquisition. DICOM files are imported from the TPS in the COMPASS software, and the 3D dose is reconstructed using fluences derived from MatriXX^Evolution measurements with the patient's planning CT data. A comparison between DVHs calculated using TPS data and COMPASS dose reconstructed is finally carried out. Adapted from (IBA; Vikraman *et al.*, 2014).

Figure 2.2 shows the comparison between the expected response in the MatriXXEvolution detector (computed from RT plan DICOM file) and the measurement taken for a CP of one of the studied cases. Besides small deviations notably distributed in the edges of the CP irradiated area, it is important to note the limited spatial resolution in the measurement.

The spatial response function of a pixel is wider than its physical dimensions and the response function is regarded as isotropic. During COMPASS dose reconstruction, the effective resolution is increased from 1 cm to 2 mm by a fit procedure, where the coefficients of a series of 2D fluence functions are adapted to best fit the response measurements (Boggula *et al.*, 2010).

Once the whole treatment plan is delivered, the dose is reconstructed on the CT images from the delivered fluence (indirectly measured dose). The purpose of

the dose reconstruction is to provide some information about the actual dose that is being delivered to the patient. In general, the reconstructed dose from the delivered fluences would help to detect any delivery errors which could go unnoticed in a regular treatment process. The dose distributions and DVHs reconstructed from the fluence measurements are then compared with the TPS calculated plan, as shown in the Figure 2.1. These reconstructed 3D dose matrices and the respective measured frames were extracted from COMPASS, for further analysis and comparison with MC simulated fluences and MC dose verification of the cases evaluated in this work.
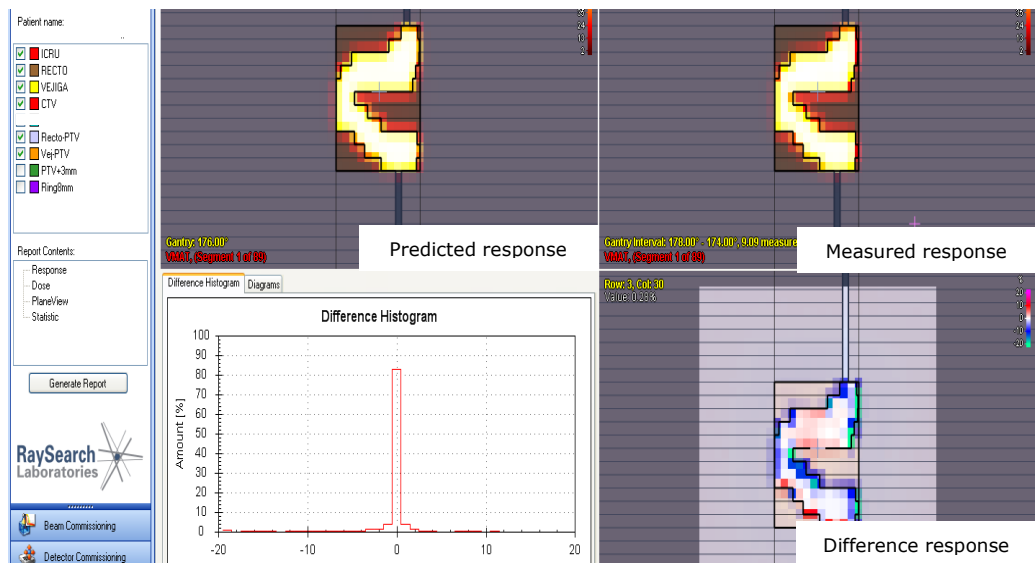
Figure 2.2. Expected detector response in the MatriXX[Evolution] array for a CP, computed in COMPASS (upper left) vs measured detector response (upper right); difference histogram and matrix difference (bottom left and right), respectively.

2.1.2 Delta4 QA system

The Delta4 QA system (ScandiDos) comprises a cylindrical phantom made of PMMA with the dimensions of 22 cm in diameter and a length of 40 cm, and the associated software. Inside the phantom there are two detector planes crossing each other in the isocenter (Figure 2.3, bottom left). The two detector planes consist of 1069 p-type Si diodes. The detection area per plane is 20x20 cm^2, and the diodes are disc shaped with a volume of 0.04 mm^3, placed with a spacing of 0.5 cm in the central area (6x6 cm^2) and a spacing of 1 cm in the outer area. An inclinometer attached to the accelerator gantry and connected to the Delta4

system gives the continuous independent information about the gantry angle during the arc delivery.

For each measurement, the Delta4 system is able to sort the dose information into sub-beam-structures, corresponding to the control points of the plan from the TPS. The sorting is made by associating the measured dose from each dose pulse from the accelerator with the actual gantry angle at the dose pulse delivery, measured by the inclinometer. The dose pulses measured during the gantry angle interval of a control point are summed together, giving the dose corresponding to that CP. The Delta4 phantom is calibrated to absolute dose measurement using a farmer reference ion chamber for the specific linac, and can thus be used to measure absolute dose level.

In its basic implementation, the one currently used at HIL, the measured dose at the detector positions is compared to the planned (recalculated on the CT-image of the Delta4 phantom in Monaco TPS), and a gamma analysis is used to verify the correspondence between dose distributions (Figure 2.3). For a more comprehensive evaluation, a 3D dose reconstruction on the phantom can also be made. For each plan CP, the rays are traced through the measurement points, and the TPS dose calculated on the Delta4 phantom along each ray is normalized to fit the measurement.
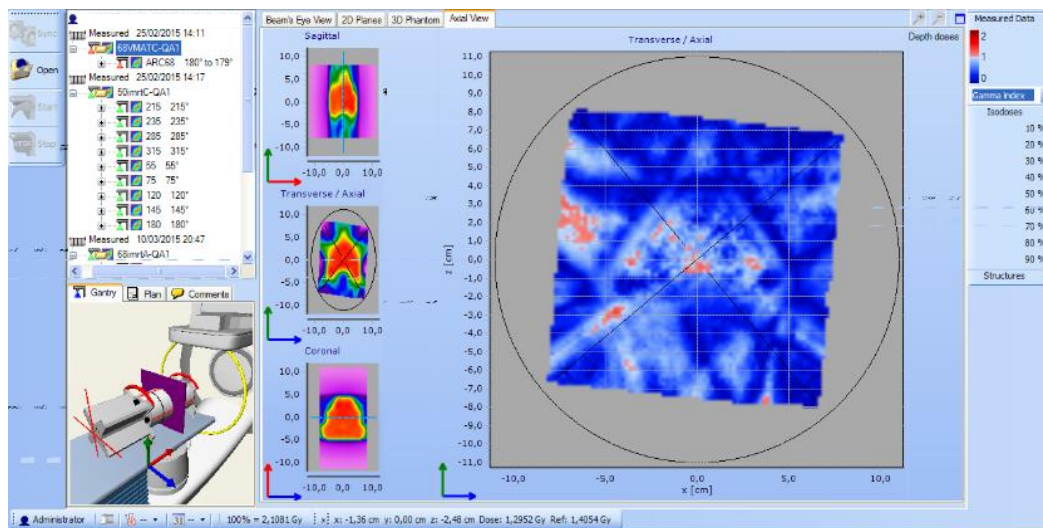

Figure 2.3. Gamma analysis in Delta4 for the axial slice corresponding to the isocenter, for the evaluated H&N case also verified with the model proposed in this work, including axial films.

2.1.2.1 Delta4 DVH Anatomy

The recently (April, 2016) version of Delta4, among other upgraded functions, contains the Delta4 DVH Anatomy 2 option, which allows the 3D patient dose reconstruction. In this option the incident fluence can be approximated from the phantom measurement and used for dose calculation on the patient dataset with a pencil beam algorithm or with the treatment plan dose including measured modification (TMM algorithm).

In order to implement this tool to obtain and compare the resulting DVHs for some of the evaluated cases, the Delta4 software of HIL was upgraded and installed in a PC with a 2.7GHz Intel Pentium CPU (G630) and 8 GB RAM, running a 64 bits Windows 7 operative system, at the University of Seville. The Delta4 DVH Anatomy license was specifically provided by ScandiDos for this work, under a collaboration agreement. This option required a commissioning process, similar to the one mentioned for COMPASS system. In this case, the head geometry including primary and secondary collimators was first described in Delta4 software, to generate the model of the Elekta Axesse linac. The required beam characterization for 6MV modality was done by importing DICOM RT dose distributions for open quadratic fields, calculated in a large water cube with 2mm x 2mm grid and a MC-Monaco uncertainty of 1%. The lateral (inline and crossline) dose profiles and percentage depth dose curves (PDDs) were then extracted in the Delta4 software, the output factors in air and water and absolute dose calibration data were also introduced, and a Gaussian source kernel was chosen for the beam characterization process. Beam characterization results, showing PDDs and profiles at different depths obtained for two of the used field sizes are represented in Figure 2.4.
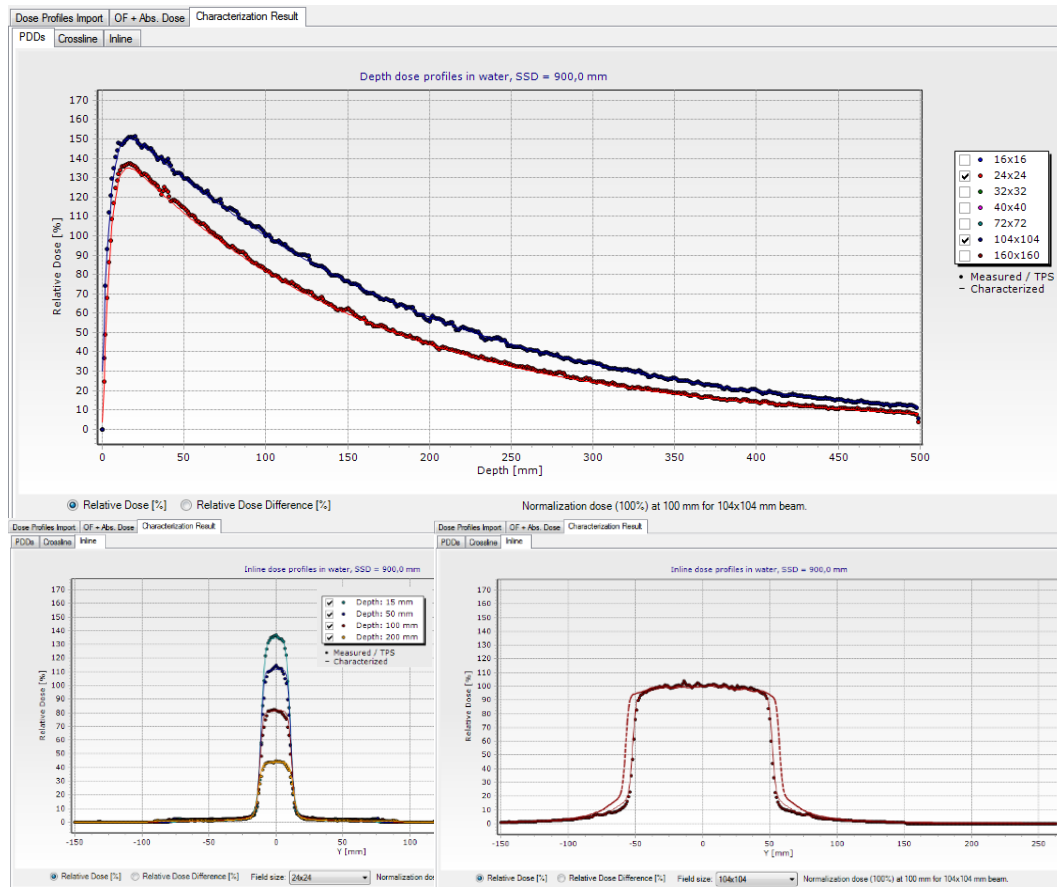
Figure 2.4. Screenshots of Delta4 DVH Anatomy software showing beam characterization results. PDDs and some dose profiles for 2.4 x 2.4 cm² and 10.4 x 10.4 cm² fields. TPS (·) and Delta4 characterization (-).

2.2 Monte Carlo simulation for VMAT QA

Monte Carlo method is a powerful tool to assess the details of the energy deposition process that accounts for all aspects of primary and secondary radiation transport inside the treatment machine head, and also within the patient. MC simulation has been already implemented as a tool for VMAT QA and treatment verification. In order to model the passage of a particle through, for example, a slab of tungsten, a particle detector, or even the human body, the ability to link the outcomes of successive interactions and particle trajectories forming the particle shower is required. The EGS (Electron Gamma Shower) code (Nelson *et al.*, 1985), developed at the Stanford Linear Accelerator Center

(SLAC), represents an unification of particle interactions for the coupled simulation of electrons and photons in an arbitrary material geometry from a few keV up to several hundred GeV. Using EGS, quantities of interest can be calculated by averaging over a given set of MC particle cases or histories.

The Monte Carlo code used throughout this work was the simulation package of the coupled electron-photon transport EGSnrc (Kawrakow, 2000a; Kawrakow and Rogers, 2000) developed by the National Research Council of Canada (NRCC). The EGSnrc is an extended and improved version of the EGS4 package originally developed at SLAC.

The BEAMnrc (Rogers *et al.*, 2011) and the DOSXYZnrc (Walters *et al.*, 2009) are widely EGSnrc-based Monte Carlo simulation user codes for simulating radiotherapy beams and calculating dose distributions in phantoms or in patients, which were developed as part of the OMEGA (Ottawa Madison Electron Gamma Algorithm) project to simulate the dose delivered by typical energy beams in radiotherapy. The former was designed to simulate radiation beams from any radiotherapy source, including Co-60 and even low energy x-rays and the latter was designed for calculating dose distributions in rectilinear voxel geometry. Both codes were already implemented for the MC simulation of the radiation transport through all the elements involved in the VMAT treatment, i.e. the linac treatment head, the phantoms employed in the dosimetric measurements and finally the patient, and their geometry (Lobo and Popescu, 2010).

2.2.1 Linac head modelling

An accurate model of the clinical linear accelerator used for VMAT delivery is an essential step during the all simulation process. In this step, the geometry of the linac treatment head of the Elekta Synergy installed at HUVR (Figure 2.5) was modelled using BEAMnrc (Rogers *et al.*, 2011) for a nominal energy of 6MV, based on the technical specifications regarding the dimensions, geometrical configuration and material composition, which were provided by Elekta, under a non-disclosure agreement. A schematic overview of the Elekta Synergy linac head is depicted in Figure 2.6.

Figure 2.5. Elekta Synergy accelerator installed at Duques del Infantado, Hospital Universitario Virgen del Rocío (left) and its MLCi2 multileaf collimator model (right). MLC images from (*Elekta*).

The Elekta Synergy accelerator is equipped with the MLCi2-type multileaf collimator (Figure 2.5), consisting of 40 leaf pairs with rounded ends and a projected width at the isocenter (at 100 cm from the source) of 1 cm, allowing a maximum field size of 40 x 40 cm^2. Once the leaves are separated from their neighbors by a small nominal gap to minimize friction and there is no tongue and groove or interlocking steps in the leaves of the MLCi2 (in contrast with the previous model MLCi), the interleaf leakage is reduced by a slight leaf bank tilt of the focused leaves. The MLCi2 leaves have the ability of interdigitation, if enabled by the linac control system, an over travel distance of 12.5 cm and a maximum leaf speed of 2cm/sec.

The MLC with 8.2 cm thick leaves is complemented with secondary collimators (see Figure 2.6), which consist of a 3.0 cm thick X backup jaws fitted below the MLC to minimize the radiation leakage and perpendicular to these, a 7.8 cm thick Y jaws for full attenuation, all made with a tungsten alloy.

To produce a photon beam, an electron beam impinges on a tungsten target giving rise to bremsstrahlung photons; the beam is collimated by the primary collimator and flattened by the flattening and difference filter, depending on the energy; the ionization chamber is used to monitor the output of the linac and the backscatter plate protects the chamber from backscatter photons; the mirror (not presented in Figure 2.6) projects a light field on the patient and allows visualization of the collimator settings. The MLC is a combination of a set of thin collimating leaves which can be positioned individually, in this way an

arbitrary field shape can be generated. The jaws are collimator blocks that can be positioned to limit the leakage and transmission through the MLC. At the exit of the linac head, the beam passes through a mylar screen, which has lines printed on it to indicate the isocenter position.
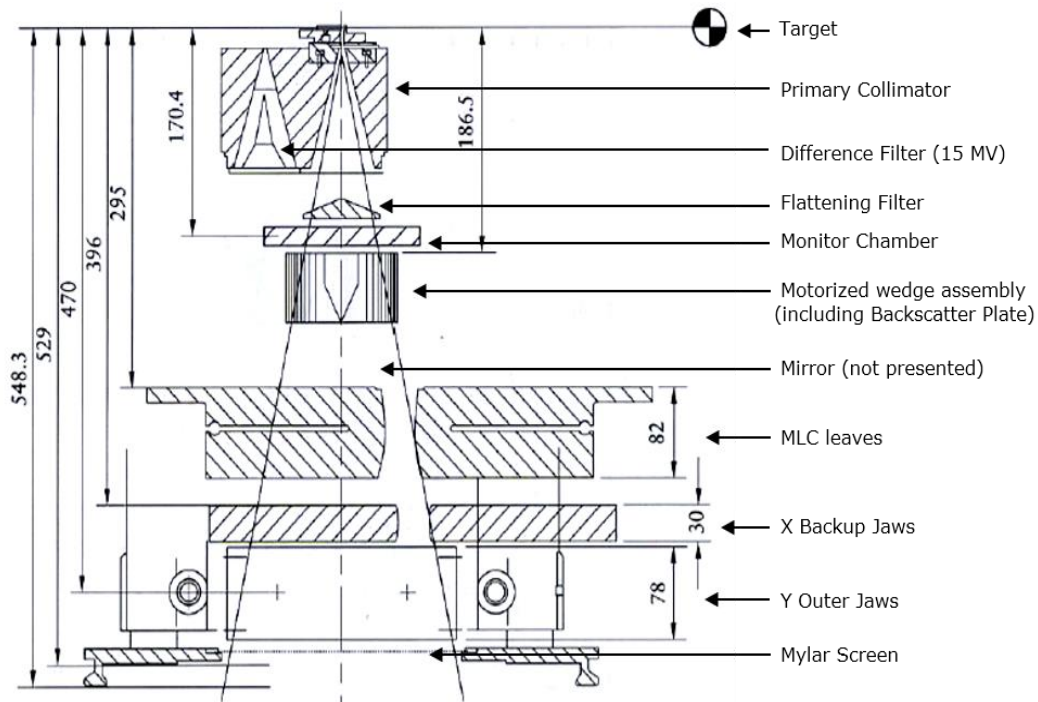

Figure 2.6. Schematic representation of the Elekta Synergy linac head for the 6 MV photon beam operating mode (property of Elekta limited).

The accelerator head geometry was built using a number of individual component modules (CMs) present in BEAMnrc that are perpendicular to the beam axis, which are specifically designed and optimized to model different geometries for different components in the treatment head. It is possible to modify the physical dimensions and material of the CM, in order to match the specific components according to the manufacturer's specification. The CMs used to model the Elekta Synergy treatment head were: FLATFILT for target and flattening filter, CONESTAK for primary collimator, CHAMBER for ion monitor chamber, MIRROR for mirror, MLCE for MLC, VARMLC for X backup jaws, JAWS for Y jaws and SLABS for the backscatter plate, the mylar screen and for the air gap between the exit mylar and the desired phase-space plane. A representation of the accelerator head modeled in BEAMnrc with all the CMs can be seen in Figure 2.7.
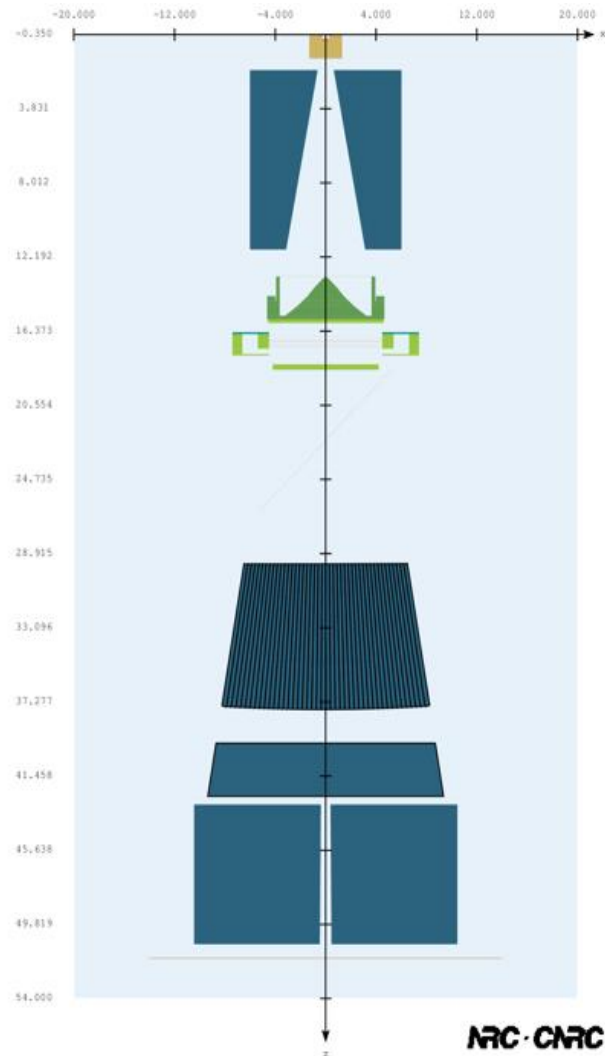
Figure 2.7. XZ-plane representation of the Elekta Synergy linac head geometry (6 MV modality), with the different component modules in the BEAMnrc user code.

Although all the information was supplied by the manufacturer, the access of some detailed specification was limited, mainly in what concerns the detailed geometry of the MLCi2 leaf. Some physical parameters, specified in the BEAMnrc component model MLCE (Figure 2.8) used for modelling the MLCi2 geometry were, therefore, completed by theoretical geometric considerations. This CM model was mostly coded by Nick Reynaert at the University of Ghent. To account for the beam divergence and minimize the geometric penumbra across the leaves, the leaf sides are focused towards the target, which means there is a difference in width between the leaf top side and bottom side for all the leaves to line up with the beam divergence. To define the top and bottom

thickness of the leaf, the projected width at the isocenter was rescaled by ray-tracing, taking into account the interleaf air gap to the Z distances of each defined thickness.

On the other hand, the rounded leaf end design of the MLC leaves and backup jaws (with parallel leaf motion), leads to a nonlinear relationship between the physical leaf opening and the projection at the isocenter plane. As a result, the actual positions were calculated by applying a correction algorithm (2.1), through trigonometric relationships, for the rounded tips, taking into account the corresponding radius of curvature. In any case, the leaf offset corrections provided by the manufacturer to account for the rounded leaf tip were similar to the corrections being applied with this correction algorithm.

$$
x_f = \begin{cases} \frac{x_0}{z_0} z_f + r \sqrt{1 + \frac{x_0^2}{z_0^2}} \text{ , leaf in its MLC bank.} \\ \frac{x_0}{z_0} z_f - r \sqrt{1 + \frac{x_0^2}{z_0^2}} \text{ ,leaf over central axis.} \end{cases}, \tag{2.1}
$$

where, x_0 and x_f are the initial and final positions, respectively, being z_0 the source-to-isocenter distance, and z_f the source-to-leaf defined radius distance, and r the radius of curvature.
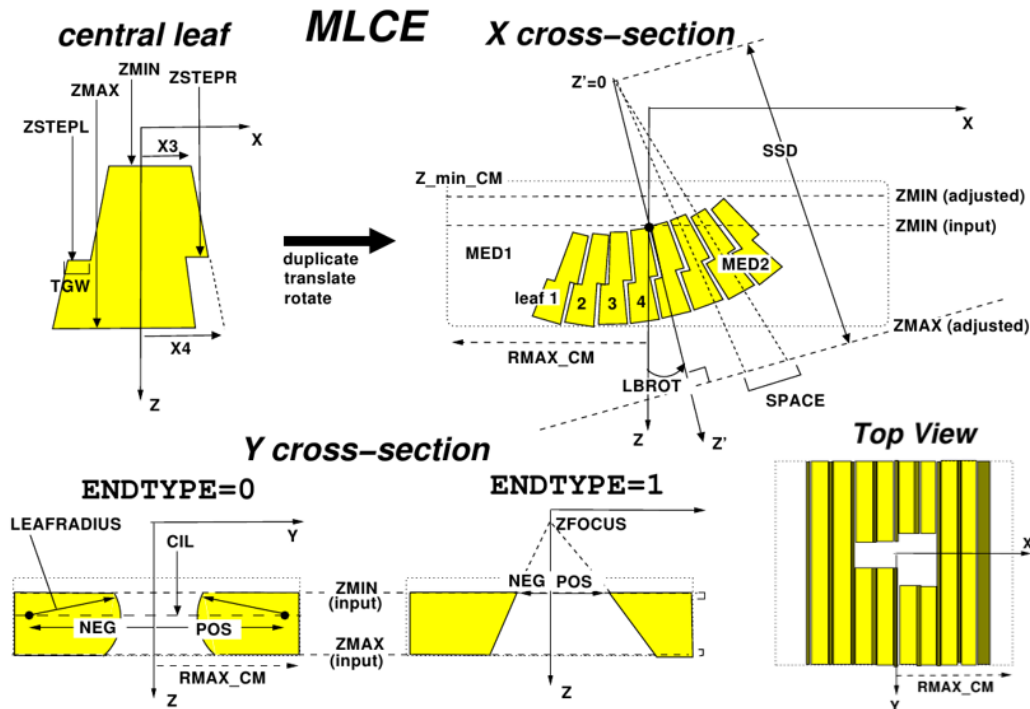

Figure 2.8. Schematic representation of the MLCE CM (*Rogers et al., 2011*), showing its geometry and the input parameters required in BEAMnrc user code for this module.

Moreover, this CM model allows the entire leaf bank rotation in a plane perpendicular to the leaf opening direction by a specified angle (in radians), to consider the previously mentioned leaf bank tilt. This slight rotation is set by the manufacturer to reduce the leakage transmission between the leaves in the MLC. As shown in Figure 2.7, this linac model has two pairs of jaws below the MLC, thus the necessary tilt can be small.

The interleaf gap was also adjusted from the recorded particle tracing of their transport simulation through the MLCE. During a BEAMnrc simulation, particle positions can be recorded when they cross air-leaf or leaf-air boundaries through this CM used to model the MLC, following the method developed by Heath *et al.* (Heath and Seuntjens, 2003). A representation of the MLC model implemented, recorded during this simulation in order to adjust the interleaf gap is shown in Figure 2.9.
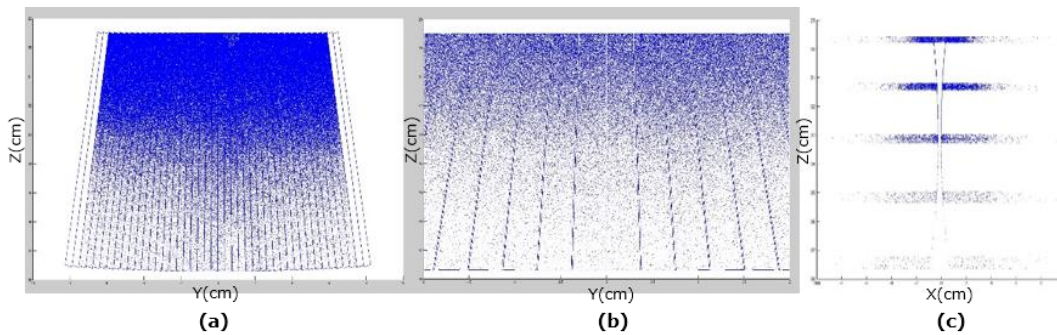

Figure 2.9. Cross-sectional views of the 40-leaf MLCi2 model generated by particles tracing recorded during BEAMnrc/EGSnrc simulation. (a) MLC end view, (b) zoom of the MLC end view, and (c) leaf side view.

A number of scoring planes can be applied at the back plane of any CM in the modelled accelerator, where a phase-space data (PSD) file can be scored. The PSD is the most important output from BEAMnrc where information of each particle's complete history, energy, position, incident angle and charge is stored. The PSD file can also be used as an input file for further Monte Carlo dose calculations, e.g. the photon beam incident at the surface of a phantom with DOSXYZnrc.

For the BEAMnrc simulation, apart from the input file establishing the parameters that control the radiation transport and specify the geometry and the materials in the linac head, the cross-section data for the media composing the CMs is required. This information is contained in a pegs4 data file (*.pegs4dat file) previously generated from the composition of the different

materials and their densities. The same is done for DOSXYZnrc regarding the media represented in the patient CT.

2.2.2 Source modelling and beam characterization

Accurate dose calculations require an accurate Monte Carlo model, which means that not only correct information about the accelerator head but also about the incident electron beam is needed.

The actual shape and spectrum of the primary electron beam source incident on the target to generate the photon beam are rarely known. Even the same accelerator model presents different spectra for the same nominal energy for each installation. Therefore, it is necessary to deduct this spectrum from reliable experimental dosimetric measurements (PDDs and lateral dose profiles), which characterize the beam. In this case, the 6 MV photon beam from the Elekta Synergy linac was modelled.

To simulate the primary electron beam incident on the target an energy spectrum with a Gaussian radial intensity distribution was modelled by the source routine number 19 in BEAMnrc (Figure 2.10). The radial spatial
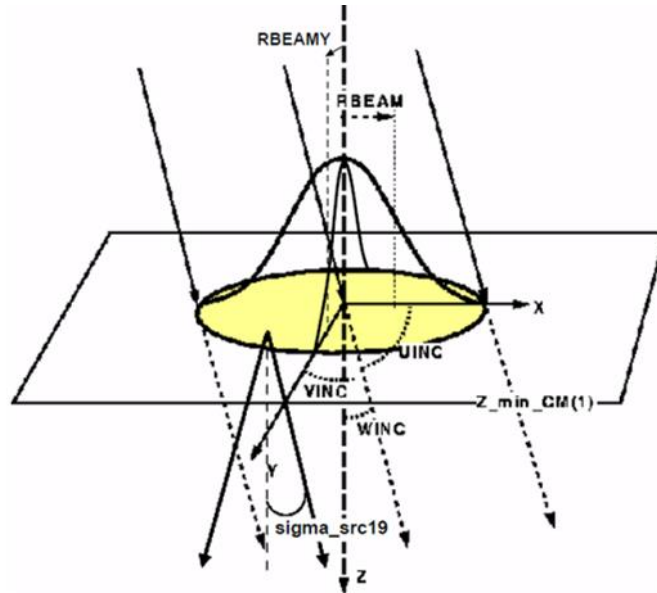
Figure 2.10. Geometry of the BEAMnrc's ISOURC=19 (Rogers *et al.*, 2011). This is an elliptical beam where the ellipse is defined by Gaussian intensity distributions in X and Y. The beam can be parallel, with specified direction cosines, or has a mean angular spread about the Z-axis. If the σ or FWHM of the Gaussian distribution in the Y and X direction are equal, the beam results in a circular beam with a Gaussian radial distribution, as it was assumed in this case.

intensity was given by the full width at half maximum (FWHM). This value is also commonly described by the standard deviation in the Gaussian distribution (FWHM $= 2\sqrt{2 \ln 2}\sigma \approx 2.35\sigma$).

As the initial electron beam leaves the accelerator vacuum and hits the bremsstrahlung target, the characterization requires a fine tuning of the different parameters for the electron beam in order to match Monte Carlo calculated dose distributions within an accepted error (less than 2%) with measured dose distributions in well-known standard conditions.

To estimate the incident electron beam energy and radial intensity distribution, BEAMnrc simulations for a set of field sizes (20x20, 10x10, 20x5, 5x20 and 2x2 cm^2) were performed. Different combinations of the mean energy and FWHM values, ranging from 6.0–6.5 MeV and 0.75–2.0, respectively, were evaluated to find the appropriate values (table 2.1). Due to the tilt presence in the MLC, the value of this parameter was also investigated during the simulations, what meant a hard task because the results showed to be very sensible to this parameter. Simulations with no tilt and with small tilt variations were performed, starting from 0.0013 rad which corresponds to a 0.5 mm displacement over the source focus.

A phase-space file was scored just below the accelerator head at 54 cm from the bremsstrahlung target for each simulation. An initial number of histories (from 5×10^7 to 5×10^8) were simulated to obtain the necessary number of particles recorded in the phase-space files depending on the field size and the required statistical uncertainty (less than 1%).

For the transport parameters, global cut-off energies for electron and photon transport, respectively, were set as follows: ECUT (including the electron rest mass energy) = 0.7 MeV, similar to AE (threshold energy for electron creation, defined in the medium file); PCUT = 0.01 MeV, similar to AP (threshold energy for photon creation, defined in the medium file). The boundary crossing algorithm EXACT and electron-step algorithm PRESTA-II were used, and for Bremsstrahlung and pair angular sampling the complete modified Koch-Motz distributions were considered. The National Institute of Standards and Technology (NIST) cross section data base was used for the bremsstrahlung production.

To improve the simulations efficiency, variance reduction techniques were also employed. In this case, it was used the range rejection with an energy cut-off of 2.0 MeV and the Directional Bremsstrahlung Splitting was also used with variable splitting field radius according to field setting.

The phase-space files obtained were used as inputs for DOSXYZnrc to calculate the dose distributions in a water phantom. The dose distributions were compared to the experimental measurements, provided by HUVR, including PDDs and lateral dose profiles at several depths (1.5, 5, 10 and 20 cm), previously obtained with ionization chamber and semiconductor diode.

Phantoms with dimensions of 10 x 10 x 36 cm^3 for 2 x 2 cm^2 field, and of 30 x 30 x 36 cm^3 for the rest of field sizes were constructed with a voxel dimension of 0.1 x 0.1 x 0.1 cm^3 in the first case, and with 0.3 x 0.3 x 0.3 cm^3, in the second case, to have a better resolution for smaller field sizes.

For these simulations, particle transport parameters were similar to those used for the BEAMnrc simulations, except the energy threshold for electron transport, ECUT, which was set to 0.521 MeV. The number of histories required in each run to get the desired statistical uncertainty is dependent on the field size and the voxel size. Smaller voxels were necessary for the smaller field sizes and therefore, a larger number of histories was required to get the desired statistical uncertainty. In all cases, the particles in the phase-space file were recycled 3 times to obtain less than 1 % of uncertainty in the smallest voxels of each simulation. In this way, the recycling considered did not incorporate systematic errors

All MC simulations were distributed on a cluster of four 12-core 2.19 GHz CPUs AMD Opteron, in a parallel architecture, installed at the *Fisiología Médica y Biofísica* Department of the University of Seville.

Table 2.1. Variable parameters for the different field sizes simulated during the calibration process of the 6 MeV energy beam delivered by the Elekta Synergy linac installed at HUVR.

Field size (cm^2)	Mean energies (MeV)	Radial FWHMs (mm)	Tilt (rad)	BEAMnrc (N hist.) / DOSXYZnrc (N rec.)
20 x 20	6.0/6.25/6.5	1.5/1.1	0.0013/0.0017	5x10^7 / 3x
10 x 10	6.0/6.25/6.5	1.5/1.1	0.0013/ 0.0017/0.01	5x10^7 / 3x
2 x 2	6.0/6.25/6.5	0.75/1.1/1.5/2.0	0.0013/0.0017	5x10^8 / 3x
5 x 5	6.0/6.25/6.5	0.75/1.1/1.5/2.0	0.0013/0.0017	5x10^8 / 3x
5 x 20	6.0	1.5	0.0013/0.0017	5x10^7 / 3x
20 x 5	6.0	1.5	0.0013/0.0017	5x10^7 / 3x

2.2.3   MC verification of VMAT TPS calculation

The 6 MV photon beam from the Elekta Synergy modelled in this work, and also the 6 MV photon beam from the Elekta Axesse linac model validated in other work (Ureba, 2015) were used to simulate several clinical cases from both hospitals, HUVR and HIL.

Different treatment locations with distinct complexity, including SBRT lung and radiosurgery (RC) cases, head and neck (H&N), prostate, and other locations, all solved with VMAT technique were included for evaluation. These cases were previously planned with commercial TPS Pinnacle V9.0, or Monaco V2.3, and verified with the aforementioned commercial systems, IBA COMPASS/MatriXX, or Delta4.

For the MC simulations of all VMAT treatments, a PSD file was first obtained from the simulation of the treatment-independent components in the linac head, in order to be used as source for the transport simulation through the geometry of beam modifiers specific to each case. This enables a considerable reduction of the global simulation time. The subsequent PSD files, were then obtained for each one of the simulated control point geometry, and scored at the exit of the linac head.

The BEAMnrc transport parameters were analogous to the ones used for the MC beam calibration process. Conversely, there was no need for DBS to improve efficiency, since the PSD file corresponding to the simulation of treatment-independent components was used as the main source for subsequent simulations of the CPs.

In order to implement a routine VMAT verification by means of an automated MC simulation system, an in-house program was developed for the automatic explicit simulation of the geometry of every CP, through the acquisition of the data contained in the RTP files from MOSAIQ system. The general workflow of this automated process is represented in Figure 2.11. The RTP file contains the parameters for the linac to deliver the treatment (gantry angle, MLC and jaw positions, and MU for each CP, mainly). However, it has a specific format and particular characteristics for VMAT, and thus differs from the previously known LANTIS structure and IMRT plans, widely used in our group. To overcome the communication problems encountered with this different RTP file format, its structure has been studied and new records were identified, which are described in the next subsection. This allowed the creation of a program written in shell (Linux) to automatically extract all the required plan parameters and automatically create the input files for the BEAMnrc user code.
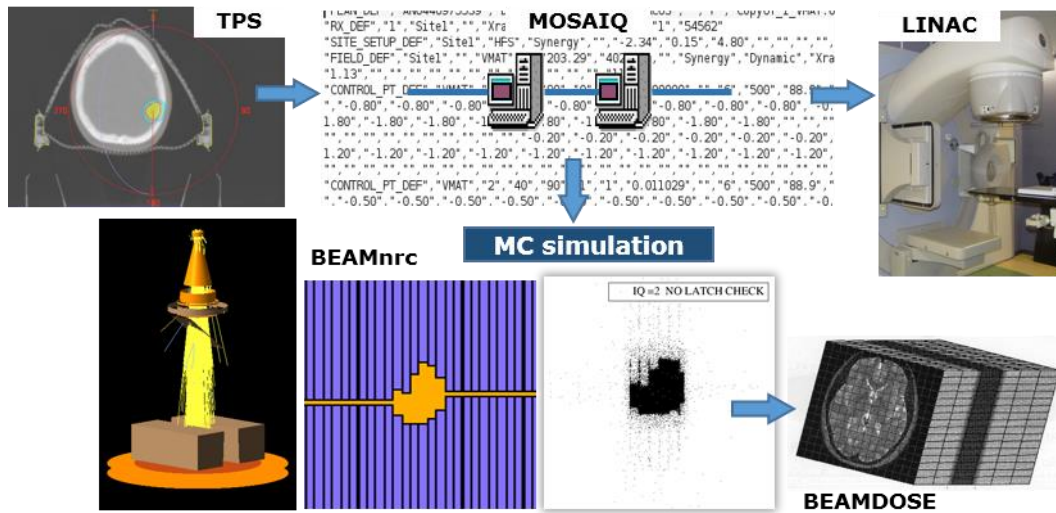
Figure 2.11. Workflow of the automated MC verification process.

Similarly, DICOM-RT plan files exported from the TPS can also be used for simulation, so this automated process was then adapted to MATLAB, in order be integrated in the CARMEN platform. CARMEN is a specific MATLAB-based platform developed by the Medical Physics group (Baeza *et al.*, 2015) with a graphical user interface (GUI) for a friendly use, which is also used in this work for the evaluation and comparison of results.

The corresponding dose calculation was carried out from the phase-space files previously obtained for each CP, by means of BEAMDOSE, a DOSXYZnrc code modification already implemented by this research group for a previous work (Salguero Castaño, 2008). This code allows knowing every aperture contribution or beamlet, in each voxel in order to score the individual dose through each voxel of the phantom representing either a patient CT or a QA phantom. In this way, the dose distribution can to be weighted by changing the MUs corresponding to each individual beamlet.

The voxelized phantom is obtained from the conversion of the CT numbers, or Hounsfield units (HU) to the correspondent physical density, and assigned material, according to the respective calibration curve obtained from the CT scan, which was used for generating the CT image involved in the simulations (see Figure 2.12). Dose calculation was performed with a high resolution grid, consisting on 256×256 voxels per slice, for a fair comparison with film, when applied. For particle transport simulation in the phantom, ECUT was chosen considering the voxel size and the electron range for the involved tissues.
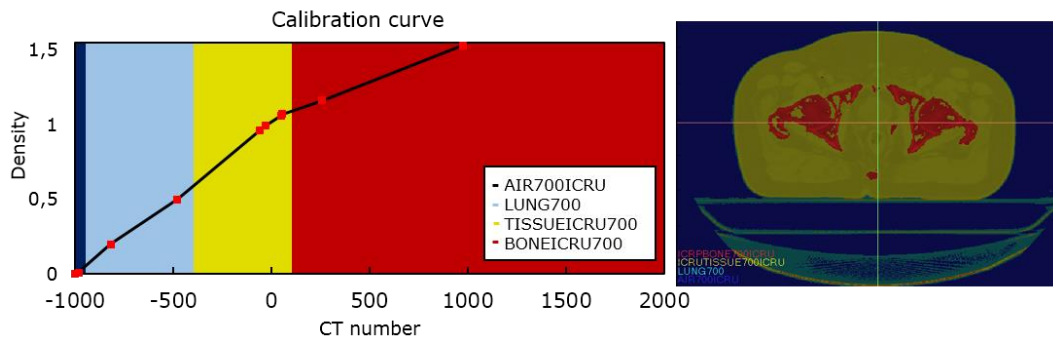
Figure 2.12. Calibration curve used to generate the MC phantom of a patient CT from the HUVR (left) and a representative slice of the converted patient CT phantom, showing the 4 different materials being considered (right).

The number of initial particles was selected according to the number of simulated CPs to ensure the statistical uncertainty below 1% in the final dose for all the voxels inside the treatment region. This number ranged from 2 to 4×10^6 particles per CP. When required, particles in the phase-space files were recycled and/or particle splitting techniques were implemented to improve statistics efficiently. A typical single arc case involving around 90 CPs took less than 3h, using the cluster previously mentioned, and simulating 2×10^6/CP.

A conversion factor from MC dose (Gy/history) to Gy/MU has been calculated for each linac model, following the formalism by Ma. et al (Ma *et al.*, 2004). The number of histories for MU conversion factor is determined by relating the absolute dose measured under reference calibration conditions (central axis, depth of dose maximum in water, 10×10 cm^2 field defined at 100 cm SSD) to MC dose obtained from the simulation of the same reference conditions. The conversion factors obtained for Axesse and Synergy linac models were, respectively, 8.76×10^{13} and 1.12×10^{14} hist/MU.

MC solution of each case was evaluated and compared in CARMEN platform, together with the solutions given by the TPS and the commercial dosimetric verification system employed. Dose distributions were compared through isodose curves and DVHs, as well as difference matrix and gamma function analysis.

2.2.3.1 MOSAIQ system and RTP file structure

MOSAIQ is an Elekta's dedicated oncology information system (OIS), which simplify the entire therapy workflow, from initial diagnosis and staging, through planning, treatment and subsequent follow-up.

At HUVR and HIL a MOSAIQ OIS is the implement platform that works as a communication network between the TPS and the Elekta linac, involving data integration supported by communication protocols as DICOM.

As it has been commented before, it is possible to export a set of DICOM files containing the patient plan data through the TPS. These are:
- **DICOM CT** files, containing the patient's CT scans.
- **DICOM RT Structures** file, including structures and volumes of interest (planning volumes).
- **DICOM RT dose** file that presents all the distribution characteristics of the dose calculated by the TPS.
- **DICOM RT Plan** file comprises all the treatment plan information of the TPS (e.g. Beams and Dose References).

When the created plan is sent to MOSAIQ from the TPS, to be then delivered by the linac, the DICOM RT Plan file is previously received by IMPAC DICOM Communication Module (DCM) product operation and is translated into RTP*Connect Import file* intended to be imported by the MOSAIQ application. MOSAIQ performs the importation process that extracts information from the RTP*Connect Import file* and stores the information in the Information Management System database. This format is defined as the link between the TPS and linac control system, and also can be used to verify and /or correct the treatment plan.

The recorded structure of these RTP files follows the hierarchy presented in the diagram of Figure 2.13. The records of the data file, which correspond to the structure, illustrated in the following figure present a specific format. Each one is identified by its *KEYWORD* and data elements appearing in a particular order. The last field of each record shall contain a calculated Cyclical Redundancy Check (CRC) for that record, which shall be a 16 bit unsigned CRC.

The main RTP file records used to extract information for the treatment simulation in MC were:
- Plan definition record [PLAN_DEF], containing the treatment plan identifiers for the patient, the plan, and the staff member who generated the plan.
- Prescription site record [RX_DEF], containing prescription site and treatment technique information.
- Site setup record [SITE_SETUP_DEF], containing the site setup information for the prescription site.
- Treatment field record [FIELD_DEF], containing treatment field information.

- Control point record [CONTROL_PT_DEF], containing the geometric and monitor unit parameters for large leaf count MLCs (i.e. greater than 50 leaves/side).
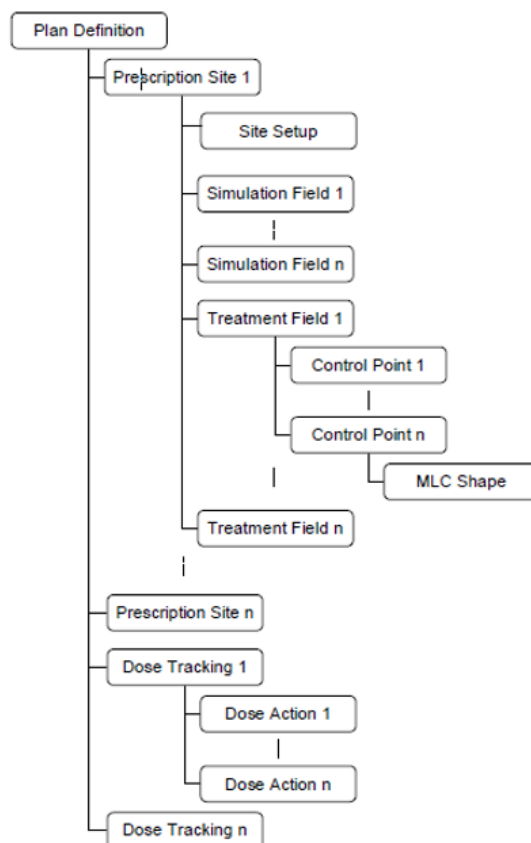

Figure 2.13. Diagram of RTP Import/Export data hierarchy. This specification defines a treatment plan (course) with multiple treatment (prescription) sites, and multiple treatment fields. From RTPConnect manual (IMPAC, 2012).

2.2.3.2 Validation of MC simulation with experimental measurements

The required experimental support was initially carried out with radiochromic film (Gafchromic EBT3, International Specialty products Inc.), in order to verify the correct MC accelerator model and beam calibration, in a homogeneous solid water phantom. Some dosimetric measurements, including irradiation with all MLC leafs closed and an E shaped segment were performed to evaluate the intra and inter leaf transmission and tilt model. The change of the energy spectrum with the central axis distance was also studied, by means of the irradiation of central axis and off-axis segments with complex geometry.

Additional experimental verification, with Gafchromic EBT3 film, of complete treatments was also included in order to validate the MC simulations of complete treatments. Films were placed on the same setup as for COMPASS/MatriXX verification and also in a cubic solid water phantom on the treatment table. The irradiation of complete clinical cases, solved with MCTP-CARMEN solution in a homogeneous solid water phantom (Ureba *et al.*, 2014), were also included to complete the validation of the MC model of the Axesse linac. MC solutions were compared to the solutions given by the TPS and the dosimetric verification carried out. The agreement between dose distributions was evaluated through dose profiles, and gamma analysis.

2.2.4 MC verification of VMAT by using log files

Despite MC verification of TPS exported files, such as RTP or DICOM-RT plan files, allows a verification of the TPS dose calculation, the verification of the continuous arc delivery of VMAT plans is not considered in this way. Moreover, this approach can be dependent on the degree of modulation between CPs in the arc, providing greater effect and produce more differences in the dosimetric verification of plans with a higher level of modulation. Therefore, log files recorded during VMAT treatment plans delivery, were considered in order to simulate the actual treatment parameters. This was achieved by means of specific software written in C++ developed by Rafael Linares from HIL, within our research group. This software allows the communication with the Elekta linac in real time, under the iCom Protocol, and is able to record all the CP parameters every 0.25s or 1s during beam on or beam off, respectively. This 4 Hz recording rate is similar to other tools implemented for log file analysis in Elekta linacs (Tyagi *et al.*, 2012).

2.2.4.1 Discretization process of log files for simulation

As part of a QA model applied to VMAT evaluation, the implementation of log files into the automated MC simulation process of every CP geometry, and dose calculation described above was also carried out. For that purpose, an in-house MATLAB program was developed, allowing the analysis and the discretization process required for the MC simulation of these files. A flowchart of log file analysis and discretization process for MC simulation is presented in Figure 2.14.
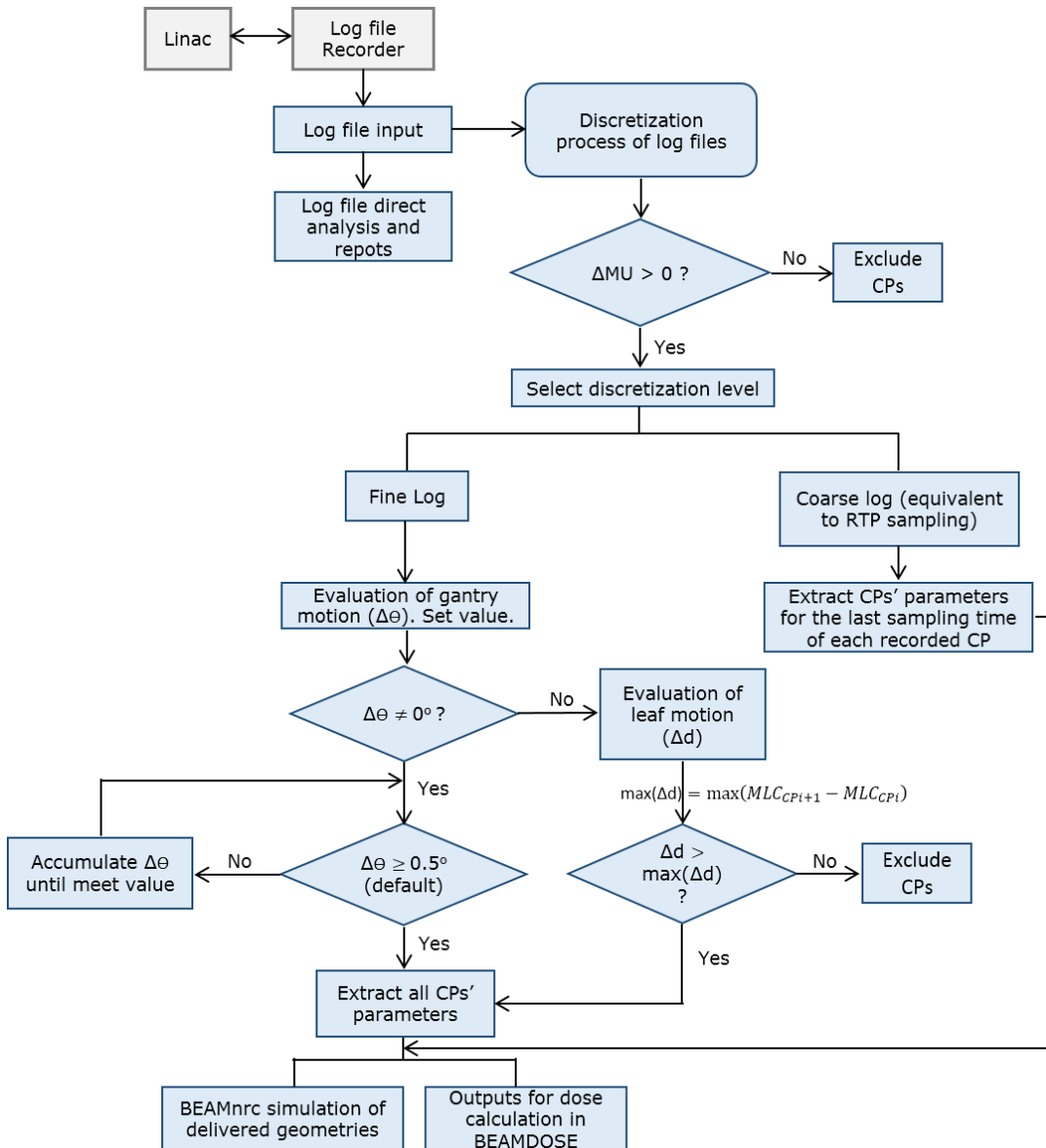
Figure 2.14. Flowchart of log file discretization process for MC simulation.

The analysis and comparison of relevant delivery parameters can always be made without further reduction of the data recorded in these log files. However, the data retrieved for MC simulation and dose calculation from log files are dependent on the discretization level required for an optimal approximation to a continuous delivery. The discretization level used for log file simulation and its effect in the developed QA model, presented in the next section was also investigated. The discretization method was designed to take into account the relationship between changes in MUs and gantry motion, for a higher sampling

when more significant changes are present in a specific sector of the arc. In this way, the dose rate is intrinsically considered for the sampling process. Obviously, this process does not lead to equi-spaced CPs along the arc, such as it was considered by others in previous related works.

For our model, the term 'fine log' was used when the delivered parameters for MC simulation were considered with more CPs describing the arc than the ones usually presented in the DICOM-RT plan file from the TPS. This latter, in turn, was identified as 'coarse log', i.e. when the considered discretization level from the log file was equivalent to one of the DICOM-RT plan file. For the coarse discretization level, after excluding CPs where there was no variation in cumulative MU, the actual cumulative value at the end of each control point was retrieved along with the actual leaf positions and the corresponding gantry angle, recorded during that sampling time. In general, the number of simulated CPs will be dependent on the original treatment plan and its complexity. In particular, this number was about three times higher for the fine approach compared to the coarse one, for the plans evaluated in this work.

2.3 QuAArC model

The main goal of this work was directly linked to the purpose of developing a QA model that could be used more effectively for evaluating the accuracy of the associated optimization algorithms, delivery systems, and QA devices.

To complement the VMAT verification by means of the automated MC simulation described so far, an in-house model called QuAArC was developed. This QuAArC model consists on a system composed by a specific phantom, integrated with MC simulation of VMAT log files in a feedback procedure, in order to implement experimental measurements with film to estimate the actual treatment delivery. This system and associated methodology, as well as, validation process with clinical cases are described in the following subsections.

2.3.1 QuAArC phantom

Regarding the volumetric nature of VMAT, a cylindrical shape polymethylmethacrylate (PMMA) phantom (physical density 1.19 g/cm³), consisting of a set of two concentric cylinders, was specifically designed. It was aimed to host radiochromic films rolled at different radial distances from the isocenter, for a 3D and continuous dosimetric verification. The detailed

description with geometrical schemes of the designed phantom prototype is presented in the Appendix I. As it can be seen in Figure 2.15, two different radial distances were selected in the phantom. This dual configuration was adopted to obtain an experimental estimation of entrance fluence, since the outer films are located close to the maximum dose depth in PMMA, while the inner hosting allows a 3D dose distribution consideration, as it will be described later. In order to ensure the films are correctly placed, the cylinders size was thought to be equal to the length of films. Moreover, the phantom has several marked reference lines to know the exact film location during the setup mounting and positioning on the treatment table with the usual laser system (Figure 2.15).

Other components allow a configuration prepared for axial or coronal films and dose point measurements with several types of ion chambers at different locations. Besides the PMMA components, it also includes a set of cork cylinders and inserts to simulate lung or air-like cavities (Figure 2.15). In order to consider the verification of several treatment regions, QuAArC phantom comprises two different setups: one with dimensions of 30 cm diameter and 30 cm length (big setup), and the other with 20 cm diameter and 28 cm length (small setup).
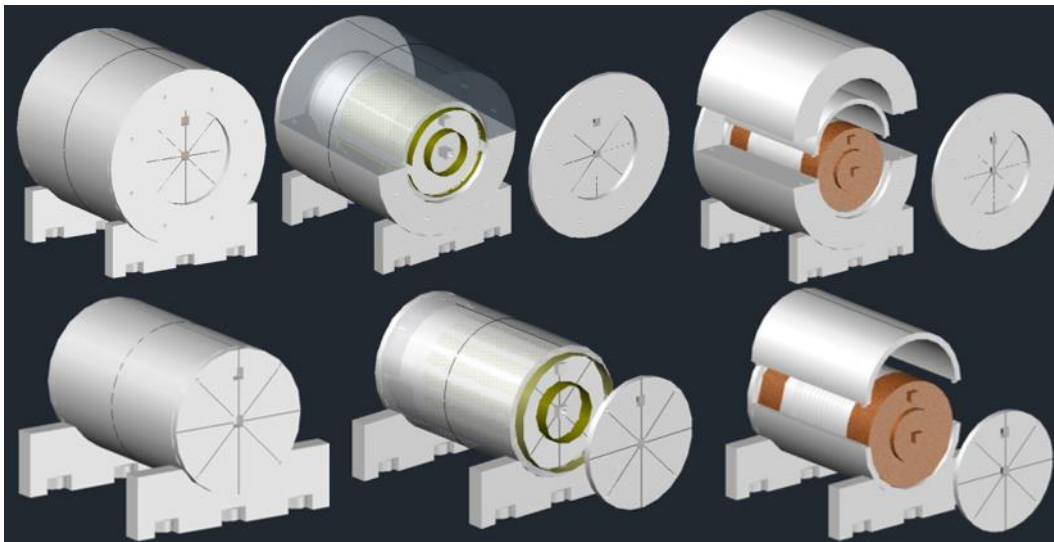

Figure 2.15. Different setups of QuAArC phantom prototype. The big (top) and small (bottom) setups are depicted with radiochromic films rolled at two different radial distances. The small setup at the bottom is an independent interior part of the phantom, also present in the big setup at the top. Two bases with screws were designed for a fine positioning with the laser system.

2.3.2   Data processing in QuAArC

2.3.2.1   Implementation of experimental measurements and film processing

For QuAArC verification of actual plans, Gafchromic EBT3 films with dimensions of 20.3 x 25.4 cm^2 were rolled around the outer cylinder, at 1 cm depth (2 films), and the inner cylinder, at 6 cm depth (1 film) in the phantom, onwards the outer and inner film scrolls, respectively. Absolute dose measurements with a CC04 and a CC13 ion chambers (IBA Dosimetry) placed at the isocenter for each treatment in QuAArC phantom were also performed. Chamber reading conversion to dose was made following the IAEA TRS-398 protocol, and then compared to the corresponding absorbed dose to water calculated by MC in the PMMA QuAArC phantom. This MC dose to water was converted by applying a conversion factor determined through MC calculation of the water-to-PMMA stopping-power ratio, considering the Bragg–Gray cavity theory.

The irradiated films were processed following a specific protocol, which included the characterization procedure of the scanner-film system, in order to minimize the related uncertainties. All films were scanned at least 12h after exposure, using an Epson Expression 10000 XL (Seiko Epson Corp.) flatbed scanner at a resolution of 75 dpi and a depth of 48-bit RGB, without applying any color correction. The films were all scanned in the portrait orientation at the center of the scanner to use its optimum part, which was determined through a characterization process of the device.

Optical density to dose conversion was done through calibration curves for each batch of radiochromic films. The calibration curve for each batch of EBT3 and 6MV photon beams was obtained by irradiating sixteen pieces of 5×6 cm^2 cut from the same film. The pieces were individually irradiated with a 10 x 10 cm^2 beam in reference conditions, with doses ranging from 0 to 400 cGy, for an appropriate characterization of the film response behavior, including more than 12 points as proposed by Bouchard *et al.* (Bouchard *et al.*, 2009). Because of film scrolls normally would receive lower doses than the films used in typical verifications, especially in outer films, it was important to have an exhaustive characterization of dose-response curve in the low-dose range. For each irradiated film, two reference film cuts (4 x 5 cm^2) from the same film, one exposed to a known dose and the other unexposed, were used to adjust the dose–response curve for the conditions applying to that film. For the conversion of the film pixel value into dose, a multichannel method was used (Micke *et al.*, 2011),

and also corrections for the non-uniformity lateral dose dependence response of the scanner were applied to the three channels. Although the same effect in the longitudinal scanner direction was also characterized, corrections were not applied since it was found to be negligible.

For this process, the support and suggestions received by the Radiophysics Department of the Virgen Macarena Hospital of Seville were invaluable.

2.3.2.2 Dose processing and evaluation

In order to process and evaluate the unusual dose distribution in the irradiated film scrolls, specific in-house software was also developed in MATLAB, which incorporates the analysis of dose distributions, profiles, dose difference maps, and 2D/3D gamma index. The cylindrical distribution of the films in the 3D dose cubic voxelized matrix ($1.25 \times 1.25 \times 1$ mm³) demands a specific recruitment process based on interpolations each 0.5° between voxel values taken from the nearest neighbors in the three axes.

In order to take into account the disagreement between different coordinate systems, one planar MC matrix was reconstructed for each, inner and outer scrolls, from 5 planar matrices generated by shifting the isocenter to ± 1 pixel (Figure 2.16). In this way, it was assumed that the uncertainty location between MC scroll and film scroll was ± 1.25 mm, for the considered grid. During the comparative analysis between both dose distributions, an efficient non-deformable mutual information method was implemented in our software to account for small shifts or rotations that could take place during the film processing.
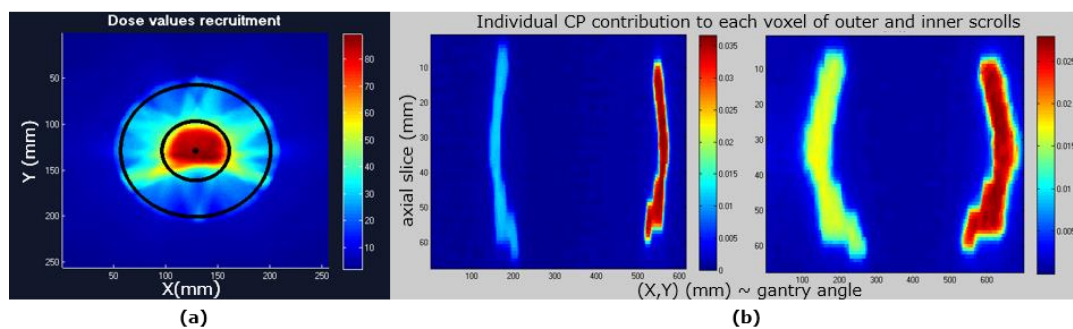

Figure 2.16. Location of the dose recruitment in QuAArC to obtain the MC dose scrolls (circle balck lines) and absolute dose (central black dot) (a). Individual CP contribution to each voxel in both scroll regions (outer in the middle and inner at the right), from each CP dose recruitment to be used for reconstruction purposes (b).

2.3.3 3D dose reconstruction

Different approaches were followed in order to reconstruct the 3D dose from the experimental measurements in QuAArC.

A method was first developed to obtain a fluence estimation for each of the simulated CPs, from the identification of entrance radiation contribution in the outer film scrolls. This would then be applied to correct the MC simulated fluence according to the parameters of log file to match the measurement, by establishing a relationship between this fluence approximation and actual fluence. As these measurements record all accumulated entrance, lateral, and exit CP dose contributions from the opposite CPs, the direct contribution of each CP was first extracted from the correspondent MC simulation. Although it is not possible to separate dose components resulting from primary or secondary particles in the measurements, MC simulated CPs from log file could be used in order to separate the direct contribution recorded in the outer film scroll from QuAArC irradiation. The procedure used for this approach is illustrated in Figure 2.17, showing a single CP direct dose contributions identified in the outer film scroll, after excluding other contribution, using the information of the whole outer MC scroll and the MC dose for a single CP. However, it can be seen that using this approach, a heterogeneous result was obtained for the CP evaluated in the film measurement (Figure. 2.17 – bottom of the right panel). This result was expected and it is common to other commercial verification systems, as a result of manage discretely a continuous phenomenon. In our case, this effect is even more evident due to the high resolution provided by the film, what is here showing as an important reason to use this detection system instead of other. Unlike other verification systems, our model provides an excellent scenario to achieve a better consideration of the continuous nature of the VMAT application. Besides having the precise calculation provided by MC, the isolated contribution of each CP in combination with the high spatial resolution measurement of experimental film allowed us to develop a novel model for VMAT verification, as it will be explained below.
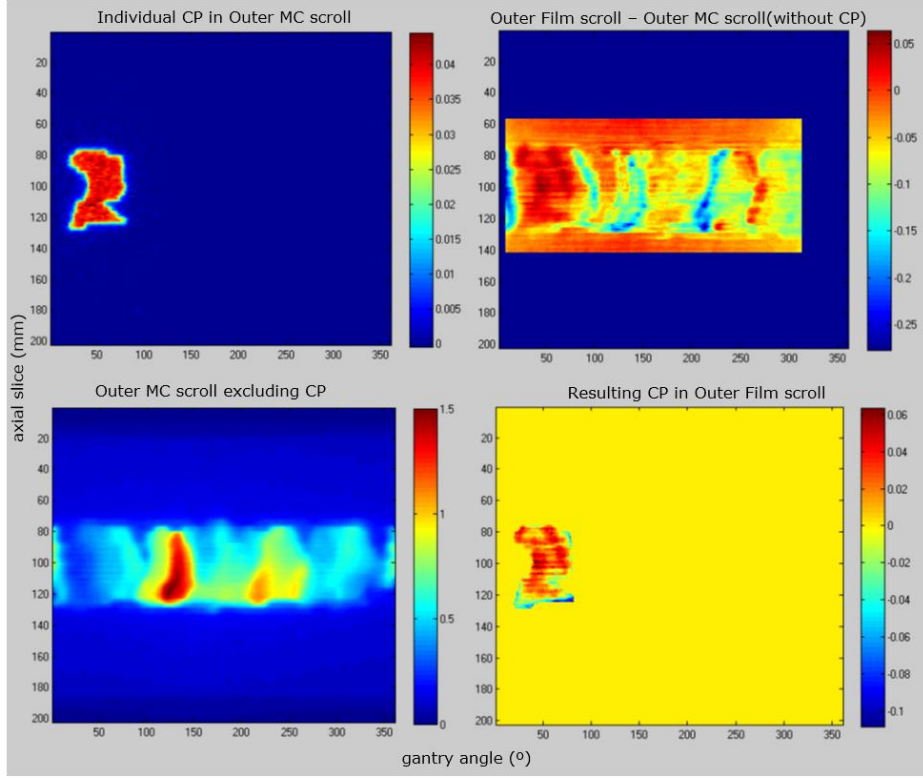
Figure 2.17. Procedure used to isolate individual CP entrance dose contribution in the outer film scroll (bottom-right). The individual CP dose contribution in the outer MC scroll (top-left) is subtracted to the total outer MC scroll (bottom-left), and the resulting difference with the outer film scroll (upper-left).

A different approach was therefore considered in our proposed model for the final 3D dose reconstruction. The measurements were implemented in a feedback process in order to experimentally adjust the MUs from the MC log simulation and to finally obtain an experimental reconstructed DVH in the patient anatomy. To this end, a least-squares optimization method following the expression (2.2) was implemented in our software, taking into account the measurements obtained with the rolled films and the absolute point dose in the phantom.

$$\min_{x} \frac{1}{2} \| C \cdot x - d \|_2^2 \ such \ that \begin{cases} A \cdot x \leq b \\ Aeq \cdot x = beq \\ lb \leq x \leq ub \end{cases} \tag{2.2}$$

C is the MC dose matrix containing the individual CP contribution to each voxel; x is a MU weight vector, considered as a percentage of MU change from either the initial solution calculated from the log file or the final proposed

solution; d is the matrix composed by the films dose matrices and the isocenter absolute dose measured with ion chamber; A and b are the linear inequality constraint to establish the tolerance of dose difference between MC dose and measurements (considering both, positive and negative differences); Aeq and beq are the linear equality constraints, specified as a vector and a scalar, respectively, which represent the original MU weight vector from log file, and the total treatment MU; lb and ub represent the lower and upper bounds for the solution x, allowing the control of the variation level on the MU values from log file to match the experimental value. In this process, the global contribution of each individual CP to the whole treatment is assessed and adjusted according to the measurements. The rolled films provide us measurements of fluence estimation (outer film scroll) and relative dose contribution (inner film scroll) of the direct entrance, lateral overlapping, and the opposite irradiation for the whole arc. The contribution of opposite irradiation present in these film scrolls, it is not a handicap because it is considered in a global manner along the optimization process. It is important to note that the values lb and ub are considered as a percentage of the original MU corresponding to each CP in the log file. In this way, it is possible to accept only relative small variations for each new MU during the iterations in the optimization process. The latter in addition to a minimum tolerance of dose difference, makes possible to obtain experimental values as a result of an average of the heterogeneity within the irradiated area in the film corresponding just to one CP. In this way, the adjustment is mainly performed by using the contribution from lateral overlapping, what is directly related to the discretization effect applied to a dynamic delivery. The latter can be observed in Figures 2.18 and 2.19, where the variations in MU for each CP obtained with our model are evaluated for an IMRT case and for a VMAT case. For the static IMRT plan (Figure 2.18), the variations in MUs are not significant, showing again, the high agreement between our MC simulations and measurements in film. Conversely, for the dynamic case, Figure 2.19, the variations in MUs are relatively more relevant for each CP, as it was expected. Also, in spite of considering the whole comparison between experimental matrices and MC matrices in the same process can be observed that the MU changes don't modify substantially the original MU distribution along the arc. Otherwise, the model would be providing a different solution, but not one experimentally reconstructed, such as it is the aim.

This approach makes possible the study of the effect of considering several discretization levels from the log file simulation, since deviations measurement

caused by a mismatching detection location can be overcome thanks to the high density detection inherent to film dosimetry.
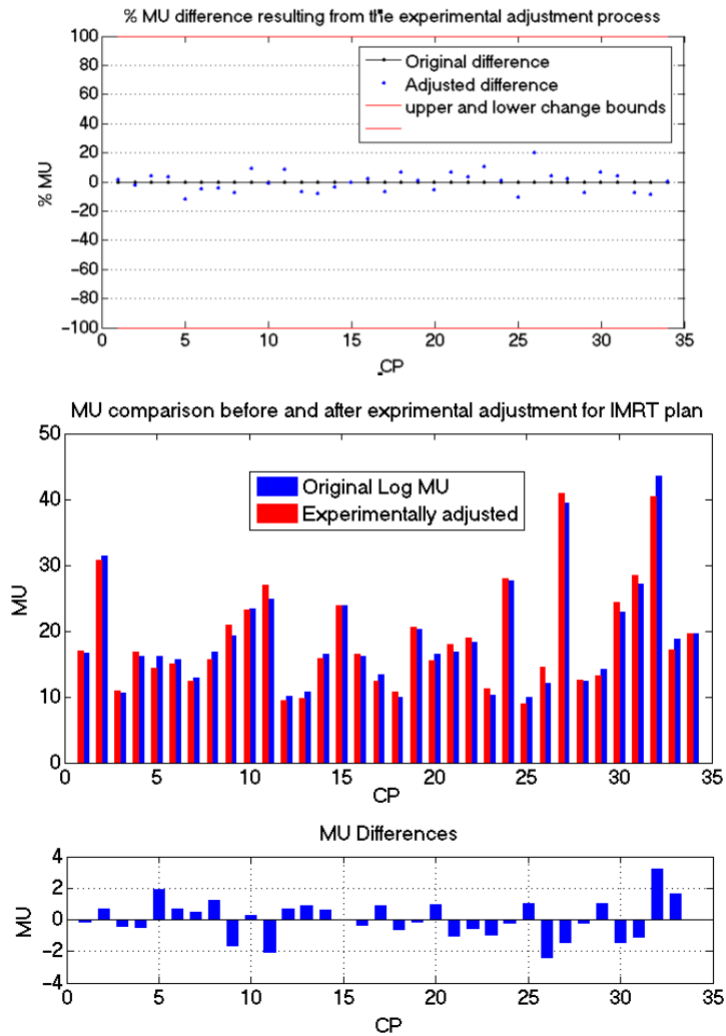

Figure 2.18. Evaluation of MU adjustment during the optimization process for an IMRT plan, showing very small changes from the original MUs, as expected. The scatter plot at the top represents the percentage of the resulting change (blue) with maximum allowed changes in MUs imposed by the upper and lower established limits. MU comparison and absolute difference are shown on the middle and bottom histograms, respectively.
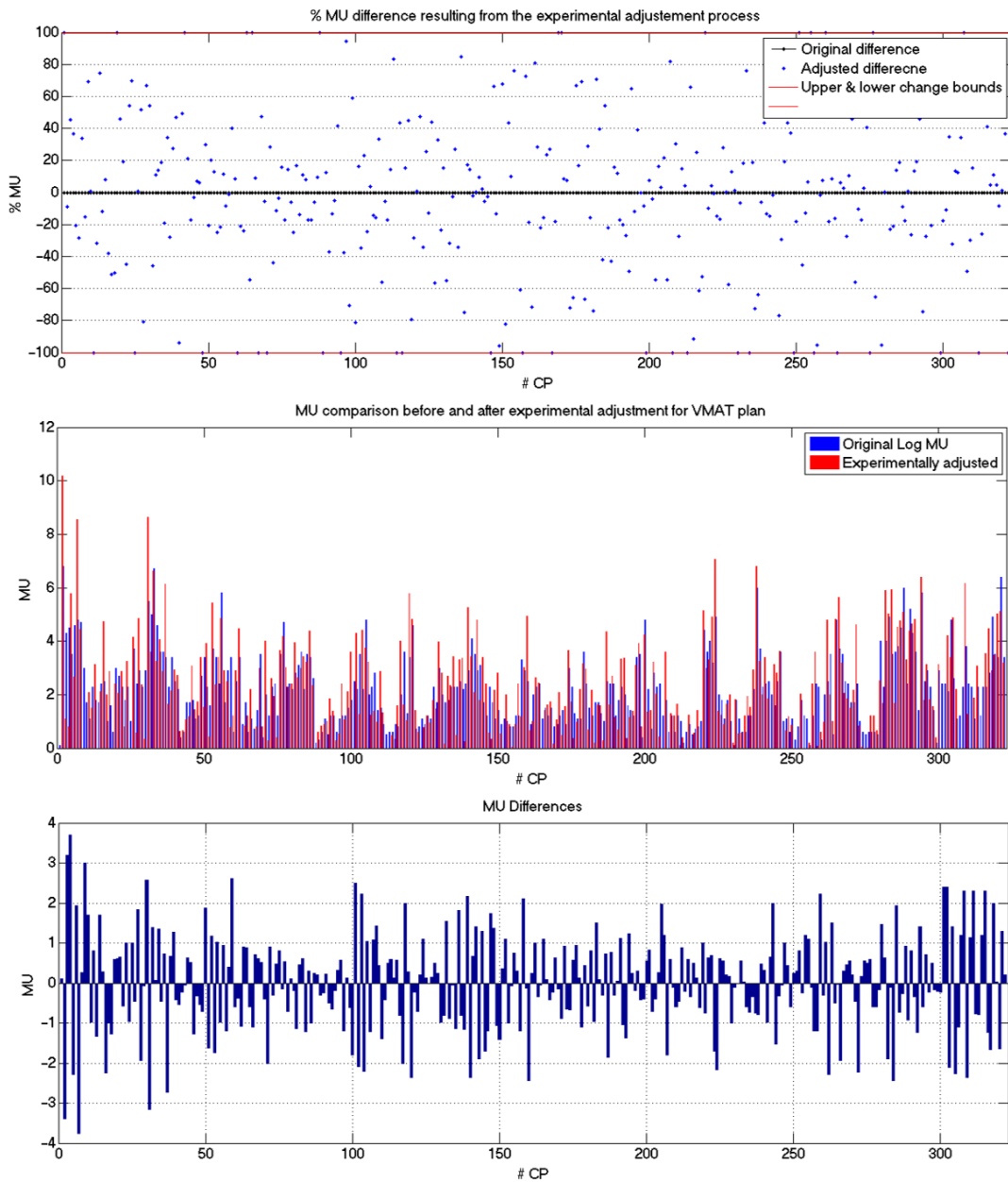
Figure 2.19. Evaluation of MU adjustment during the optimization process for a VMAT plan. The scatter plot at the top represents the percentage of the resulting change (blue) with maximum allowed changes in MUs imposed by the upper and lower established limits. MU comparison and absolute difference are shown on the middle and bottom histograms, respectively.

On the other hand, the control of parameters in this feedback process would also allow obtaining a new proposal of a treatment plan with larger variations in MU values, but still in accordance to the experimental measurements, able to provide a final DVH on patient CT clinically acceptable. Although this last operative option of our method was considered, it was not evaluated for this work.

Finally, before describing the clinical application evaluated in this work, a general flowchart describing the proposed model is presented in Figure 2.20.
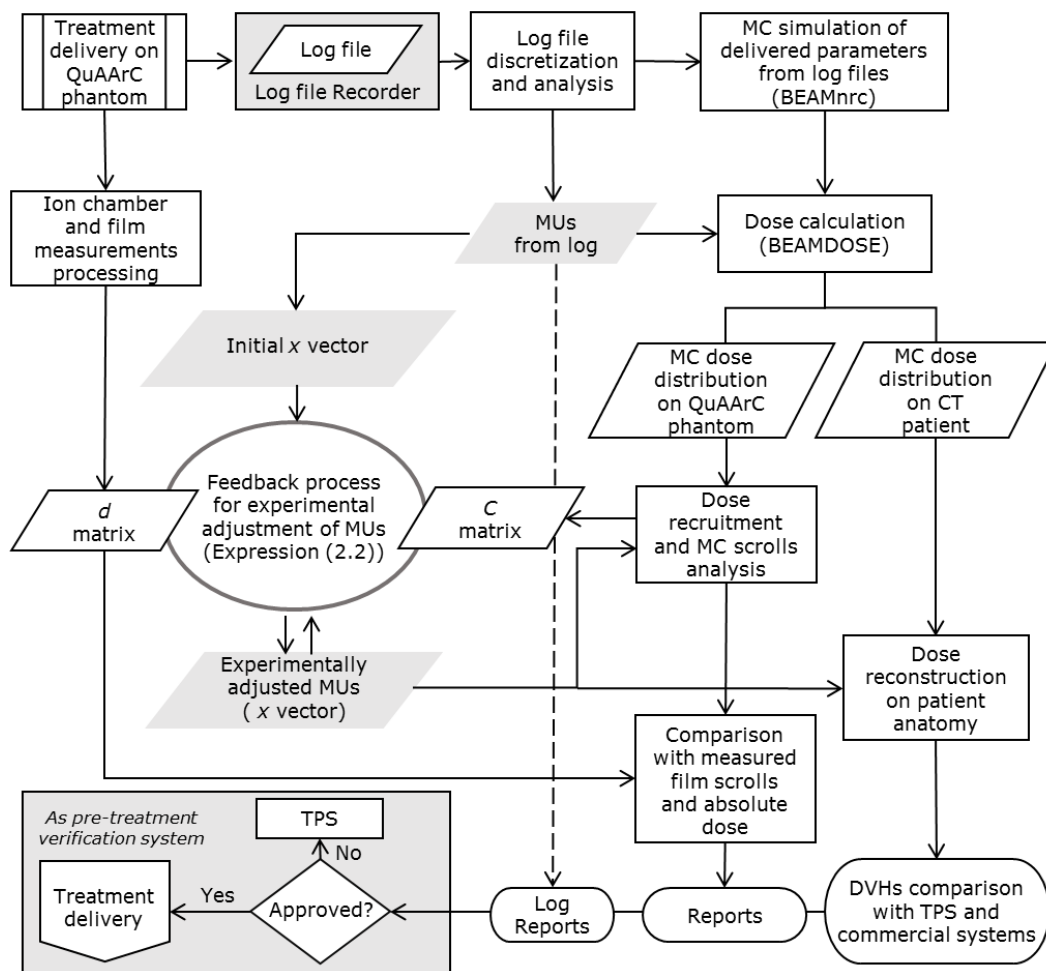
Figure 2.20. General workflow followed in the proposed model.

2.4 QuAArC model validation with clinical cases

The proposed model was tested by applying it to several clinical cases, from both collaborating hospitals, HUVR and HIL, solved with different TPSs, involving distinct VMAT algorithms and verified with different commercial systems, in each center.

From HUVR, two clinical cases corresponding to prostate and H&N VMAT treatments were additionally verified with QuAArC. Both treatments were previously planned with Pinnacle TPS and verified with COMPASS system. These VMAT plans consisted of a single arc with 90 equi-spaced CPs treated with a hypofractionation scheme (3Gy/fx), for the prostate case, while for the H&N case consisted of a double arc with a total of 180 equi-sapced CPs. Furthermore, both plans have met the acceptance criterion, which was based on the DVHs comparison between TPS and COMPASS solutions, through relevant dose metrics.

QuAArC solutions were then compared to the planned TPS solution on the patient CT data, as well as the corresponding QA system solution.

From HIL, also prostate and H&N treatments were selected. For these cases, four treatment plans in total were evaluated, two solutions for each one: one which was accepted by the commercial verification system and the other which not. For the real clinical application, these cases were planned with Monaco commercial TPS and verified with ScandiDos Delta4 system. For both cases, during the verification procedure with Delta4, the first treatment plan (plan A), did not meet the acceptance criteria, which consisted on more than 95% of the evaluated points with a global gamma index < 1, for 2.5% dose difference (DD) and 2mm distance to agreement (DTA) criterion and a dose threshold of 20%, in the Delta4 detector planes. A second treatment plan (plan B) was proposed for both cases, in order to find solutions that meet these acceptance criteria when verified with Delta4. In particular, the plan A for both cases, prostate and H&N, failed with a passing rate of 91.8% and 76.9%, respectively, while the plan B passed with 95.6% and 99.6%, respectively.

The prostate case was selected for this study due to the high similarity between the DVHs presented by Monaco TPS solutions for both plans, A and B, which consisted of a single arc VMAT treatment composed by 87 and 78 CPs, respectively. On the other hand, the H&N case consisted of a boost phase treatment. In this case, a single arc VMAT plan with 93 CPs was the plan A, and the second plan proposed (plan B) was a static IMRT technique, which did pass the Delta4 QA and was accepted for treatment. This IMRT plan, consisting

of 34 segments distributed in 9 incidence angles (ranging from 205º to 180º CW), and it was specifically considered as a static example to check the correct implementation of our software, since potential discrepancies between MC and the film scrolls generated by the discretization process would not be present in this scenario.

The QA results in Delta4, from these two cases were then rescued, in order to calculate the corresponding DVHs, by means of the Delta4 anatomy option, later implemented for that purpose. The solutions were then compared to QuAArC solutions.

Results and Discussion

In this chapter, some relevant results obtained from the work carried out to accomplish the objectives established within this thesis are presented and discussed.

3.1 Monte Carlo linac head model and beam characterization

Monte Carlo dose calculations of the different field sizes were compared with the experimental measured data in order to characterize the 6 MV photon beam used for the MC verification of VMAT treatments.

These results were achieved with a statistical uncertainty lower than 1%, and an agreement within 2% was obtained between experimental measurements and MC calculations.

Furthermore, some experimental measurements with radiochromic film are presented, which were included to validate the Monte Carlo simulation of the detailed Synergy linac head geometry, including its MLC. Also, some results regarding adjustments of the Axesse linac model, made by means of additional measurements of specific segments are presented.

3.1.1 Central axis depth-dose curves and off-axis ratios

Despite a description of beam parameters (energy spectrum and radial distribution) was provided by the manufacturer, the fine characteristics of the electron beam could only be determined by means of a deep comparison with empirical measurements. This comparison was done for the multiple values in the table 2.1 presented in Materials and Methods chapter, which corresponded to a set of interdependent parameters, describing the electron source from the waveguide. Considering those values, the incident electron beam on the target

found for the best fit had an energy distribution, which was assumed to be Gaussian with a mean energy of 6.0 MeV and a FWHM of 0.5 MeV. The electron beam radial intensity distribution was also taken as a Gaussian with a FWHM of 1.5 mm for the nominal 6 MV photon beam.

The tilt of the whole MLC bank was also considered during this characterization process, using a value of 0.0013 radians. Since profiles analyzed during the beam calibration process, using standard fields, were found to be insensitive to small tilt changes, it was decided to adjust this parameter later by means of experimental measurements with film. The backup jaws present in this linac model are also used to minimize the MLC transmission, thus this tilt effect was not so evident in this first stage. Figure 3.1 shows the agreement achieved between PDDs calculated with MC and the corresponding experimental measurements provided by the HUVR for several field sizes.
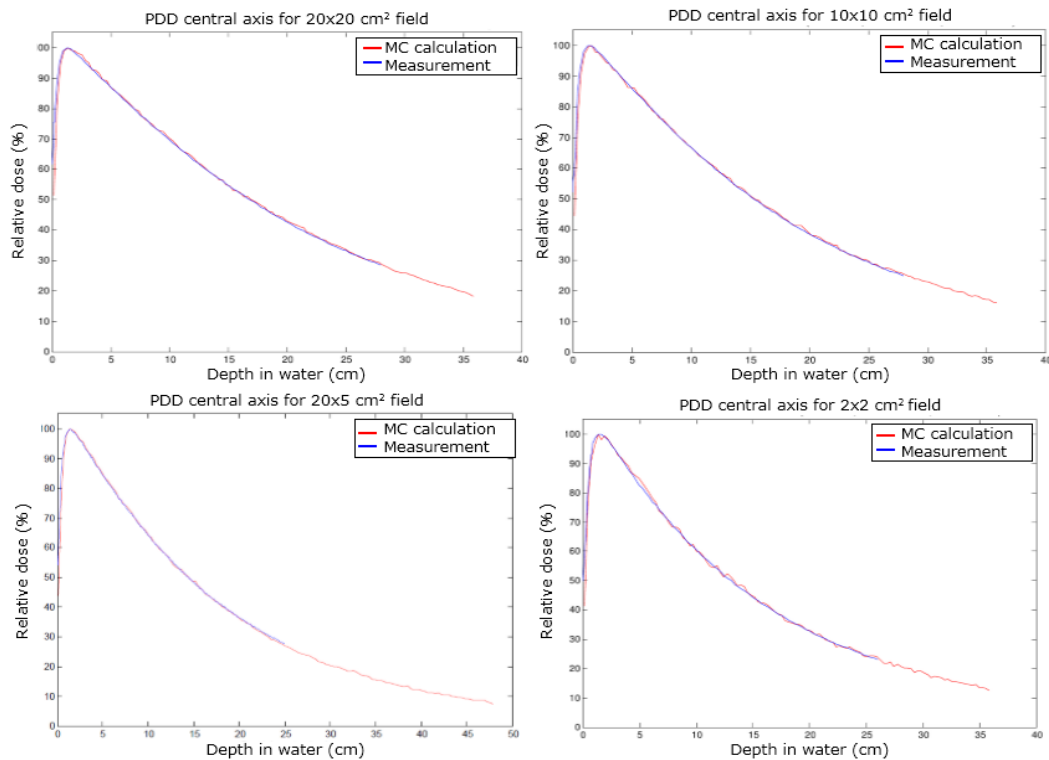
Figure 3.1. Measured (blue) and MC calculated (red) PDD curves in water for 20x20, 10x10, 20x5 and 2x2 cm² field sizes at 90 cm SSD, normalized to dose maximum.

Although the parameters described above showed high agreement with the measured depth–dose profiles, additional comparison was made using the same parameters to check the experimental lateral dose profiles for standard field sizes at different depths. Figures 3.2-3.7 show MC-calculated dose profiles and measurements in both, crossplane and inplane directions, in order to check the correct simulation of both jaws and MLC. The large number of histories simulated to obtain the phase-space files, which have been considered as input for dose calculations, ensured the statistical uncertainty below 2% in the regions under the open field region. Nevertheless, this uncertainty was less than 1%, considering the implemented PSD recycling for dose calculation. For better visualization of these results, the error bars were not represented in the corresponding figures.
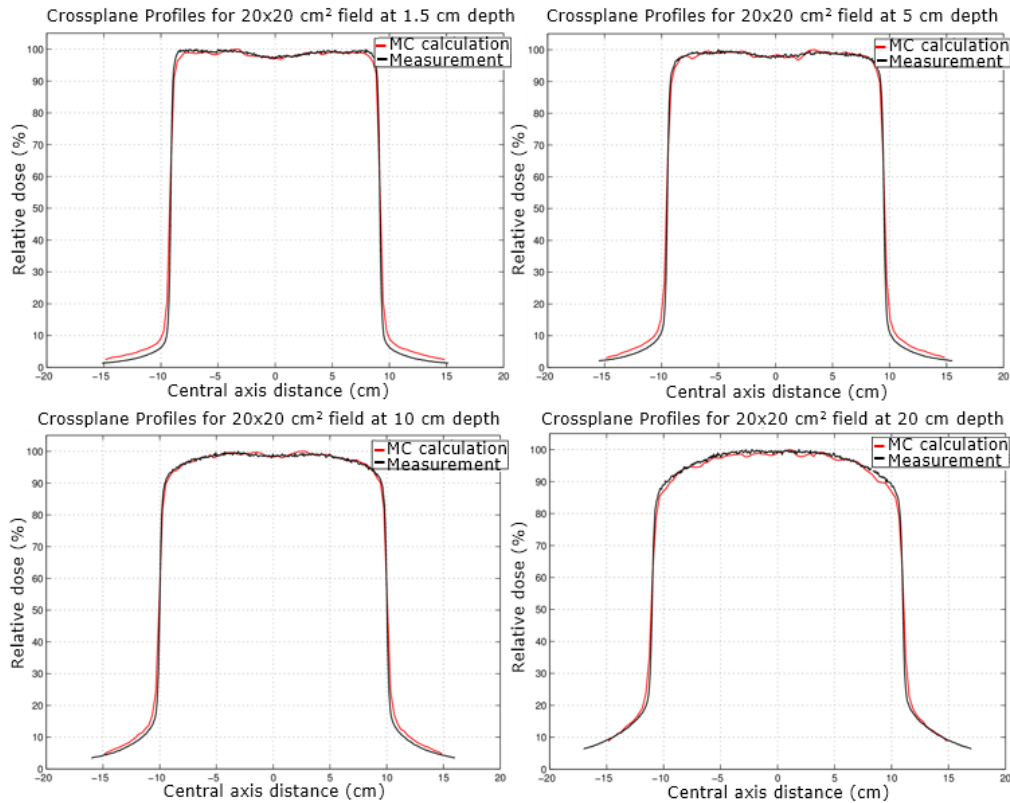
Figure 3.2. Measured (black) and MC calculated (red) crossplane dose profiles in water for 20x20 cm² field at 90 cm SSD, and 1.5, 5, 10 and 20 cm depth.
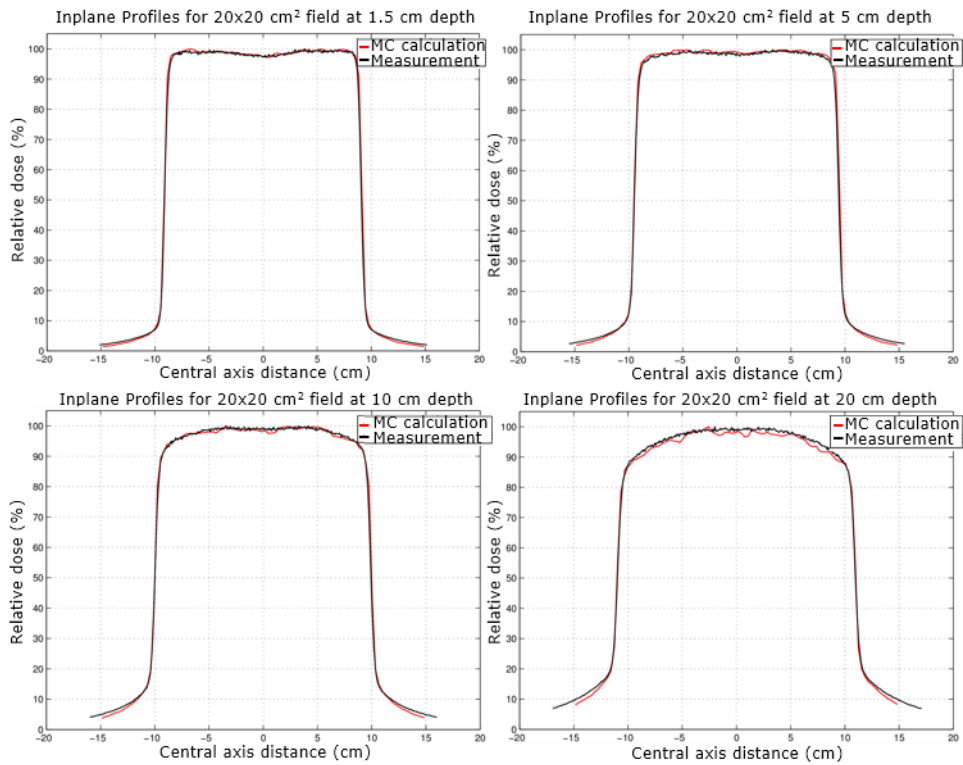
Figure 3.3. Measured (black) and MC calculated (red) inplane dose profiles in water for 20x20 cm² field at 90 cm SSD, and 1.5, 5, 10 and 20 cm depth.
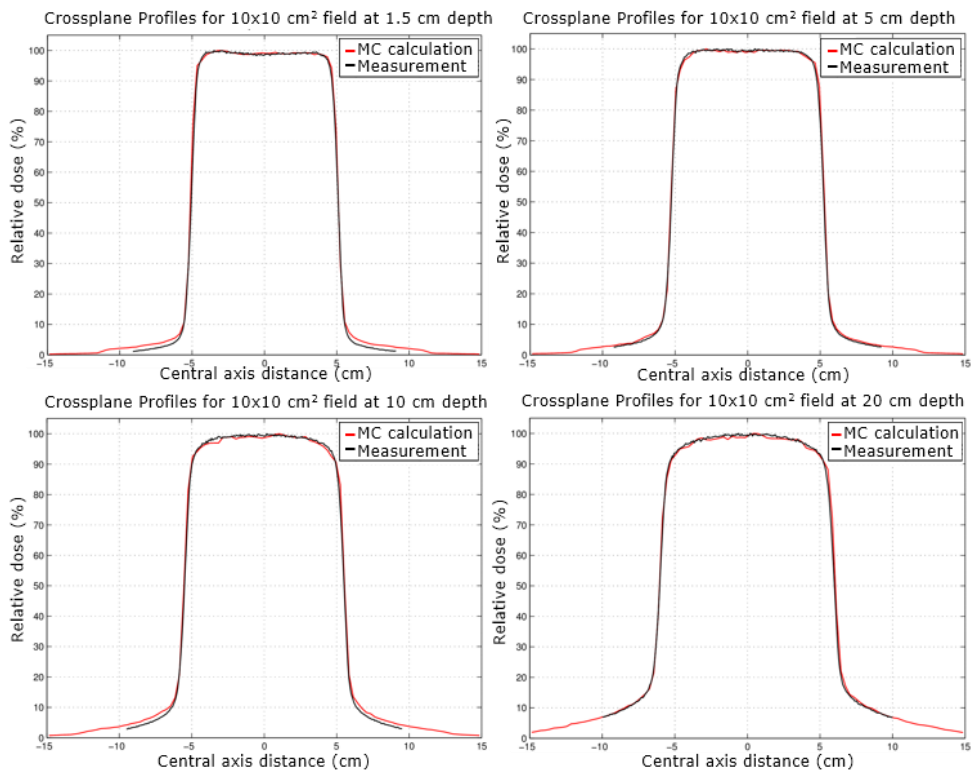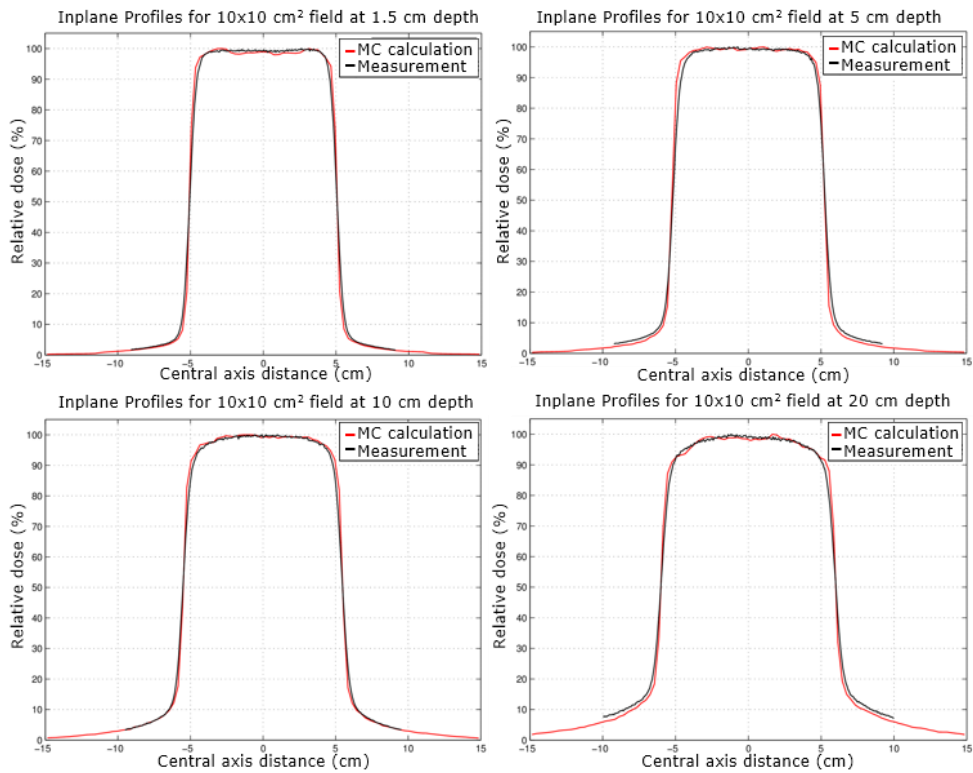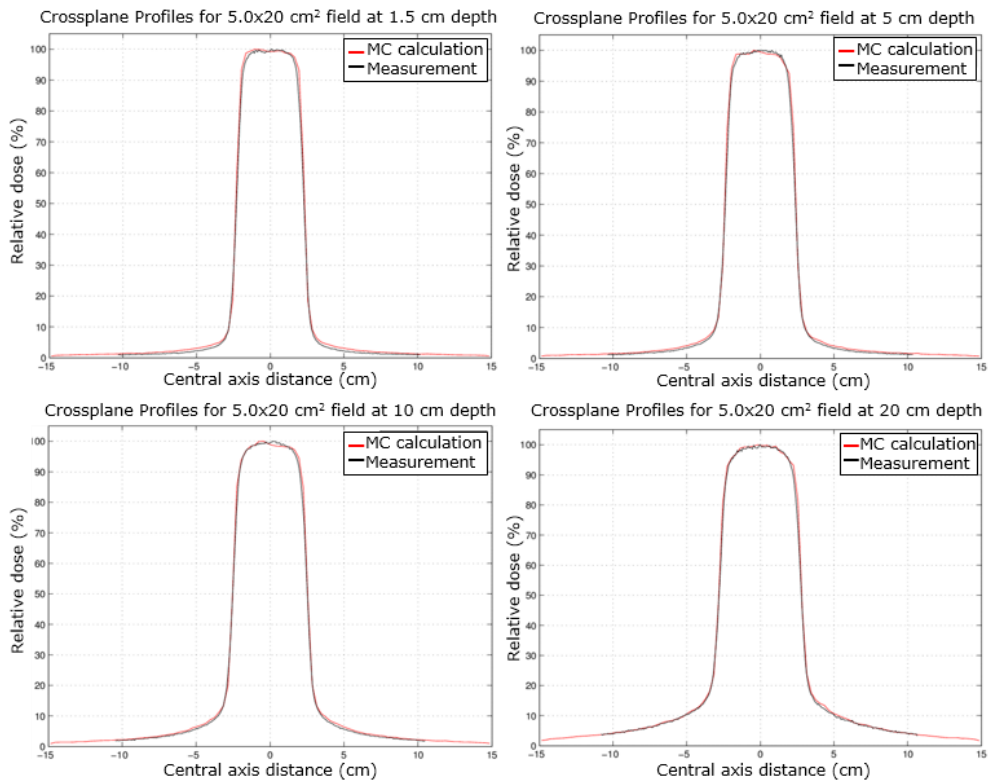

Figure 3.4. Measured (black) and MC calculated (red) crossplane dose profiles in water for 10x10 cm² field at 90 cm SSD, and 1.5, 5, 10 and 20 cm depth.
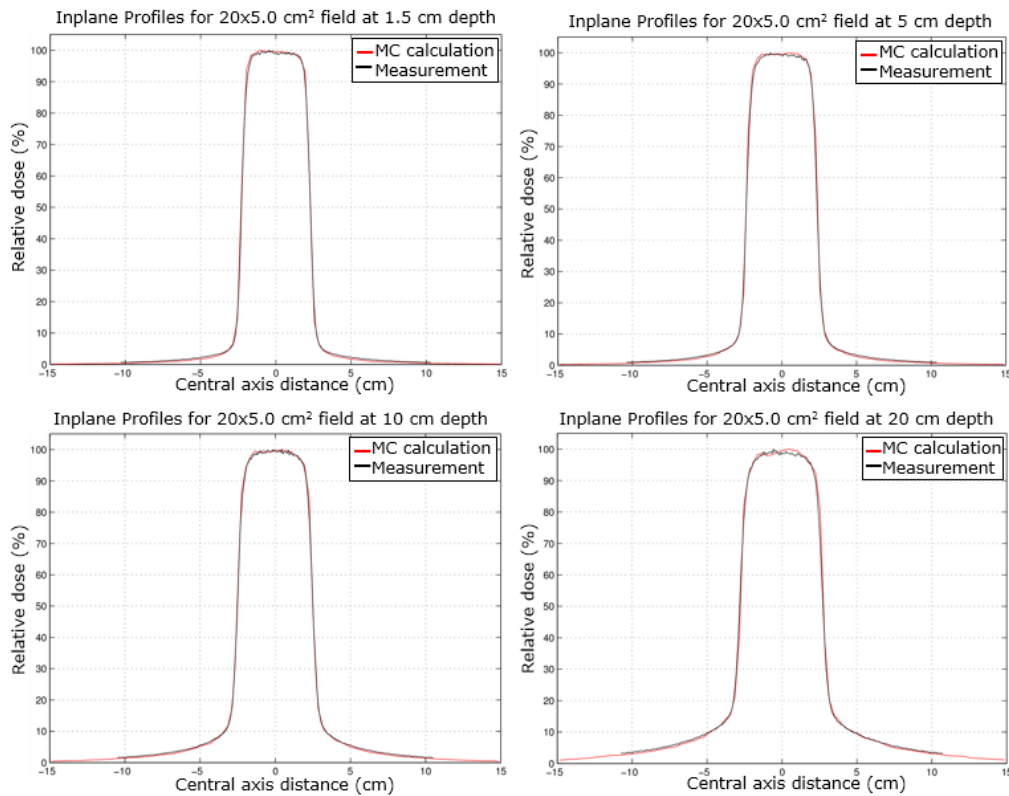
Figure 3.5. Measured (black) and MC calculated (red) inplane dose profiles in water for 10x10 cm² field at 90 cm SSD, and 1.5, 5, 10 and 20 cm depth.

Figure 3.6. Measured (black) and MC calculated (red) crossplane dose profiles in water for 5.0x20 cm² field at 90 cm SSD, and 1.5, 5, 10 and 20 cm depth.

73

Figure 3.7. Measured (black) and MC calculated (red) inplane dose profiles in water for 20x5.0 cm² field at 90 cm SSD, and 1.5, 5, 10 and 20 cm depth.

The agreement between the simulated and experimentally measured profiles was high, although not so much in the tails outside the open field. In these regions, MC statistical uncertainty was slightly higher and the experimental results were less reliable. The dosimetry systems employed present some limitations in these regions, due to their relative size and even energy dependence, in the case of diode. In any case, this lower agreement outside the field is consistent with the literature. Moreover, this validation was checked for small fields with additional film measurements, as it will be shown later.

3.1.1 Validation of MC model with experimental measurements

Smaller field sizes, as the 2x2 cm² or less, were also evaluated, but were not considered for initial MC calibration purpose, since the conventional dosimeters employed in their measurements could compromise this calibration. The detection resolution for small fields required the use of radiochromic film. Usually, the physical dosimetry routinely considered as input data for analytic

algorithms implemented in commercial TPS, does not fulfil this requirement, so once the beam characterization was achieved, the evaluation of single small segments taken from whole real treatment was considered.

Some of the experimental measurements with radiochromic film carried out to validate the implemented MLC models, are presented in the following figures. Figure 3.8 shows the comparison between MC calculated dose distribution for an E geometry made with 3 open leaves and film measurement, in a solid water slab phantom. This pattern allowed the verification of dosimetric characteristics regarding inter and intra leaf transmission, tilt, and gap modelling of the MLCi2, implemented in the MC Synergy model. From the corresponding gamma analysis and the dose profile, also presented in Figure 3.8, it is possible to see that the 'peaks' and 'valleys', created by this E geometry, were very similar in both distributions and matched accordingly to what was expected, in the case that the correct tilt was being applied.
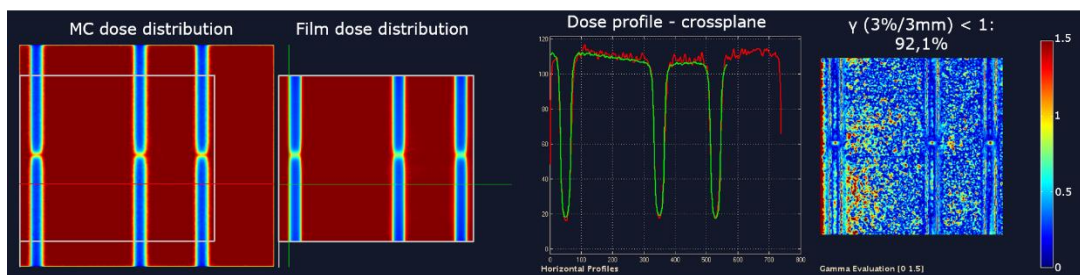

Figure 3.8. MC and film dose distributions, crossplane profile, and gamma analysis corresponding to an E shaped field made with MLCi2 of Synergy linac model. Dose distributions are normalized to maximum dose.

Figure 3.9 shows the comparison between measurement and MC calculated dose distributions for a specific segment, selected from a H&N IMRT treatment solved with MCTP-CARMEN for the Axesse linac model. From the different tilt values evaluated, the result corresponding to the final adjusted tilt is presented here.
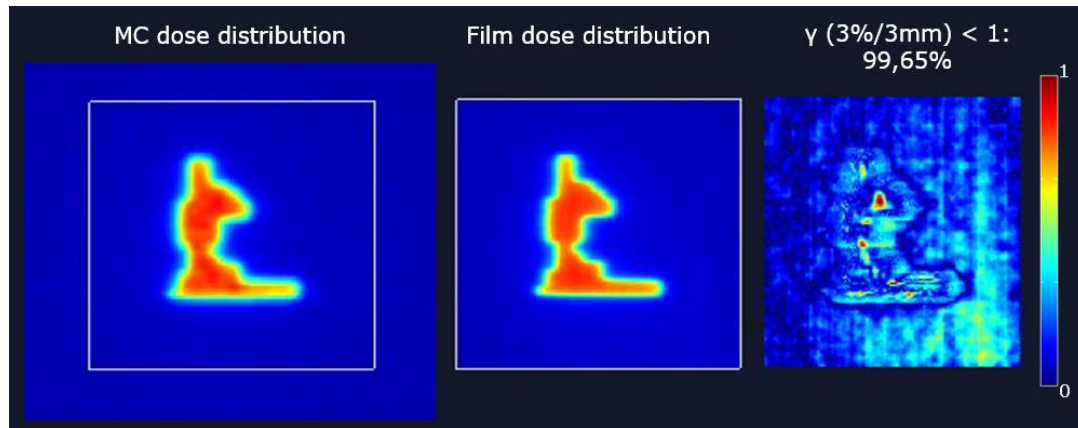
Figure 3.9. MC and film dose distributions (normalized to prescription dose), and gamma analysis corresponding to an IMRT segment created by Beam Modulator MLC of Axesse linac model.

3.2   Monte Carlo verification of VMAT TPS calculation

VMAT treatment verification by means of the automatic MC simulation of the parameters in the RTP file corresponding to TPS solutions was carried out for selected cases from HURV and HIL.

A prostate bed VMAT treatment from HUVR, planned in Pinnacle with two arcs equi-spaced in 4º, is presented in Figure 3.10.

DVHs obtained from the MC verification were compared to the TPS and COMPASS solutions, where some differences in planning target volume and organs at risk (PTV and OARs, respectively) were observed. The different heterogeneities consideration by both algorithms could be relevant in this case, and the consideration of the explicit transport by MC for the complex geometries could be contributing to the differences at OARs. Therefore, COMPASS and TPS present similar behavior at OARs. Although the measurement considered by COMPASS could be approximating better the actual dose delivered to the patient, this system still includes similar algorithm approximations as the TPS, which would explain these similar results for both solutions. In other words, the COMPASS system checks the experimental fluence, but not checks the accuracy of the calculation, which analytical procedure is called into question especially for structures subject to different density heterogeneities, such as rectum with air cavities, or bladder, compromised by the beams crossing the femoral heads. In this regard, it is important to remark that for the lesion, where this issue do not play an important role, the three solutions showed high agreement.
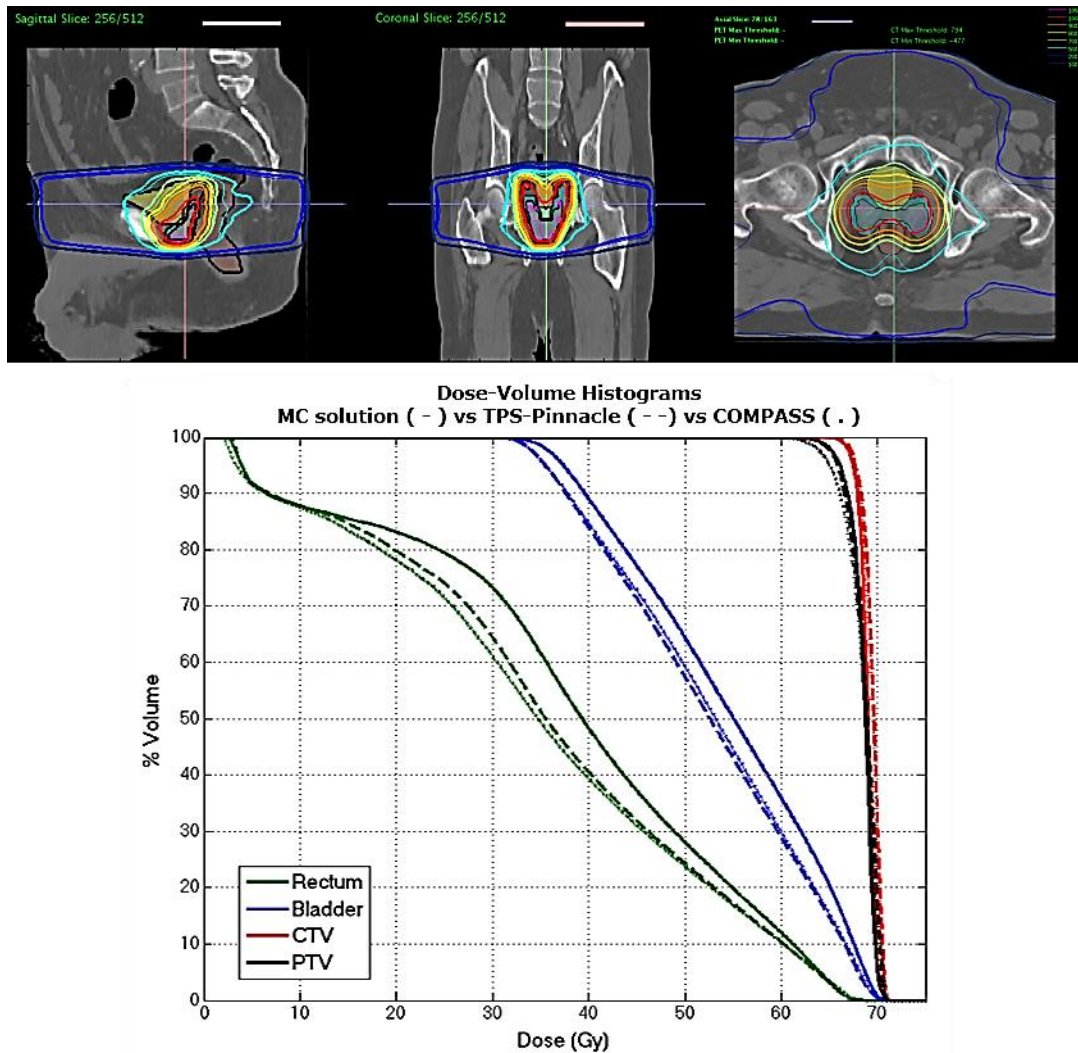
Figure 3.10. MC verification of prostate bed VMAT case. Isodose lines comparison (top) between MC (thick line) and TPS (thin line) in representative planes (sagittal, coronal and axial views), and DVHs comparison (bottom) between MC, TPS and COMPASS solutions.

The same comparison of the three solutions for other two cases is presented in Figures 3.11 and 3.12, where similar differences were found for the OARs. Although, also important discrepancies were found in the PTVs. Dose distributions and DVHs results for a H&N case corresponding to a Hodgkin lymphoma are shown in Figure 3.11 and a lung case treated with SBRT in Figure 3.12. The H&N case corresponds to a two arc VMAT treatment plan (equi-spaced in 4º), while the SBRT lung treatment was planned with 4 partial arcs equi-spaced in 2º, resulting in 101 CPs each.
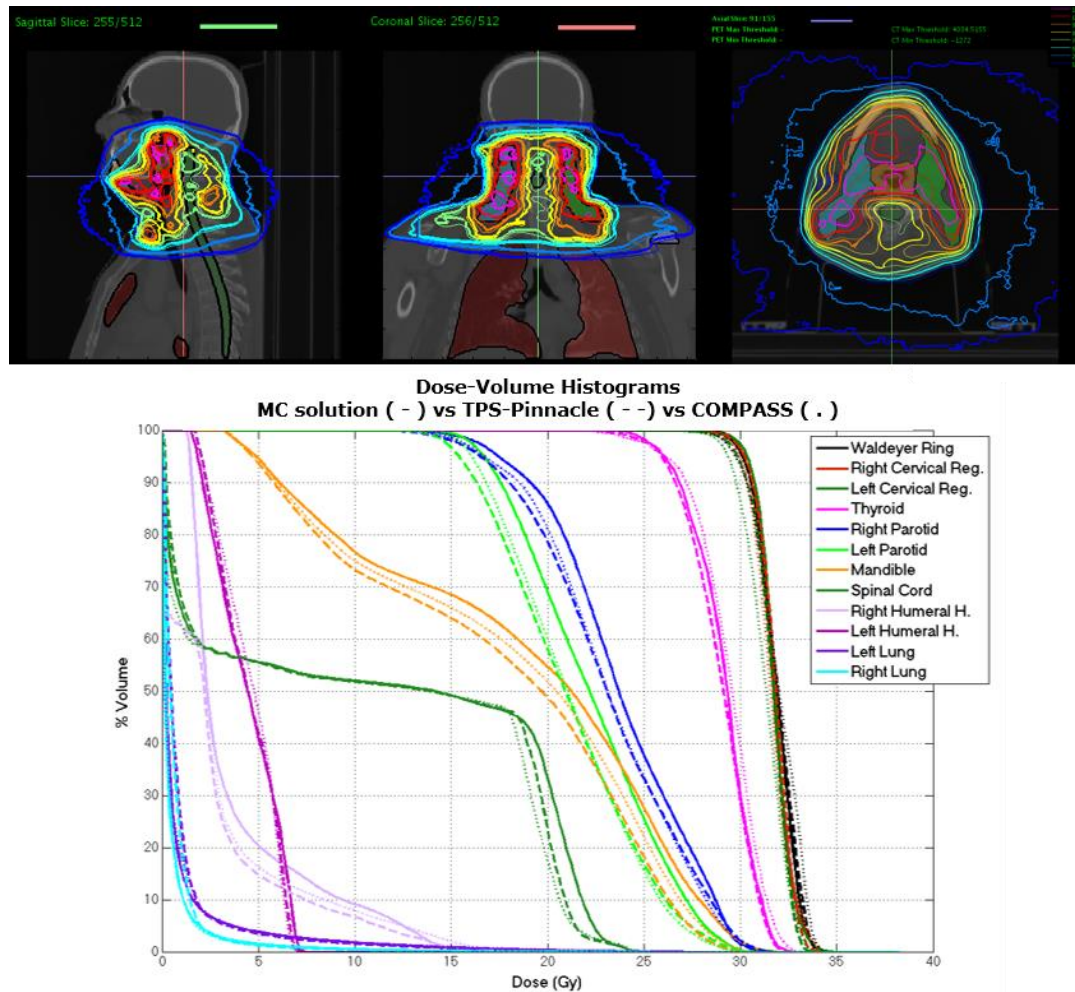
Figure 3.11. MC verification of a VMAT H&N case. Isodose lines comparison (top) between MC (thick line) and TPS (thin line) in representative planes (sagittal, coronal and axial views), and DVHs comparison between MC, TPS and COMPASS solutions.

Unlike the previous prostate case, and as mentioned above the targets of the H&N case in Figure 3.11 showed some differences between MC verification and TPS and COMPASS solution. This could be explained by the usual presence of greater density heterogeneities in these treatment locations.

In the lung case (Figure 3.12), planned to be delivered with SBRT technique, more relevant differences were found between the DVHs corresponding to the PTV, and internal target volume (ITV). This was expected because the lesion is completely surrounded by healthy lung tissue, and the consideration of the electronic density by the analytic algorithm (the same can be applied to TPS and COMPASS) is less reliable in this scenario than in homogeneous regions like

prostate. These specific results confirmed previous works, strongly justifying the need to implement fMC in the QA protocol for cases as lung with SBRT (Ojala *et al.*, 2014).
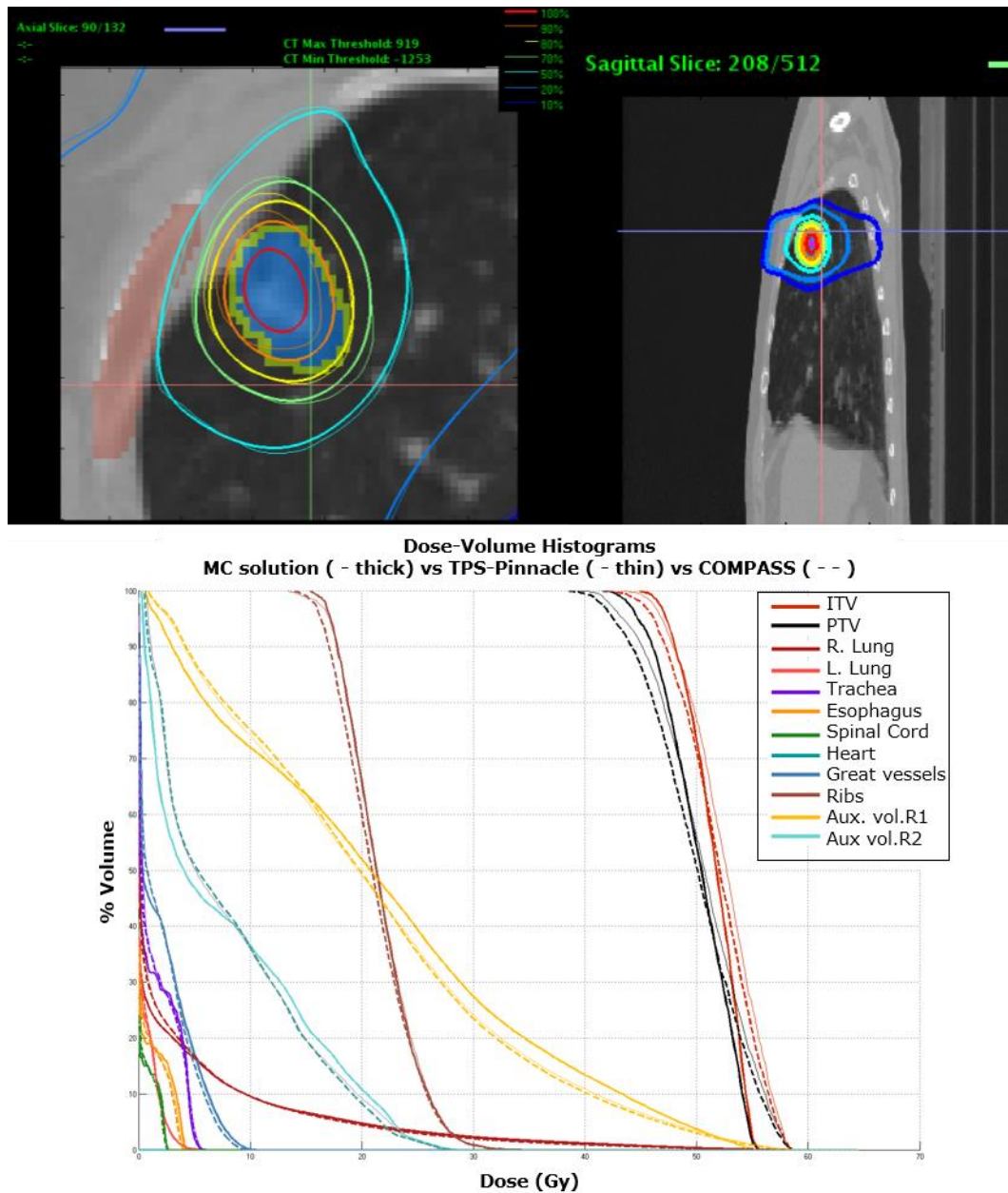

Figure 3.12. MC verification of a VMAT lung case. Isodose lines comparison (top) between MC (thin line) and TPS (thick line) in representative planes (axial and sagittal, views), and DVHs comparison between MC, TPS and COMPASS solutions

In general, MC verification (considering the RTP file) of TPS solutions showed a tendency to an increased dose in organs at risk (Figure 3.10-12), regarding the TPS and COMPASS solutions. These observed differences, as commented before, seem to be mainly linked to the different algorithm used for dose calculation and the potential discrepancies between the planned solution and the actually delivered by the linac.

Similar results were found for MC verification of cases given by HIL with Monaco TPS solutions and Delta4 pre-treatment verifications. These results were not included here to not overextend this document. Nevertheless, specific considerations related to Monaco and Delta4 will be discussed later, with other results.

It would be risky to say that the conventional verification systems are wrong when they do not agree with MC. For similar reasons, it would not be correct to say that our MC model is valid when it is in agreement with the TPS solution, as it was erroneously assumed by others (Asuni *et al.*, 2013). In fact, considering the results from Figures 3.10-3.12, the similarity between TPS and COMPASS solutions would lead us to suspect that our MC verification model was not properly developed. Besides, if we would only be confident on our MC model when it coincides with TPS, what would be the reason for using MC for VMAT verification?

It seems clear that this kind of evaluation, based on MC verification, which was stated as efficient for VMAT in previous works, is not suitable to establish the reasons of the differences found between the planning and the measurements from commercial verification systems for VMAT, and what is more relevant, it is not possible to accurately verify if our planning corresponds to the dose distribution that the patient will receive during delivery.

This MC verification procedure only based on the simulation of parameters involved in the RTP file from TPS could be enough for a robust verification of static IMRT cases (Leal *et al.*, 2003), but needs to be enhanced, such as outlined in the hypothesis of this work, to cover the two VMAT uncertainties stated in the Introduction section. Before to present results directly associated to the model proposed for covering both uncertainties, some complementary results are included below in order to show the feasibility of radiochromic film to complement MC simulation, such as it is intended to demonstrate. The comparative MC vs. film in Figure 3.9 was positive and it could be used as a validation support for our MC model but, for VMAT verification treatment, it is

necessary to also check if our software is sorting and automatic managing correctly all the CPs for the verification of a whole treatment.

In order to experimentally test our model, experimental verification with film placed in the same setup used for COMPASS/MatriXX measurements were performed and compared to MC solution, for the same cases presented above.
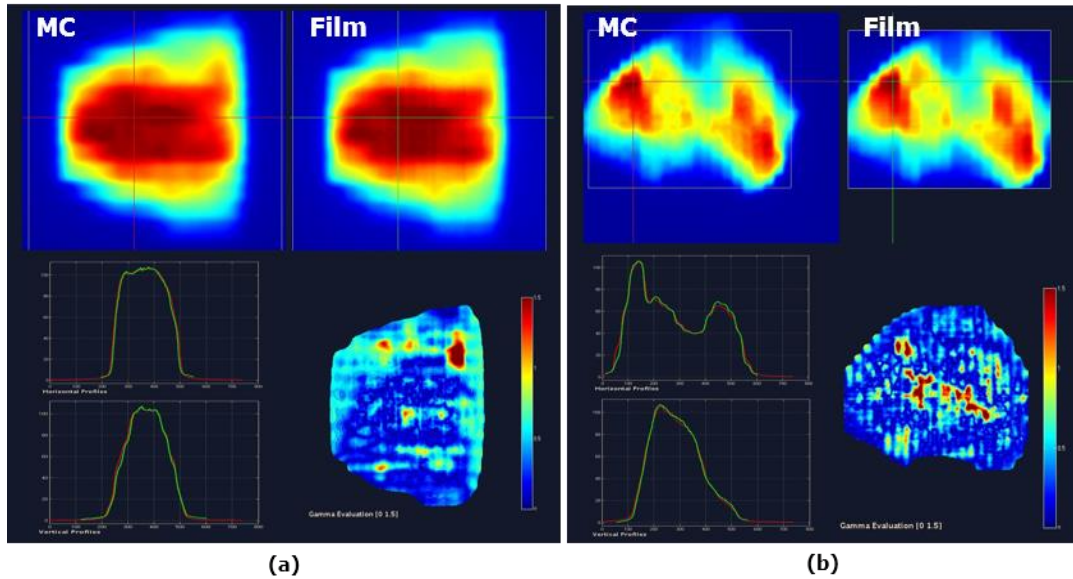

Figure 3.13. Dose distributions for MC (top left) and EBT3 film (top right) at the measured plane (between 2 cm of solid water and MatriXX^{Evolution} detector), dose profiles (bottom left) and gamma analysis (bottom right) for the same VMAT prostatic bed case (a) and VMAT H&N case (b).

This comparison showed a high agreement with more than 95% of points having a gamma index (3mm/3%) <1. These results are represented in Figure 3.13 for the previous cases except for the lung case because, being this one a SBRT case with 4 arcs, it had gotten saturate the grey in film. These results confirmed that our MC model was correctly implemented.

In the Introduction section of this work, two important sources of uncertainty in VMAT application were declared: the accuracy of the dose distribution calculation and another linked to the continuous delivery of a discrete calculation.

On one hand, it could be argued that the contribution of scattered and transmitted radiation, through the beam modifiers to the final dose, is being accurately considered by MC while it could be underestimated by TPS and COMPASS algorithms. It does not seem a weak argument in light of the Figure

3.14, where a qualitative fluence comparison for a representative CP of the VMAT prostate bed case is presented. MC simulated fluence is compared to the measured frame extracted from COMPASS showing the potential effect to the total dose due to secondary radiation not well considered by the detection system implemented in COMPASS. The commercial verification system and TPS not only share the same inaccurate dose calculation algorithm, but also a too simple approximation model of the incident beam corresponding to each CP.
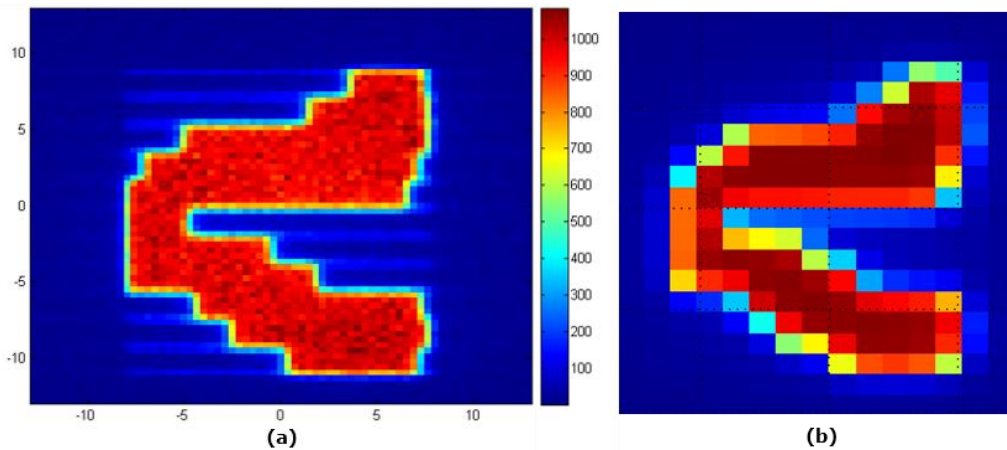

Figure 3.14. Spatial fluence distribution of a representative VMAT CP from a prostate bed case, obtained from the MC simulation (a) and from COMPASS acquisition (b).

It is necessary to remark here how important is the level of spatial resolution for experimental detection in this work. Commercial systems used for VMAT verification do not reach the resolution provided by the film. In our opinion, for a deep discussion about the precision involved in these verification systems, it is necessary to establish similar comparison as above, before including the results corresponding to the verification of complete actual clinical cases. In this case, a gantry-mounted MatriXXEvolution detector array provides COMPASS system with the experimental data for checking the dose previously calculated by the TPS. From this double comparison between MC vs. film (Figure 3.9) and MC vs. COMPASS (Figure 3.14), it is justified the need to include a verification system with the adequate resolution to establish a fair experimental correction of the explicit MC calculation from log file parameters. This means, the best measurement for the experimental comparison of this theoretical calculation, which describes the actual delivered irradiation.

On the other hand and following the discussion regarding the comparison shown in Figure 3.13, despite the high agreement between MC and film for complete treatments, one still might wonder about the small differences which are slightly higher than expected after seeing the comparison MC vs. film for a single CP in Figure 3.9. Although ideally our MC model not present absolutely any difference with film in Figure 3.9, it may still appear differences in Figure 3.13, due to the inherent limitations of a discrete solution to represent a continuous irradiation in the film. It is clear that a better MC verification will have to simulate the geometry of the log file, not those in the RTP file. Also, the geometry corresponding to each CP has an associated intensity by means of a MU value. This assignation is just an approximation to the continuous delivery, so it seems clear that a greater CP sampling from the log file will provide us a more realistic simulation.

3.2.1 Monte Carlo verification of log files

As it was already described in the Material and methods chapter, to carry out this work, it was necessary to develop software for automatic acquisition of parameters recorded by the linac control system during the delivery. An algorithm was also designed to make a CP sampling with different level of discretization by taking the CPs from log file, non-equi-spaced, but according to the density of changes along the arc. Therefore, it could be considered our model is based on a variable CP sampling. In Figure 3.15 is presented a comparison of treatment parameters from the RTP and log files simulated for one of the previous cases.
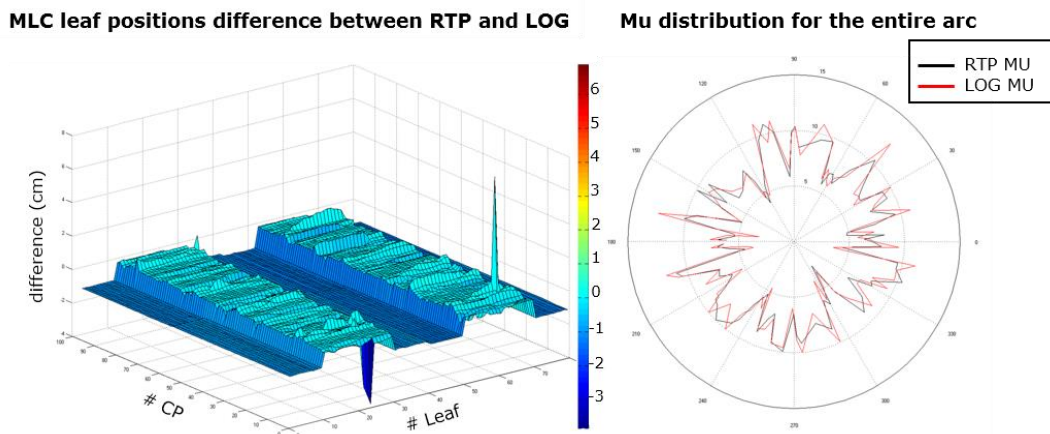

Figure 3.15. Comparative analysis of the planned treatment parameters (RTP) and those recorded on log file for the same discretization level.

As can be seen, by setting the same level of discretization of the RTP file, i.e., the same number of CPs for MC simulation of the log file, little differences can be found. No major differences in the geometries or positions of the MLC, neither in the corresponding MUs. Therefore, it was not expected that the corresponding MC solutions for RTP and log file, would have been very different.

Returning to the discussion about the detection density of verification devices for VMAT, the question arises about the benefit provided by experimentally verify the treatment plan maintaining the same discretization level used by COMPASS system. This kind of verification system is, therefore, designed to check the planning software, but not give information of what actually occurs during the delivery of the plan under evaluation, i.e., estimate the dose that the patient can receive.

To be more ambitious, the verification system has to recalculate a better approximation to the continuous delivery by increasing the sampling of parameters from log file. But also has to take experimental measurements with a detection device with enough spatial resolution for a fair comparison.

In Figure 3.16 is presented a comparison against film between the two MC verifications corresponding to the information in RTP and log files presented in Figure 3.15. The differences found by comparison the irradiated film with both simulations are equally relevant, so that a high-density detection as film reveals that the recalculation of log file may provide little if not done with greater sampling than the one in the RTP file.

Moreover, one cannot predict the final effect on the whole treatment volume, just from the analysis in a single plane (or several planes), as in Figure 3.16. A drawback of using a high resolution system as film in this situation is to obtain a 3D measurement, necessary for the reconstruction of DVH and so properly reporting how degenerated is the planning and its clinical transcendence.
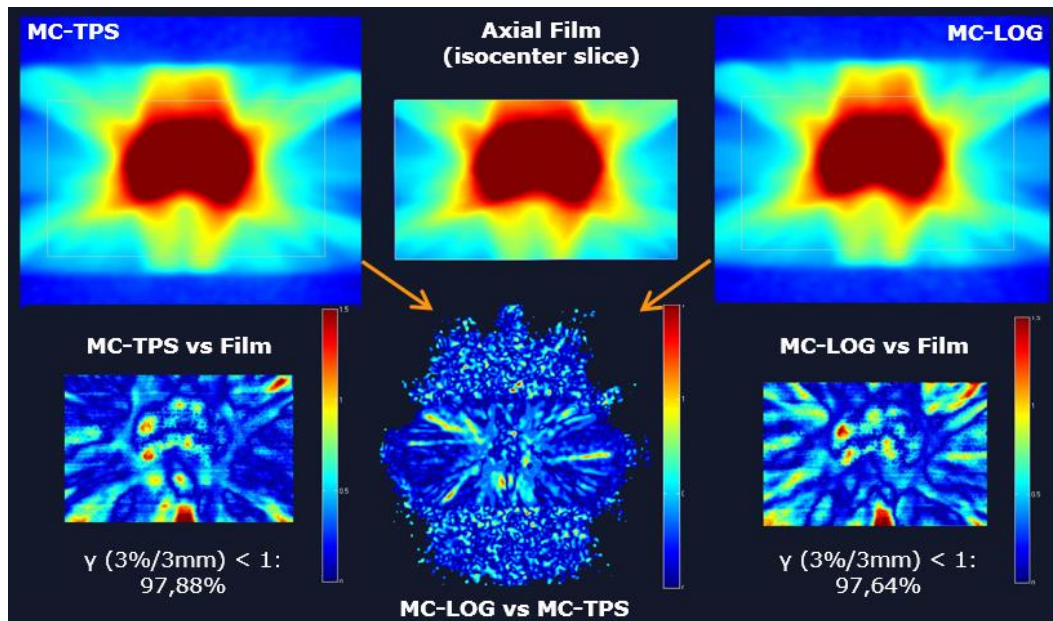
Figure 3.16. Comparison of dose distributions from MC RTP verification and MC LOG file verification with axial film at the isocenter plane and respective gamma analysis for the same VMAT prostatic case in Figure 3.15.

In view of these results and according to the discussion held, we decided to go further in the use of MC simulation for VMAT verification. Once developed an automatic verification model based on the log file with a sampling adaptable, the challenge was to implement a system able to provide an experimental correction to the simulated parameters of log file. The high detection resolution provided by film was considered as necessary to evaluate a higher sampling by means of the model. Therefore, it was necessary to develop a new phantom able to host film for 3D dose reconstruction. An ideal scenario would be having fluence measurements, 3D detection and absolute dose for complete experimental information about the delivery. Thus, the most accurate dose calculation based on MC simulation of the parameters related to the delivered geometries during irradiation, would be supplemented by a high resolution detection system for providing information on the input beam, as COMPASS, plus 3D dose measurements, as Delta4 or ArcCheck.

3.3 QuAArC Model

3.3.1 QuAArC phantom and data processing evaluation

The designed phantom prototype was constructed and implemented for a QA applied to VMAT treatments (Figure 3.17). Although it is an intermediate result, it was developed as one of the objectives established in this thesis. Beyond the aim of this work, this phantom can also be used for commissioning and other dosimetric purposes. The measurements performed with this phantom were integrated with the QuAArC model, developed for the evaluation of VMAT and other QA systems.

Figure 3.17. Final PMMA phantom QuAArC with rolled radiochromic EBT3 films (left) and PMMA slices for axial films with cork cylinders (right).

In order to evaluate the reproducibility of these unusual rolled film measurements (film scrolls) in the new phantom, repeated verifications of the same VMAT treatment plans were carried out.

Figure 3.18 shows a comparison between film dose distributions obtained for the same VMAT plan, verified in two different days, where the gamma index passing rates for a 3%/3mm criterion were greater than 99% for the 3 films, constituting the outer film scroll and inner film scroll.

All the technical specifications necessary for the construction of QuAArC phantom are included in the Appendix I. The phantom has been extensively used for this work and other experiments within the research group showing a high stability, easy handling and accurate positioning in the treatment table.
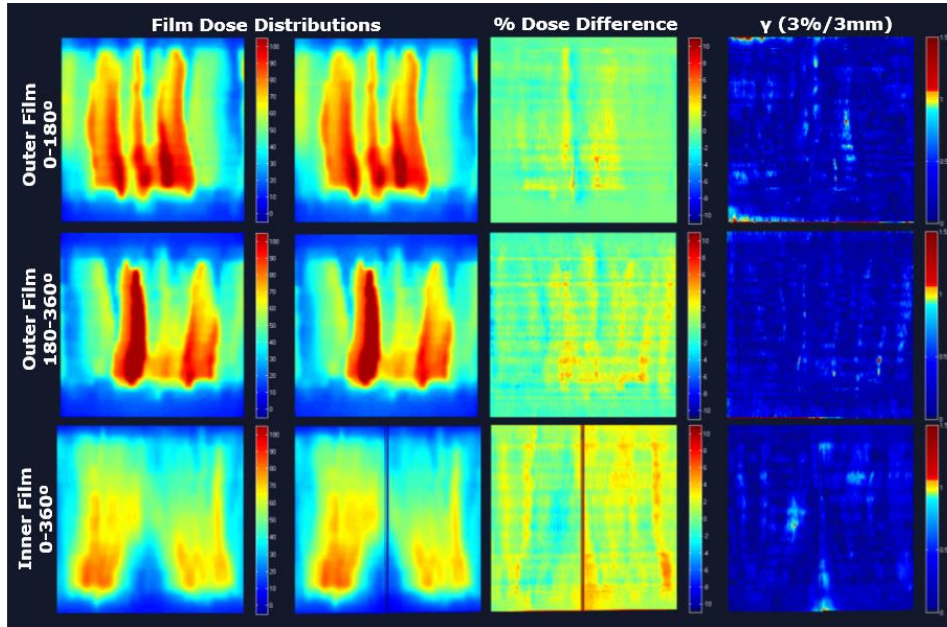
Figure 3.18. Film dose distributions, dose difference matrices and gamma analysis, obtained from two QuAArC verifications of the same VMAT plan with rolled films (2 at the outer cylinder and 1 at the inner cylinder).

Regarding the data processing in films, potential effects of considering a different discretization level from the log files for MC simulation in treatment verification was analyzed by comparison after processing of the film scrolls irradiated in the QuAArC phantom (Figure 3.19). These effects can be observed in the corresponding DVHs experimentally reconstructed on the patient CT data (Figure 3.20(c), (f)) by means of the QuAArC model proposed in Materials and Methods (section 2.3). Although in the Figures 3.19 and 3.20, only results for a prostate VMAT plan are shown, the following considerations can be extended to the other plans evaluated in this work. As expected, the more pronounced discrepancies between MC log calculation and film were found for the coarse discretization, as it is shown in the left column of Figure 3.19.

Furthermore, the different level of discretization between coarse and fine also had an impact on the procedure for obtaining the dose distribution experimentally reconstructed (QuAArC solution) from the measurements in the QuAArC phantom, as it can be observed in the right column of Figure 3.19. This shows how our model could establish the required level of discretization to obtain an adequate VMAT verification based on MC simulation of log files free-dependent on detection density. It is important to remark that these differences would not have been so evident whether a lower density detection implemented

in other VMAT verification systems would have been employed. On the other side, the consistency of these results provides confidence on our model.
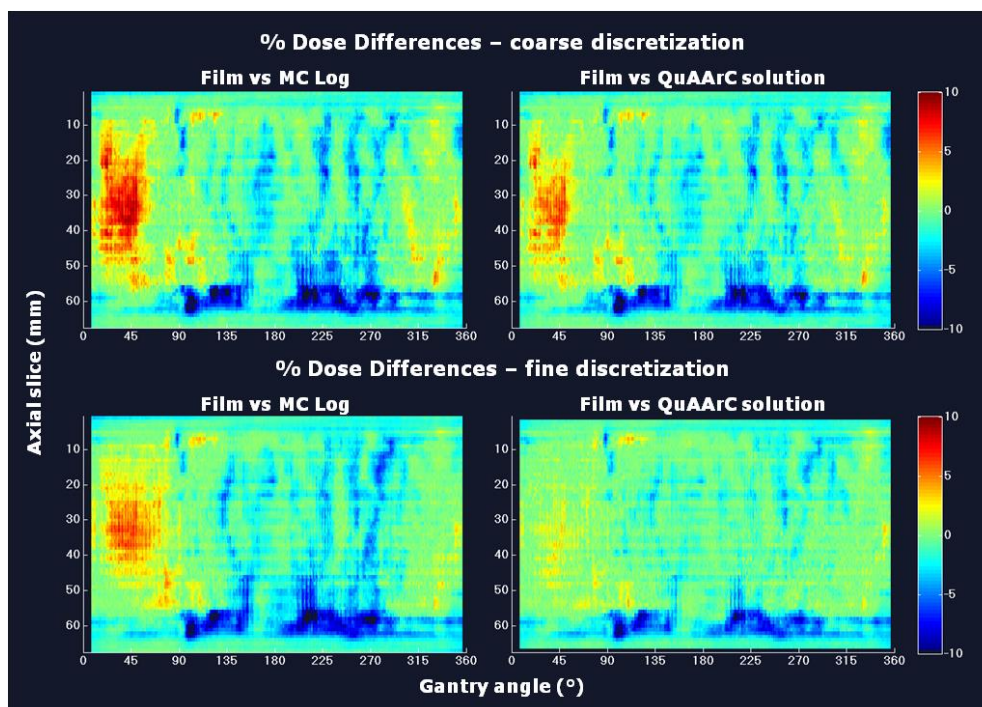

Figure 3.19. Effects of considering a different discretization level from the log files. Percent dose difference matrices of the inner film scroll versus MC Log (left) and versus the corresponding QuAArC solution (right) for coarse discretization (top) and fine discretization (bottom), corresponding to a prostate VMAT plan.

After experimental adjustment, the more relevant MU changes were found at the same arc locations for both discretization levels, showing that the procedure described in section 2.3.3 did not work randomly along the whole arc, but the algorithm proportioned the bigger changes where the differences between theoretical and experimental values were higher. Also, as expected, the global change was more uniformly distributed along the arc for the fine (Figure 3.20(d) and (e)) than for the coarse discretization (Figure 3.20(a), (b)). This latter showed that the MU adjustment was mainly carried out with the lateral contribution from the contiguous CPs, what was our goal in order to achieve a reconstruction of the accumulated MU in the log file with the information continuously registered in the film.

According to the comparison followed in Figure 3.19 with the rest of measurements in the phantom, the finer approach provided a more reliable reconstructed DVH solution (Figure 3.20(c), (f)), and was considered as the necessary option in QuAArC verification procedure for this case. Although

coarse QuAArC approach provided a similar DVH solution that could have also been approved, the same was not observed for the rest of analyzed cases. Anyway, the evaluation of a larger number of clinical cases would be necessary to prove what level of discretization could be enough for an efficient verification procedure in shorter times. With this work, we suggest that this kind of studies with verification systems different to the proposed model could be biased due to the use of lower detection density and to different spatial distribution.
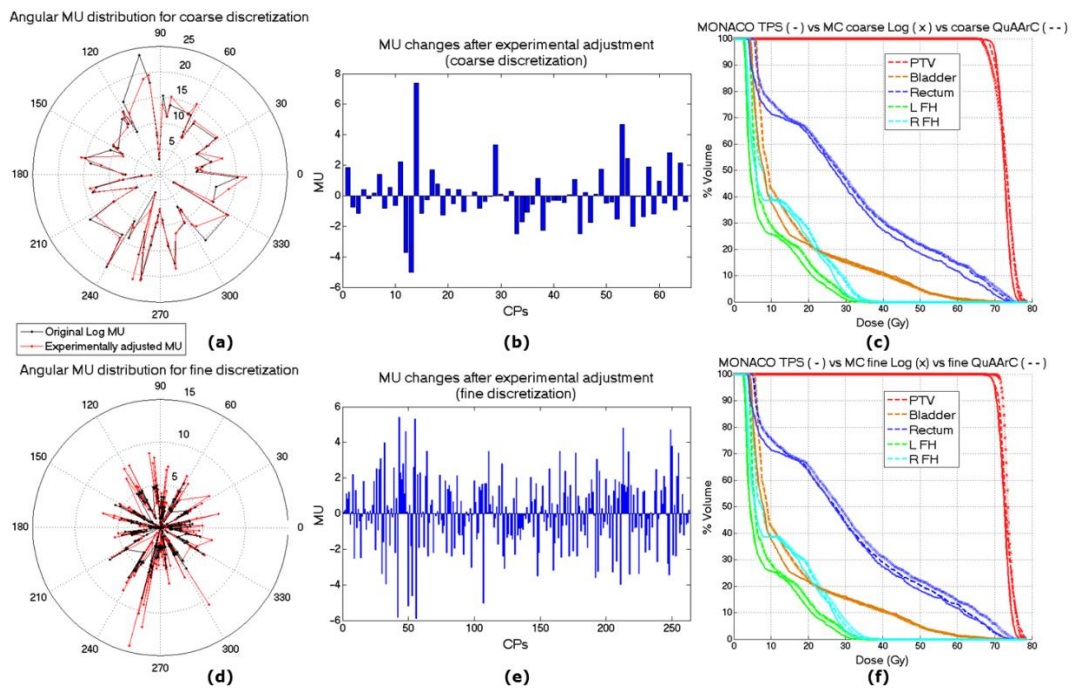
Figure 3.20. Comparative reports between original and experimentally adjusted solutions for fine and coarse discretization. Angular MU distributions from the original log file MC simulation and the experimentally adjusted with QuAArC (a) and the corresponding MU differences for coarse discretization (b). The same for fine discretization (d and e). DVHs comparison between Monaco TPS solution, MC log file simulation and QuAArC reconstructed solution, for coarse (c) and fine discretization (f). All for a prostate VMAT plan.

3.3.2 QuAArC model implementation and validation with clinical cases

In this section, the verification by means of the proposal, QuAArC model is presented for VMAT plans from HURV, which were approved for clinical treatment after verification with COMPASS system. Also the results obtained with QuAArC are presented for other cases, from HIL, including approved and not approved solutions with Delta4 verification.

Before, a proof of concept was established to indicate the feasibility of the feedback procedure explained in sections 2.3.2 and 2.3.3. Figures 3.21 and 3.22 show the comparison between film scroll dose distributions and QuAArC scroll dose distributions, and corresponding dose difference matrices and gamma analysis.
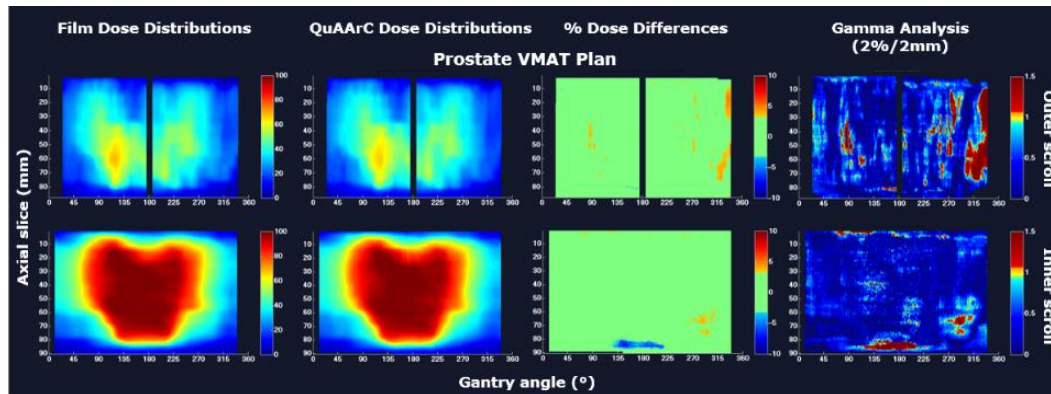

Figure 3.21. Film and QuAArC dose distributions for the verified prostate VMAT plan porvided by HUVR to prove the experimental feedback process. Corresponding percent dose differences and gamma analysis are shown for outer and inner scrolls in QuAArC phantom.
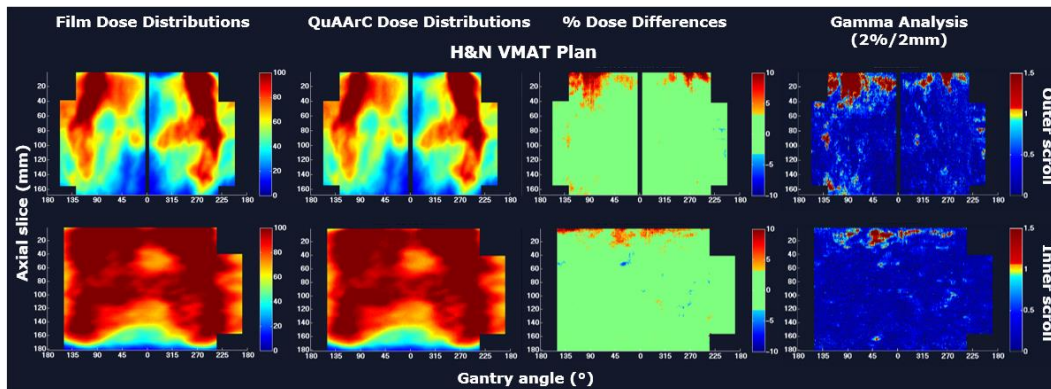

Figure 3.22. Film and QuAArC dose distributions for the verified H&N VMAT plan provided by HUVR to prove the experimental feedback process. Corresponding percent dose differences and gamma analysis are shown for outer and inner scrolls in QuAArC phantom.

The respective values are presented in Table 3.1, and also the absolute dose values obtained with CC13 ion chamber measurements in QuAArC and obtained for MC simulations of fine log discretization (MC LOG) and QuAArC solutions after experimental adjustment.

Table 3.1. Summary of absolute doses, percent dose differences and gamma index passing rates for HUVR evaluated treatment plans.

Absolute dose (Gy) (% deviation)			Dose difference passing rates (%) (<3%)				γ-index passing rates (%) (2%/2mm)			
			Outer scroll		Inner scroll		Outer scroll		Inner scroll	
CC13	MC LOG	QuAArC	MC LOG	QuAArC	MC LOG	QuAArC	MC LOG	QuAArC	MC LOG	QuAArC
Prostate Case										
3,67	3.56 (-3.00)	3.57 (-2.72)	99.05	99.53	97.55	96.63	96.51	90.53	95.45	96.62
H&N Case										
2.03	2.13 (4.93)	2.16 (6.40)	77.08	90.78	80.43	94.16	78.64	91.90	82.78	97.84

These positive results gave us confidence to apply QuAArC model to obtain the experimental reconstructed DVHs. These QuAArC reconstructed DVHs are presented in Figure 3.23, for two cases.
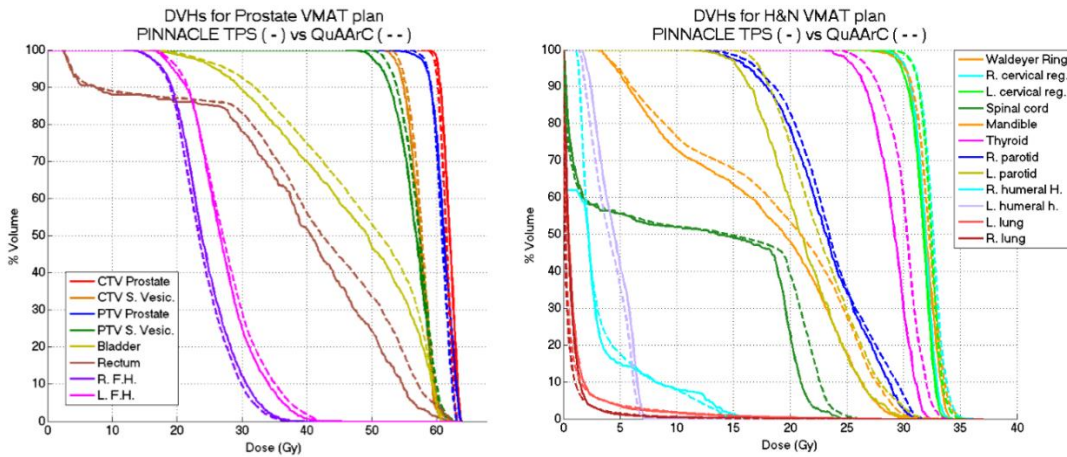

Figure 3.23. DVHs comparison between Pinnacle TPS solution and QuAArC reconstructed solution of both evaluated plans, prostate VMAT plan (right) and H&N VMAT plan (left).

As observed in Figures 3.21 and 3.22, a high agreement was obtained between QuAArC and film dose distribution for both verified treatment plans. This is also reflected in the corresponding 3% dose difference and gamma passing rates presented in Table 3.1, where overall, QuAArC solution after experimental adjustment, showed better results or comparable to MC LOG solution after a simple MC simulation, as presented in section 3.2, for all relative dose distributions. The color code used to represent the percent dose

difference matrices was set according to the passing rate values presented in Table 3.1 (% pixels having a dose difference within 3%). Gamma analysis based on 2% DD/2mm DTA criteria was also included. When a 3%/3 mm criterion was used for gamma evaluation of QuAArC solution, passing rates were greater than 97%, for both scroll regions (outer and inner), in both plans. Absolute dose values agreed well within the 3% for prostate VMAT plan, while for H&N VMAT plan, this result was worse, and it was not improved with QuAArC solution. Although this disagreement could result in some absolute dose difference when reconstructing the DVH, we considered these results acceptable. For this case, the reference point or another point should have been chosen in a location less exposed to high dose gradient. This measurement should be repeated for further evaluation, but the high agreement with film and improved results for QuAArC compared to the MC LOG were considered to be sufficiently acceptable to obtain a reconstructed DVH, which better estimates the delivered dose.

It is important to note here that the evaluated cases were approved in clinical practice after experimental verification carried out with the COMPASS system used at the HUVR. In this sense, the solutions provided by QuAArC were consistent. However, it was necessary to evaluate the behavior of QuAArC system in cases where a conventional check would not have approved the plans.

To cover this scenario, as a part of the proof of concept of the model, comparisons of outer and inner film scroll dose distributions with the ones obtained by means of QuAArC system were carried out (Figures 3.24 and 3.25), for prostate case and H&N case from HIL, respectively. As it was described in section 2.4, two solutions were previously planned with commercial TPS (Monaco, Elekta) and verified with ScandiDos Delta4 system, for each case: one solution failing (plan A) and other passing (plan B) the Delta4 acceptance criteria in the clinical application.
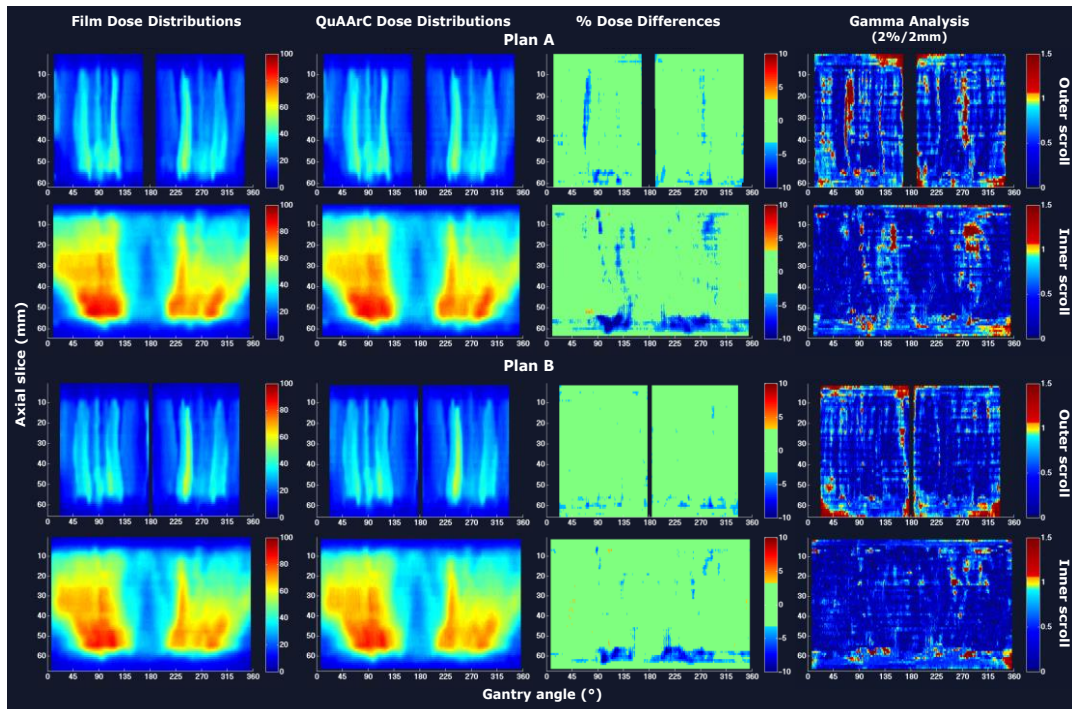
Figure 3.24. Film and QuAArC dose distributions for the prostate case provided by HIL to prove the experimental feedback process. Corresponding percent dose differences and gamma analysis are shown for outer and inner scrolls for VMAT Plan A (first and second rows, respectively), and the same for VMAT Plan B (third and fourth rows).
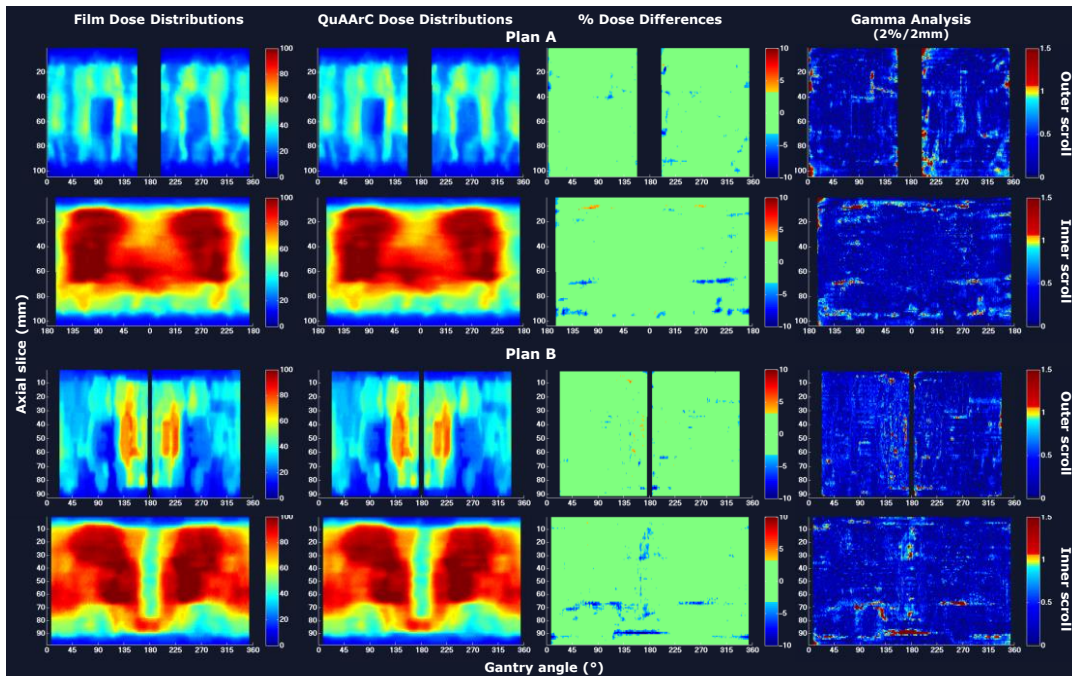

Figure 3.25. Film and QuAArC dose distributions for the H&N case provided by HIL to prove the experimental feedback process. Corresponding percent dose differences and gamma analysis are shown for outer and inner scrolls of VMAT Plan A (first and second rows, respectively), and the same for IMRT Plan B (third and fourth rows).

All QuAArC scrolls showed a high agreement with the measured film scrolls for both, percent dose differences and gamma analysis, which values are given in Table 3.2. Since there is always a limitation regarding the discrete calculation, even with the fine discretization under consideration, minor differences were assumed. Anyway, these small differences observed were mostly located outside the treatment field or at the edges. Note that this comparison was carried out with the MC scrolls resolution (1 x 0.7854 mm^2 for outer scroll and 1 x 0.3523 mm^2 for inner scroll) obtained after the dose recruitment described in Material and Method section.

Table 3.2. Summary of absolute doses, percent dose differences and gamma index passing rates for HIL evaluated treatment plans.

Plan	Absolute dose (Gy) (% deviation)			Dose difference passing rates (%) (<3%)				γ-index passing rates (%) (2%/2mm)			
				Outer scroll		Inner scroll		Outer scroll		Inner scroll	
	CC04	MC LOG	QuAArC	MC LOG	QuAArC	MC LOG	QuAArC	MC LOG	QuAArC	MC LOG	QuAArC
Prostate Case											
A	2.48	2.51 (1.21)	2.53 (2.02)	92.95	91.94	78.33	84.85	90.77	90.12	87.91	93.19
B	2.45	2.42 (-1.22)	2.45 (0.00)	92.78	95.48	80.83	91.19	88.34	92.66	89.94	97.09
H&N Case											
A	2.02	2.01 (-0.49)	2.06 (1.98)	96.89	97.61	89.52	96.04	96.28	97.45	91.19	98.18
B	2.06	2.07 (0.48)	2.07 (0.48)	97.53	98.16	93.16	94.51	97.87	98.40	96.84	97.60

As in Table 3.1, Table 3.2 shows a summary of passing rates for dose differences within 3% and global gamma index with 2%/2 mm criteria obtained for MC LOG and the corresponding QuAArC. The values for the absolute dosimetry performed with ion chamber in QuAArC phantom and the obtained from MC LOG and QuAArC solutions, were also included in Table 3.2. All MC LOG and QuAArC absolute dose values were obtained with less than 1.25% of statistical uncertainty, and agreed with the experimental measurement within 2%. In general, the passing rates improved for QuAArC solution after experimental adjustment regarding the MC LOG in both, 3% dose difference and gamma analysis. For QuAArC solution, all evaluated plans had a γ index < 1 passing rate greater than 90% using 2%/2 mm criteria in both scroll regions (outer and inner). For 3%/3 mm criteria, passing rates were greater than 98%, in all cases. As expected, this same test based on coarse discretization approach provided worse passing rates.

For the IMRT H&N plan B (last row in Table 3.2), the results were practically the same for MC LOG and QuAArC solution, meaning that our model did not modify the MUs when the delivery was static. It is important to remark that this agreement for the static IMRT case was also observed in the DVHs comparison with Monaco TPS solution (Figure 3.26(d)), since Monaco calculation is strongly based on MC, what is similar to our full MC model. The minor discrepancies in OARs could be due to the different consideration of beam modifiers contribution to the dose.

In the static plan, the MC log simulation represented the measurement well enough, but it was not the same for VMAT plans, as it can be seen in Table 3.2. MU adjustment approach proposed in our system showed to be necessary for exhaustive dynamic treatment verification. Apart from the IMRT commented above, the VMAT cases which were not accepted with Delta4 verification, were well adjusted by our model (plan A in Figures 3.24 and 3.25), although the resulting DVHs (Figure 3.26 (a) and (c)) showed to be significantly different to the planning with Monaco TPS, while the DVH corresponding to the VMAT plan B accepted with Delta4 (Figure 3.26(b)) showed to be very similar to the Monaco solution. These results obtained with our model showed to be in tune with Delta4 verification. Unlike this, greater differences, especially in OARs, were observed with other commercial algorithm, not based on MC, as the one implemented in Pinnacle (Figure 3.23). In any case, considering the two uncertainties pointed out in the Introduction chapter, it could be estimated that the potential discrepancies involved in the continuous delivery of a discrete calculation can become more significant than those due to the dose calculation accuracy.

Essentially, all the results showed in figures and tables, indicated that the model developed was robust and consistent, and were included in this work to prove the feasibility of the novel feedback procedure and to provide confidence about the experimental reconstruction of DVHs.
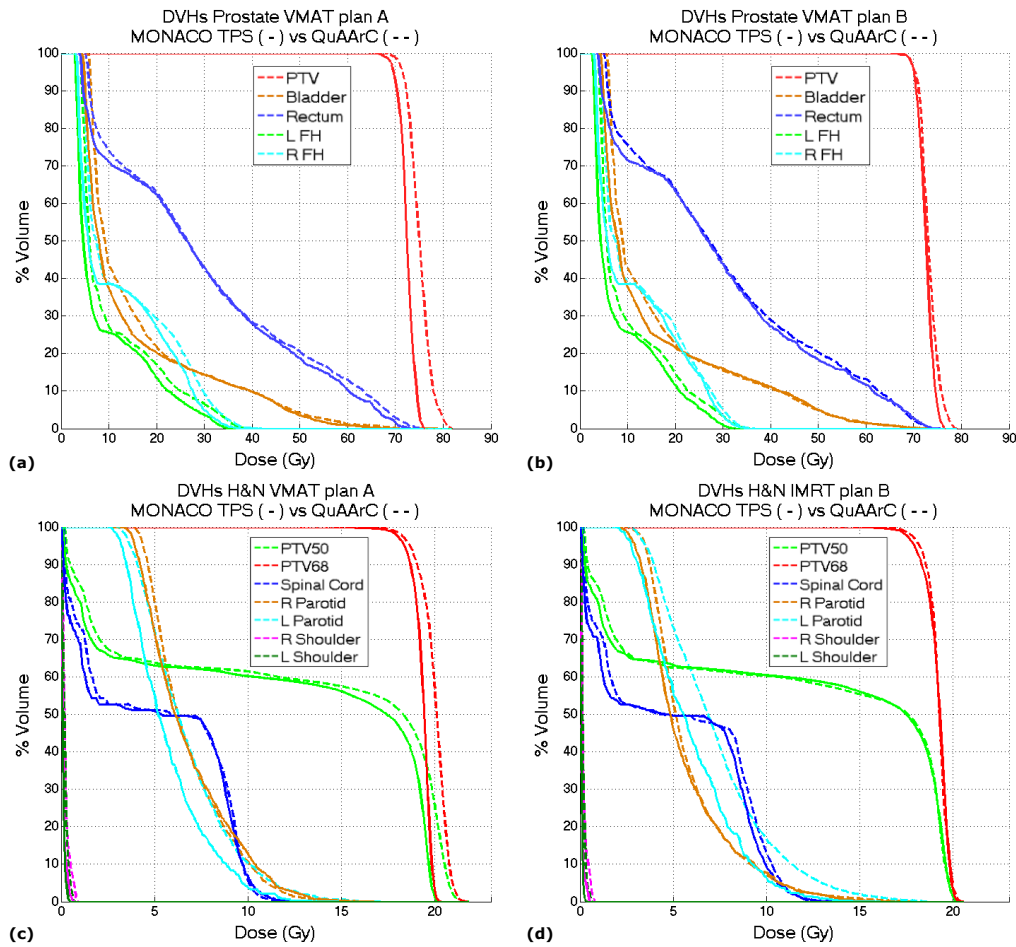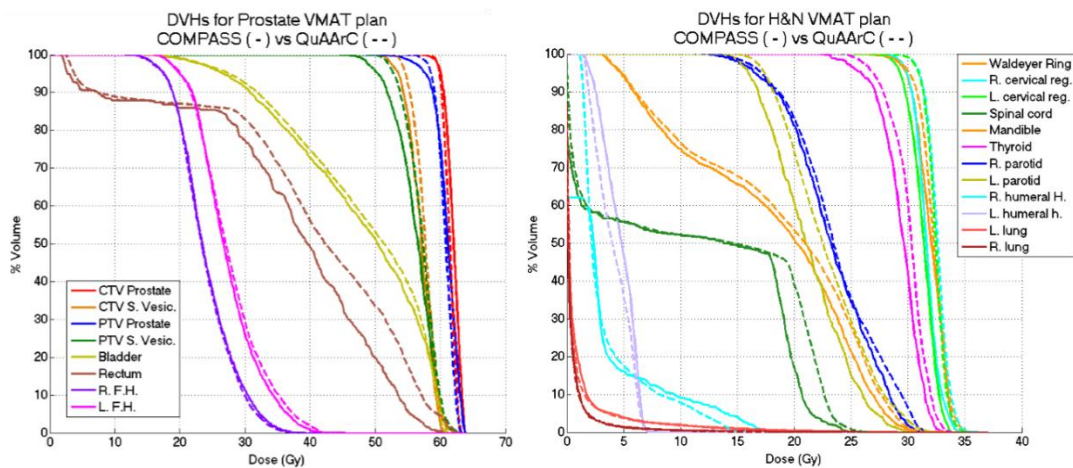
Figure 3.26. DVHs comparison between Monaco TPS solution and QuAArC reconstructed solution of both evaluated plans, VMAT plan A (a) and B (b), for the Prostate case and VMAT plan A (c) and IMRT plan B (d), for the H&N case.

The comparison between experimental measurements and TPS dose distributions recalculated in the QuAArC phantom was also carried out. Anyway, the different location of detection points in commercial systems and QuAArC phantom, makes inappropriate the direct comparison. In the next section, the DVHs provided by the evaluated VMAT verification systems, including the recent Delta4 DVH Anatomy option, are presented in order to analyze a direct DVH comparison with QuAArC solution.

3.3.3 Comparison of QuAArC solution and commercial solutions

DVHs obtained with QuAArC model compared to both solutions provided by the evaluated commercial systems are presented, in Figures 3.27 and 3.28, for the same treatment plans used for QuAArC model validation.

When comparing QuAArC and COMPASS solutions (Figure 3.27), very similar results to the ones observed in the previous comparison QuAArC versus Pinnacle, were obtained. These results could be expected, since both plans have been accepted for treatment with COMPASS and this system also use the same type of analytic algorithm to reconstruct the dose in the patient anatomy as Pinnacle.

Figure 3.27. DVHs comparison between COMPASS solution and QuAArC reconstructed solution of both evaluated plans, prostate VMAT plan (left) and H&N VMAT plan (right).

From the DVHs results of Delta4 Anatomy, using pencil beam algorithm, compared to QuAArC solutions, in Figure 3.28, it can be seen that our model showed to be consistent for all the plans. Similar results were obtained with QuAArC for the plans previously approved with Delta4 (plans B), as expected, except small discrepancies that are assumed due to different detection methods and reconstruction algorithms. This latter, can be more evident for plans, which falied the acceptance criteria with Delta4 (plans A), where this different detection density and location, even the distinct approach implemented, could introduce more discrepancies in the reconstruction. Therefore, the major differences were found for one of the plans A. However in this situations, where verified solutions could be different, Delta4 Anatomy can still present the same

result as QuAArC, which means that the final solution is also dependent on the degeneration of that treatment plan, regarding the optimization algorithm being used, and probably the relative locations of verified CPs and detectors in the system.
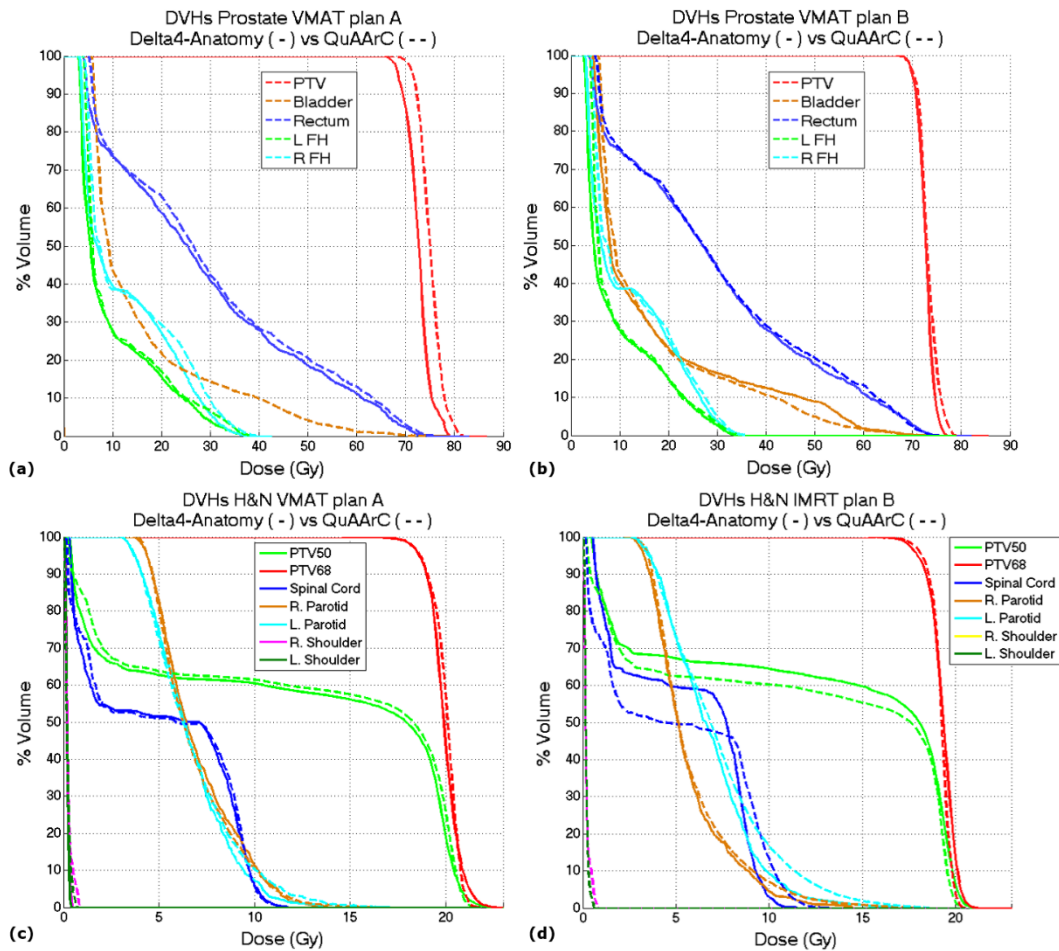

Figure 3.28. DVHs comparison between Delta4 DVH Anatomy with PB and QuAArC solutions for all plans of both evaluated cases.

Summarizing the evaluation of the clinical implementation, it is important to remark that this work was not focused to make a comprehensive study on the different verification systems and dose calculation algorithms for dynamic techniques. Anyway, few clinical cases were evaluated to check the feasibility of our model.

On one hand, for those cases which were approved with Delta4 and COMPASS, QuAArC system provided similar DVHs to the solutions from TPSs

corresponding to planning targets, Monaco and Pinnacle, respectively. More important disagreement was observed for DVHs corresponding to OARs in the cases from Pinnacle/COMPASS. The dose calculation uncertainty using Monaco TPS was observed to be not as relevant as the uncertainty linked to the dynamic delivery. However, greater differences were found when QuAArC solutions were compared with Pinnacle TPS, where this uncertainty, linked to the dose calculation accuracy, also added discrepancies, as expected.

On the other hand, for those cases which were not previously approved with Delta4 from Monaco TPS solutions, QuAArC did show a greater disagreement for DVHs of PTVs. All these results proved that QuAArC system was consistent with expected results, what support the viability of the model for this kind of studies.

In addition, it is important to note that the QuAArC phantom based on film could be implemented apart from MC log calculation, whether the TPS is able to provide individualized CP dose contribution. This would lead to more efficient computational times for routine pre-treatment verification, although with our approach based on fMC calculation, the results were more reliable and, in fact, they were ready at time of film processing stage.

Chapter 4

Conclusions

The results achieved in this work allow us to drawn the following conclusions:

1. The model developed in this work allows the VMAT evaluation with high accuracy provided by the MC explicit radiation transport simulation of the actual delivery treatment parameters from the log files, and with the high spatial resolution provided by film dosimetry.

2. The stated uncertainties inherent to complex dynamic techniques can be controlled and reduced with the proposed model, what will be useful for further studies about VMAT efficiency in specific clinical cases and for the evaluation of other QA systems.

3. The detection density level and its location in a specific phantom have to be adequately considered to obtain a more reliable DVH. This could be useful to detect potential wrong decisions based on the results from commercial VMAT verification systems, due to mismatching between control points used for dose reconstruction and the detector locations.

4. The specific phantom designed for the implementation of the model together with the software developed for data processing have shown to be robust and efficient to be considered as a pre-treatment VMAT verification alternative for clinical practice.

APPENDIX I

This appendix contains the description and geometrical schemes of the designed prototype of the VMAT phantom (QuAArC), for manufacturing.

VMAT Phantom

1. Phantom:
   - General Description
   - Possible setups for different applications
2. List of components
3. Schemes

1. PHANTOM

Description and setups

1. Phantom

Description:

It consists of a set of two concentric cylinders of different diameter to roll up around one and/or two radiochromic films, apart from axial slices to interpose films. This set is surrounded by two covers, enclosing both the cylinders and the slices. In addition, it also presents housings for inserts with ionization chambers with different dimensions. All components are manufactured in some type of plastic (polystyrene, PMMA) plus other replaceable parts in cork.

Radiochromic film dimensions:
20.30cm(W) x 25.40cm(L) x 0.03cm(T)

→ **20.30cm** ←

25.40cm

0.3mm thickness

Closed phantom view
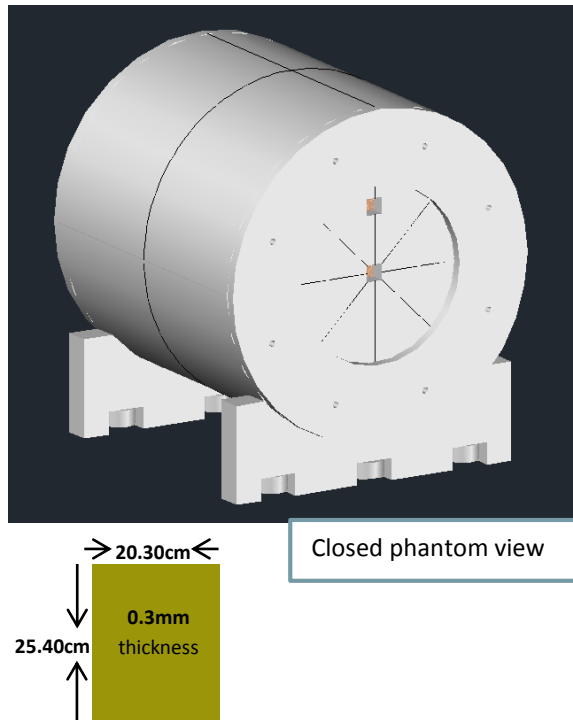
1. Phantom

Setups:

The phantom allows two setups, which are adapted in size for the verification of treatments in different locations. Both setups support cylinders and slices.
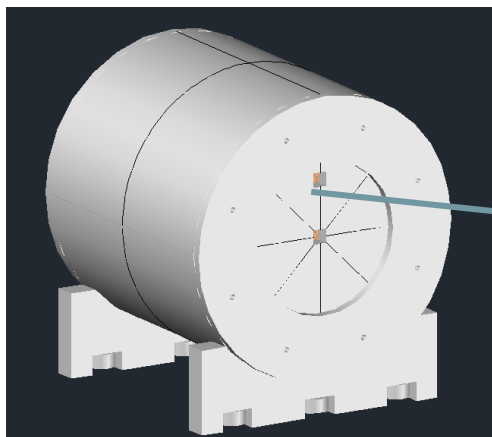
Phantom setup for larger treatment fields. From now on **big setup**.
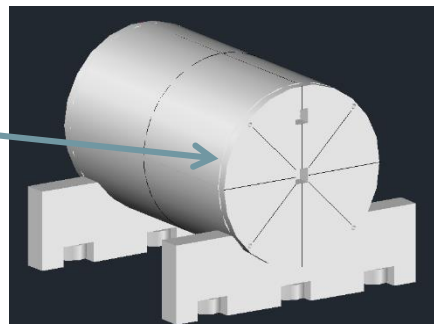
Phantom setup for smaller treatment fields. From now on **small setup**.

Below it is shown, for the two setup types (big and small), the location of the films rolled up around the two cylinders, as well as slices and other components.

Setups – rolled up films option (scrolls)

20.30cm

0.3mm Thickness

25.40cm

Big Setup with 3 rolled up films

Inserts and films slightly extracted for their visualization

Films

Small Setup with 3 rolled up

Setups – axial films option:

To place axial films in both setups (big and small), the two concentric plastic cylinders from previous figures are replaced by slices. Additionally, two cork cylinders are included at the ends (outside the region of interest).

Big setup with slices to place axial films

External Cover

Small setup with slices to place axial films

Internal Cover

Inserts and small cylinder slightly extracted for their visualization

The covers (external and internal) encompass the two setups and are closed with front and back lids.

Setups – other images:

Big setup with cylinders to place an ionization chamber in the center

Small Setup with cylinders
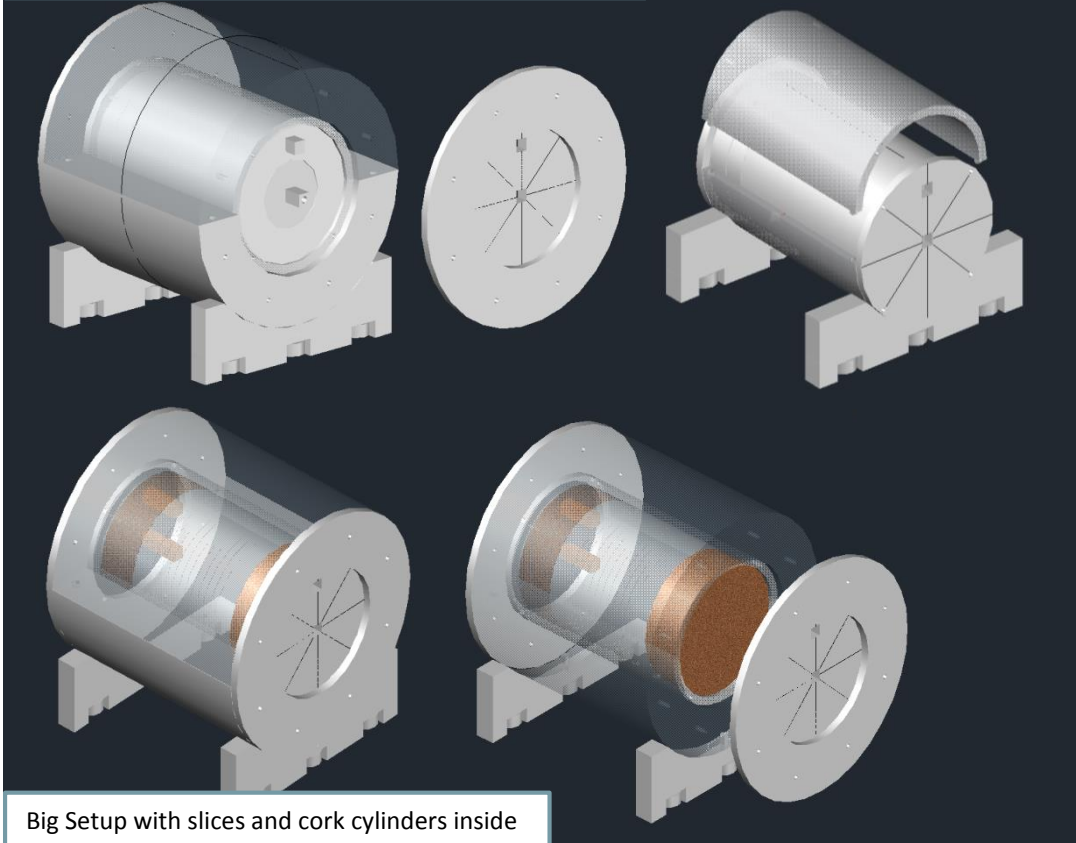
Big Setup with slices and cork cylinders inside

2. LIST OF COMPONENTS

2. List of components

- **2 Covers** (external and internal):
    - 4 hemi-covers (C_{E1}, C_{E2} ; C_{I1}, C_{I2})

- **1 Plastic Cylinder G** (big):
    - 2 hemi-cylinders (G_1, G_2)

- **1 Plastic Cylinder P** (small):
    - 2 hemi-cylinders (P_1, P_2)

- **2 Cork Cylinders G**:
    - 4 hemi-cylinders (G_{11}, G_{12} ; G_{21}, G_{22})

- **2 Cork Cylinders P**:
    - 4 hemi-cylinders (P_{11}, P_{12} ; P_{21}, P_{22})

- **13 Slices**: R_{1-9} of 1cm; $R_{10,11}$ of 0.5 cm; $R_{12,13}$ of 2.5cm.

- **30 Screws**:
    - For the lids: 16 of 3.5cm and diam. 0.8cm and 8 of 3.5cm and diam. 0.6cm;
    - For the supports: 6 of 3cm and diam. 1cm (planar surface head of 3cm of diam., which act like legs).

- **4 Lids**: front (T_{E1}, T_{I1}) ; back (T_{E2}, T_{I2}).

- **2 Supports** (S_1, S_2): 2 plinth + 4 bases.

- **18 Inserts** (prisms): $I_{1,2}$ of 20.3cm (1 of them is cut); $I_{3,4}$ of 2.5cm; I_{5-8} of 5cm in cork (2 of them are cut), for phantom filling; I_{9-11} of 15cm for chambers together with I_{12-18}: 1x7.8cm + 2x5cm + 2x1cm + 1x0.5cm + 1x0.3cm.

2. List of components
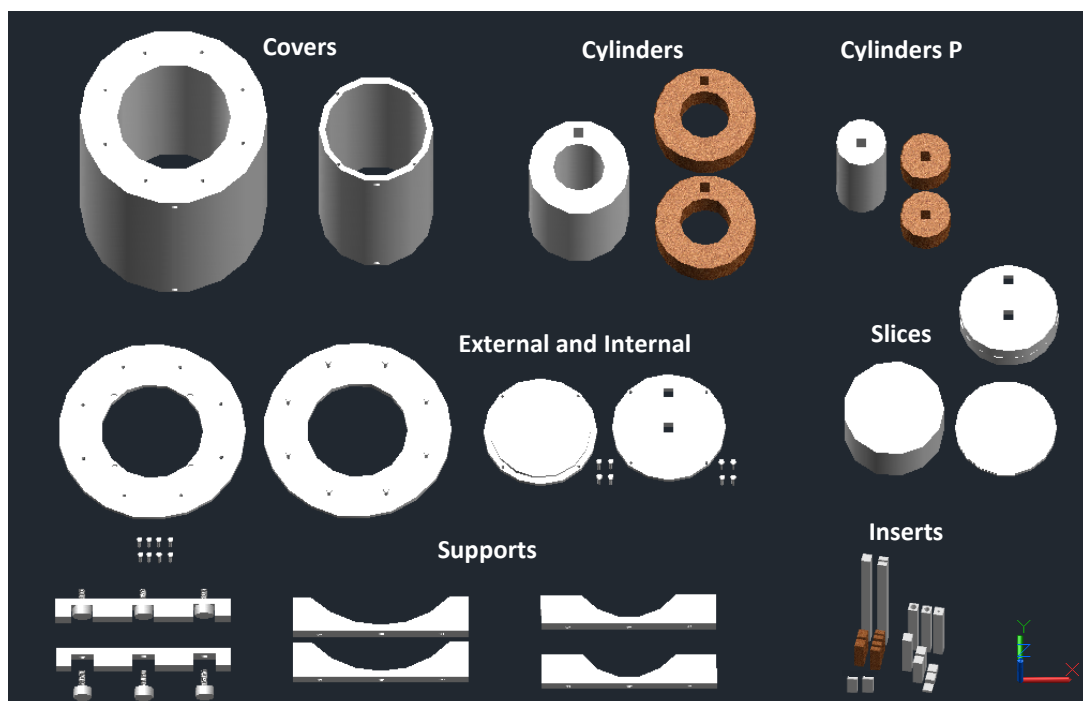
3. Schemes

Schemes and description of each component from the list

External Cover (C$_{E1}$, C$_{E2}$)

- Hollow cylinder with 30cm of outer diameter, 20cm of inner diameter and 28cm length, which is cut longitudinally in the central XZ plane, forming 2 symmetrical parts (hemi-covers C$_{E1}$ & C$_{E2}$) with tongue and groove between them. Both hemi-covers remain closed with the external lids, involving the other components. Big setup.

- **References for localization/positioning:** Besides the cover's longitudinal cut that serves as lateral references, it also presents two marked references, one longitudinal on the top and one axial at its center.
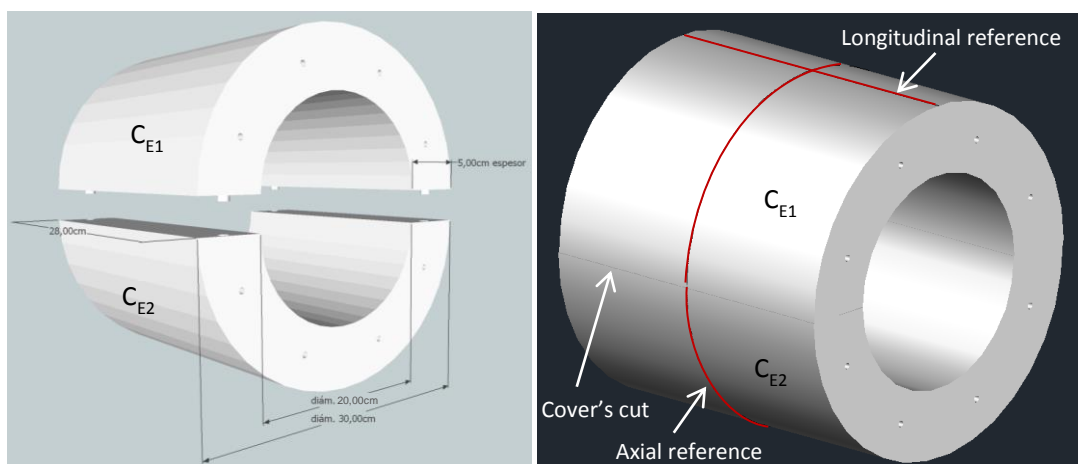
External Cover (C_{E1}, C_{E2})

- The hemi-covers fit in four points (tongue and groove), what will keep them joined providing more stability to the big setup. The hemi-cover C_{E1} has four cylindrical junction points of 1.0cm of diameter and 0.5cm thick that fit into the four holes of equal dimensions (0.5cm of depth and 1.0cm in diameter) present in the hemi-cover C_{E2}.
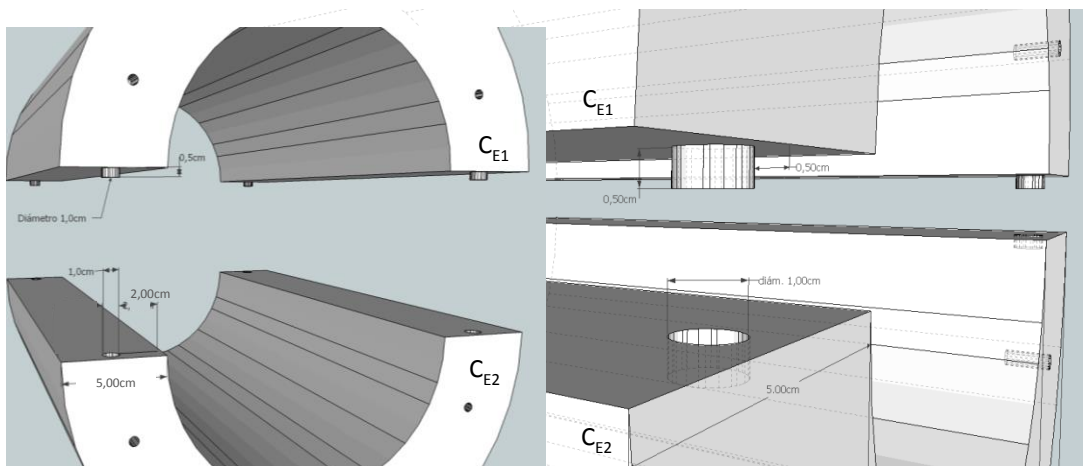

Schemes of the external cover
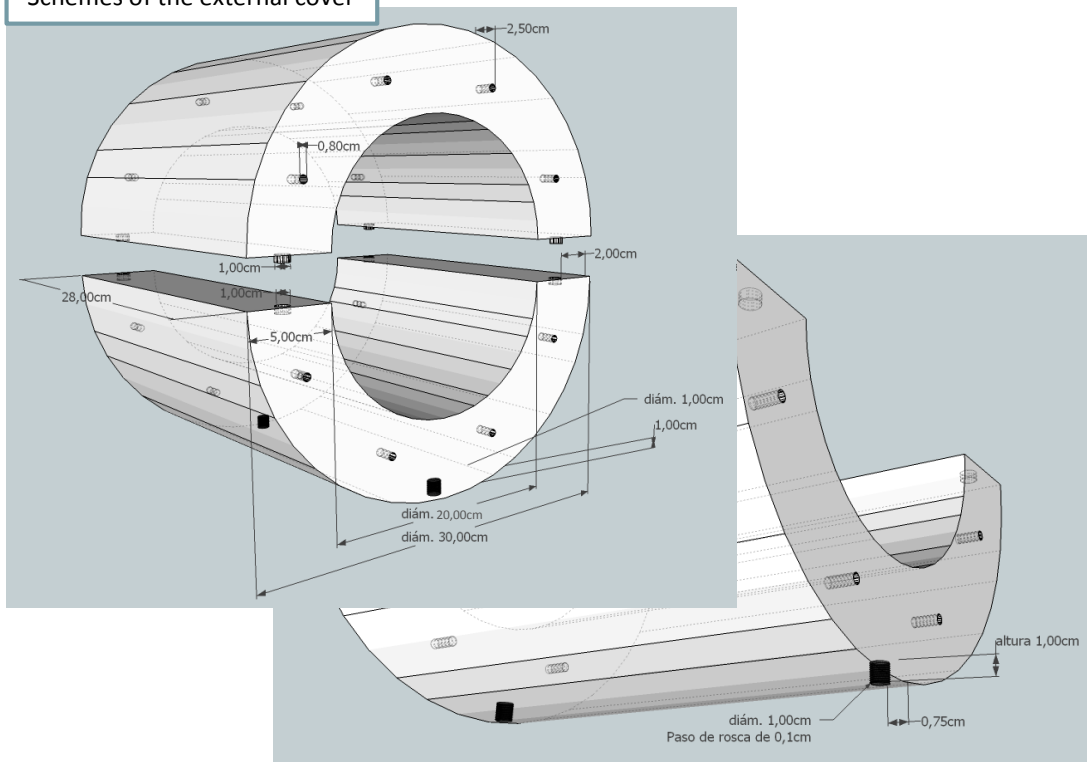
Internal cover (C$_{I1}$, C$_{I2}$)

- Hollow cylinder with 20cm of outer diameter, 18cm of inner diameter and 26cm length, which is cut longitudinally in the central XZ plane, forming 2 hemi-covers (C$_{I1}$ & C$_{I2}$). It works as a structure to fix the cylinders and slices of the phantom, along with the internal lids. Small setup.
- **References for localization/positioning:** Besides the cover's longitudinal cut that serves as lateral references it also presents two marked references, one longitudinal on the top and one axial at its center.
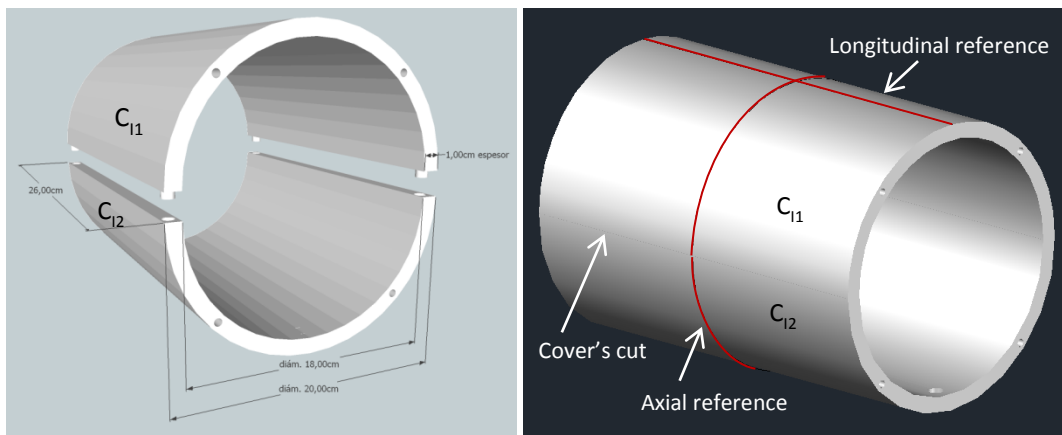
Internal cover (C$_{I1}$, C$_{I2}$)

- The hemi-covers fit in four points (tongue and groove), what will keep them joined providing more stability to the small setup, as for the external cover. However in this case the junction points have a diameter of 0.8cm.

Scheme of the internal cover
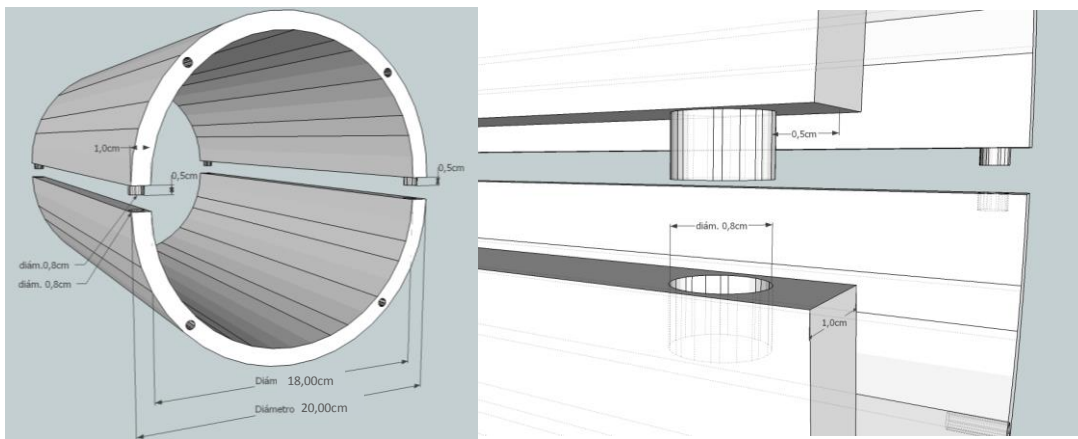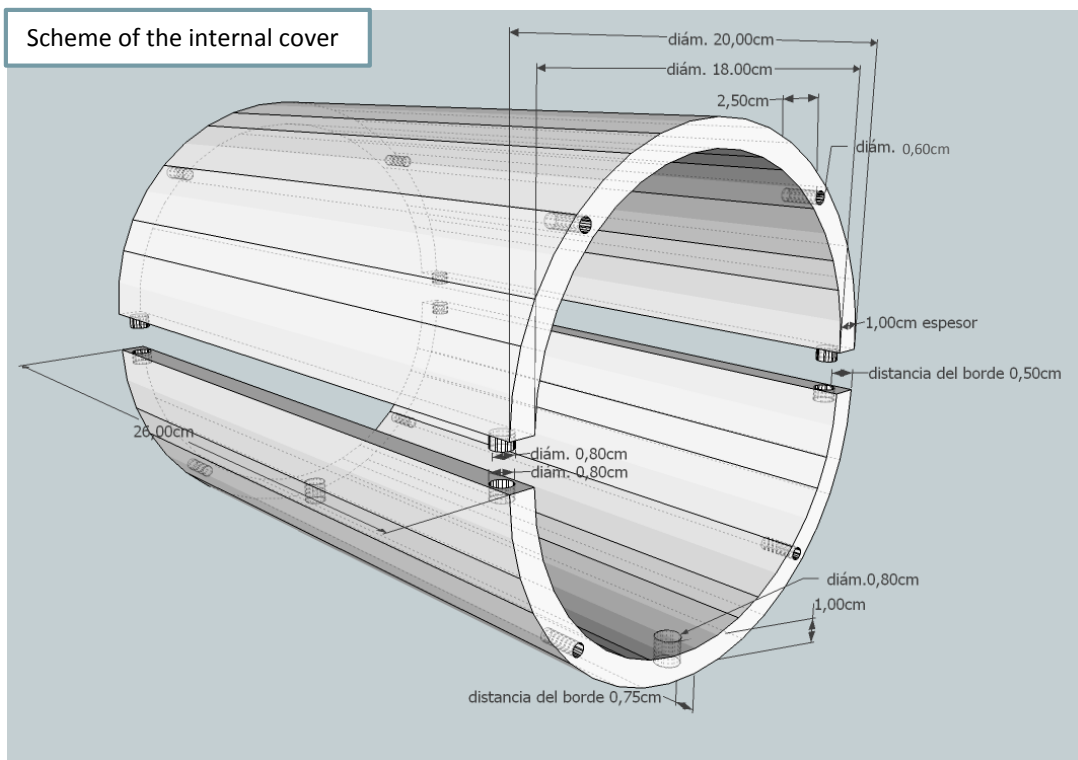
Cylinders G – Plastic (G$_1$; G$_2$)

- A hollow cylinder with 17.97cm of outer diameter (plus 0.03cm of film thickness, reach the internal cover's inner diameter of 18cm), 8.13cm of inner diameter and 20.30cm length, longitudinally cut by the central XZ plane, forming two symmetrical parts (hemi-cylinders G1 and G2).

It allows up to **2 radiochromic films rolled up around the outer diameter** (by the longer side of the film) and comprises its entire length (by the shorter side).

Schemes of the plastic cylinder G
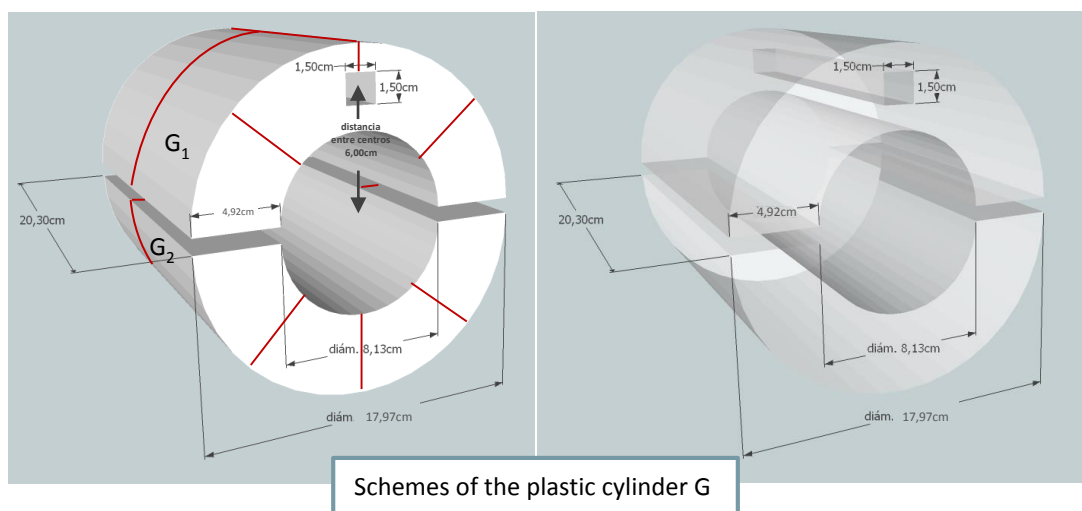
Cylinders G – cork (G$_{11}$, G$_{12}$; G$_{21}$, G$_{22}$)

• Two hollow cylinders with 17.97cm of outer diameter, 8.13cm of inner diameter and 5cm length, longitudinally cut by the central XZ plane, forming 4 symmetrical parts (hemi-cylinders G$_{11}$, G$_{12}$, G$_{21}$, G$_{22}$).

Allow up to **2 radiochromic rolled up films** (by the longer side of the film, by default) and comprises 10cm of film length.
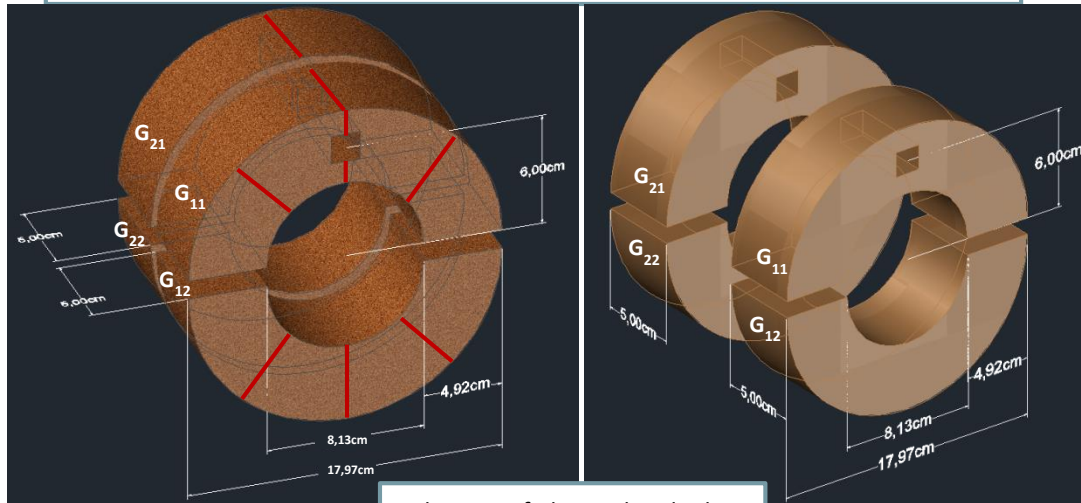

Schemes of the cork cylinders

Cylinders G – plastic and cork

References for localization:

Longitudinal – for plastic and cork: at the center, one upper and one lower;

Front - for plastic and cork : at 0°, 45°, 135°, 180°, 225° and 315°;

Axial – for plastic: two at **12,5cm** from the edge, one around the cylinder, which matches with the axial of the covers (the phantom's half) when the cylinder is placed at the front end, and the inner axial reference.
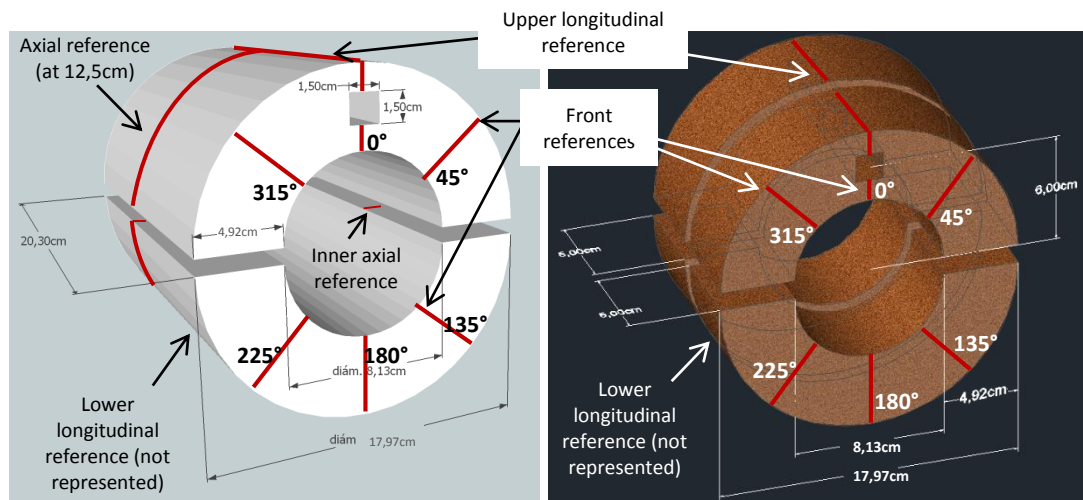

Representation of references (in red) for plastic and cork cylinders G

112

Cylinders P – plastic (P_1 ; P_2)

- One cylinder with 8.10cm of diameter and 20.30cm length, longitudinally cut by the central XZ plane, forming 2 symmetrical parts (hemi-cylinders).
- **References for localization:** the same as the plastic cylinder G (see above).

It allows to roll up **1 radiochromic film** (by the longer side, by default) and comprises its entire length (by the shorter side).
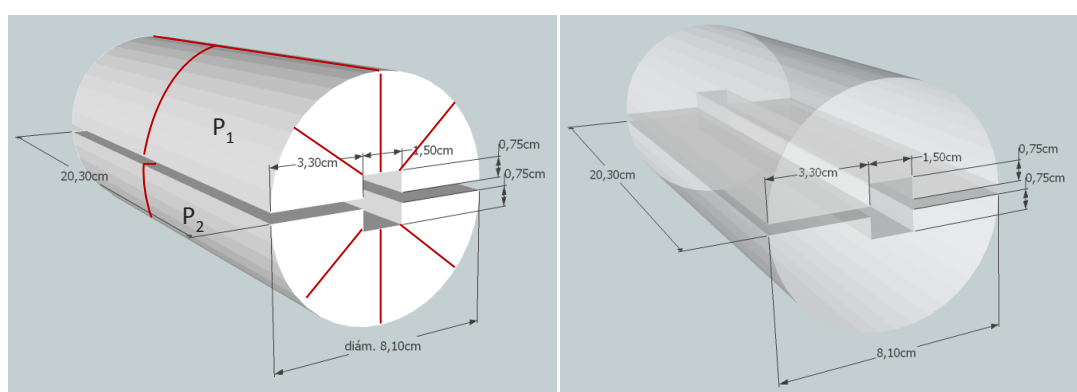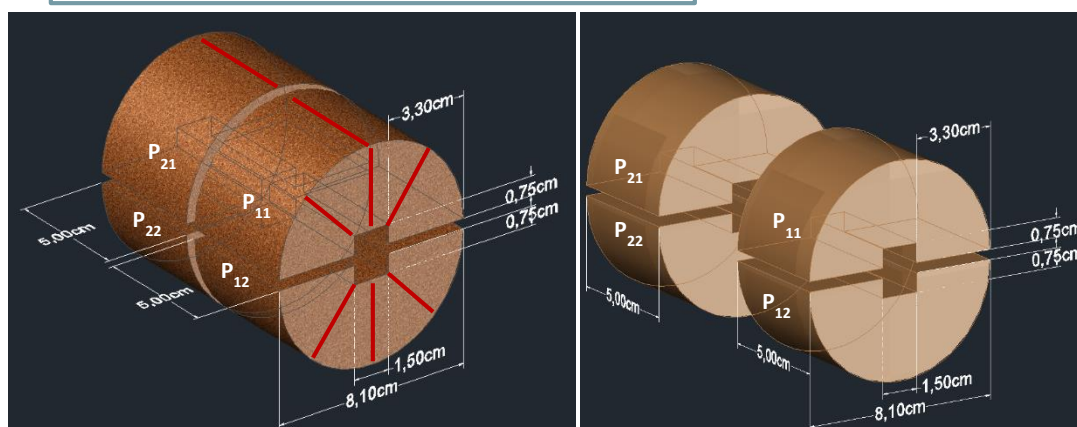

Schemes of the plastic cylinder P with references depicted in red

Cylinders P – cork (P_{11}, P_{12} ; P_{21}, P_{22})

- Two cylinders with 8.10cm of diameter and 5cm length, longitudinally cut by the central XZ plane, forming 4 symmetrical parts (hemi-cylinders P_{11}, P_{12} , P_{21}, P_{22}).
- **References for localization:** the same as cork cylinders G (see above).
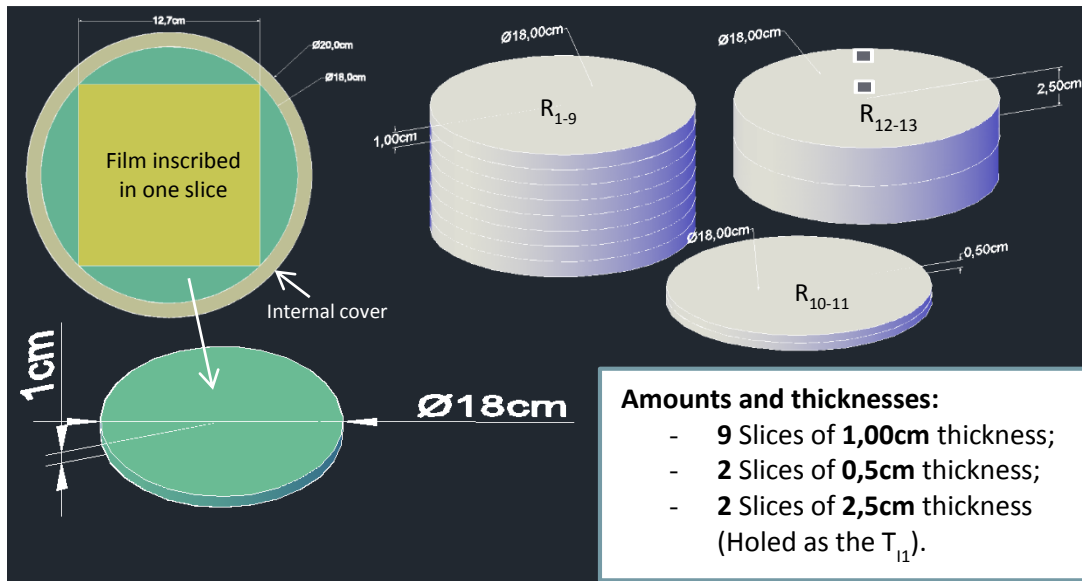
Allow to roll up **1 radiochromic film** (by the longer side of the film) and comprise 10cm of film length.

Schemes of the cork cylinders P with references depicted in red

Slices (R_{1-9} of 1cm; R_{10-11} of 0,5 cm; R_{12-13} of 2,5cm)

• Thirteen slices of different thickness, with 18.0cm diameter, allowing the irradiation of axial films of 12.7 x 12.7 cm^2, inscribed in the slices (see 2D image).

• **Both 2.5cm slices** are holed in the same way as the front internal lid, with holes of the same dimensions, in order to match once closed.
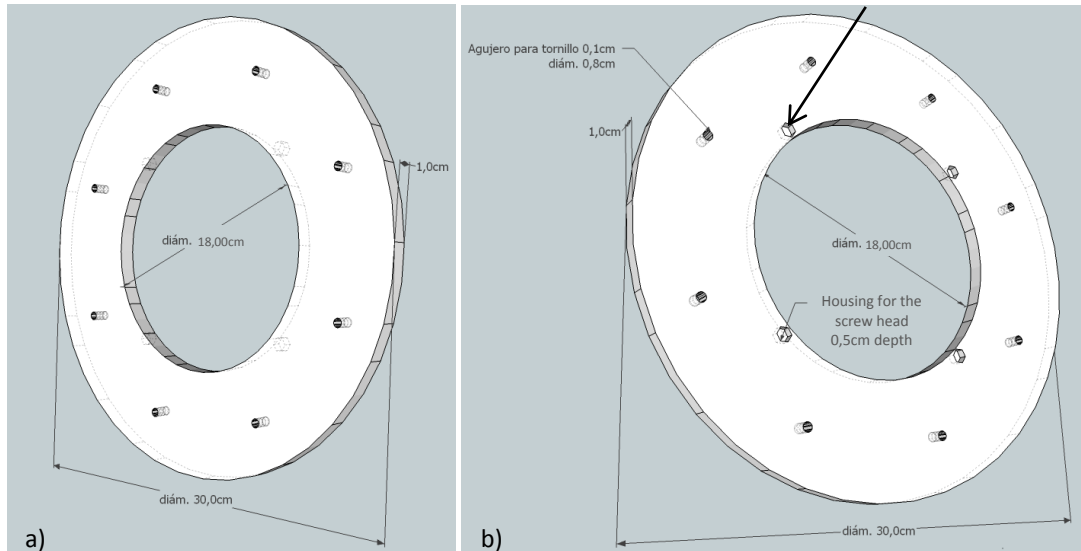

Amounts and thicknesses:
- **9** Slices of **1,00cm** thickness;
- **2** Slices of **0,5cm** thickness;
- **2** Slices of **2,5cm** thickness (Holed as the T_{I1}).

External lids (T_{E1}, T_{E2})

• Two external lids of 1cm, front (T_{E1}) and back (T_{E2}), are screwed to the external cover, allowing their closing through 8 perforations. Closer to their center, they present 4 housings for the screw heads of the internal covers, which go up to the half of their thickness (0.5 cm depth).

View of the outside part of the lid with screws

View of the inside part of the lid
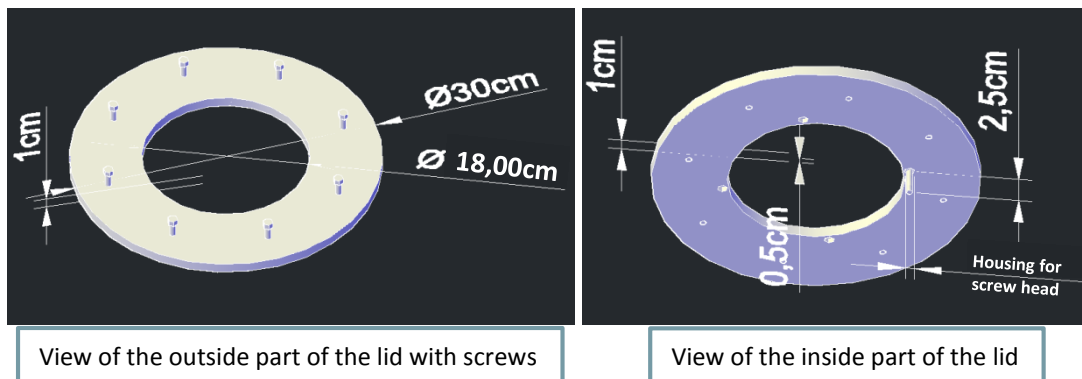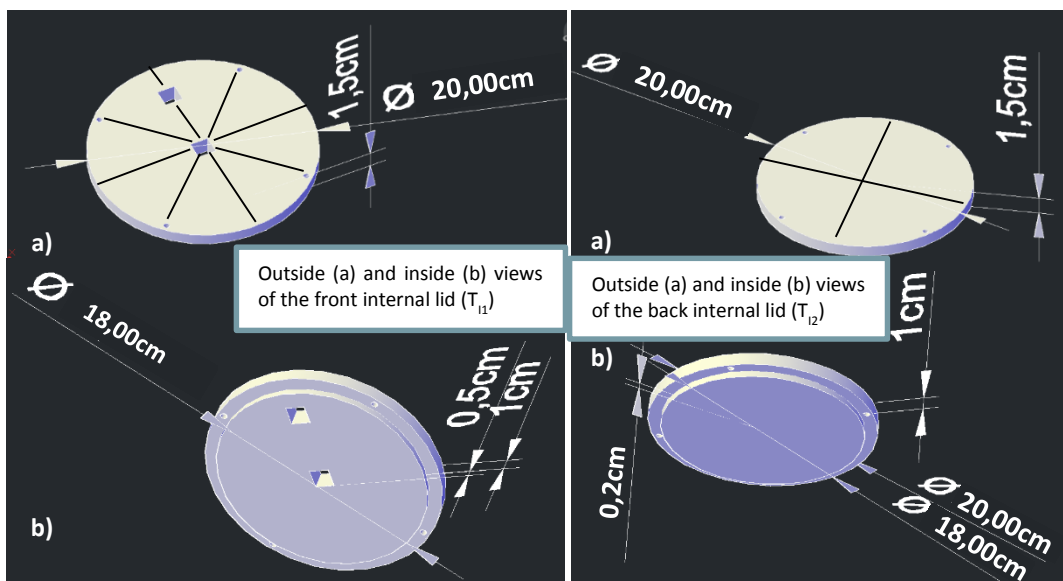
External lids (T$_{E1}$, T$_{E2}$)

These housings for screw heads have circular shape and not hexagonal as shown in the figure (simply it is represents their location and depth). Their diameters correspond to the screws head of 0.8cm diameter and circular head.

a)

Agujero para tornillo 0,1cm
diám. 0,8cm

1,0cm

1,0cm

diám. 18,00cm

diám. 30,0cm

b)

diám. 18,00cm

Housing for the screw head 0,5cm depth

diám. 30,0cm

Outside (a) and inside (b) views of one of the external lids
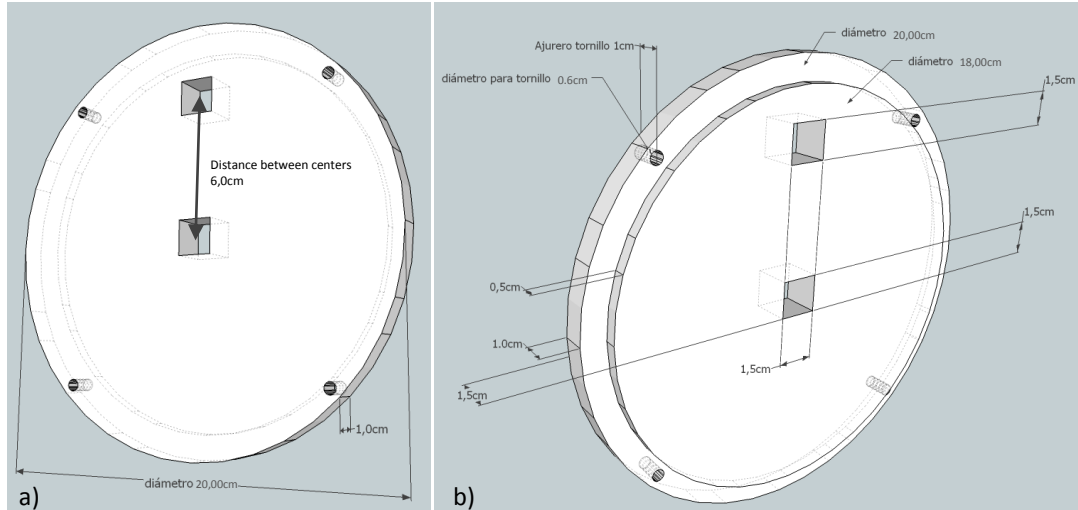
Internal lids (T$_{I1}$, T$_{I2}$)

- Two internal lids, the front one (T$_{I1}$) of 1.5cm thickness and the back one (T$_{I2}$) of 1.2cm, are screwed to the internal cover, allowing their closing through 4 perforations. The front lid (T$_{I1}$) allows the introduction of the prism shaped inserts into the phantom at its center and near to its edge.

1,5cm

Ø 20,00cm

a)

18,00cm

b)

0,5cm 1cm

Outside (a) and inside (b) views of the front internal lid (T$_{I1}$)

20,00cm

1,5cm

a)

Outside (a) and inside (b) views of the back internal lid (T$_{I2}$)
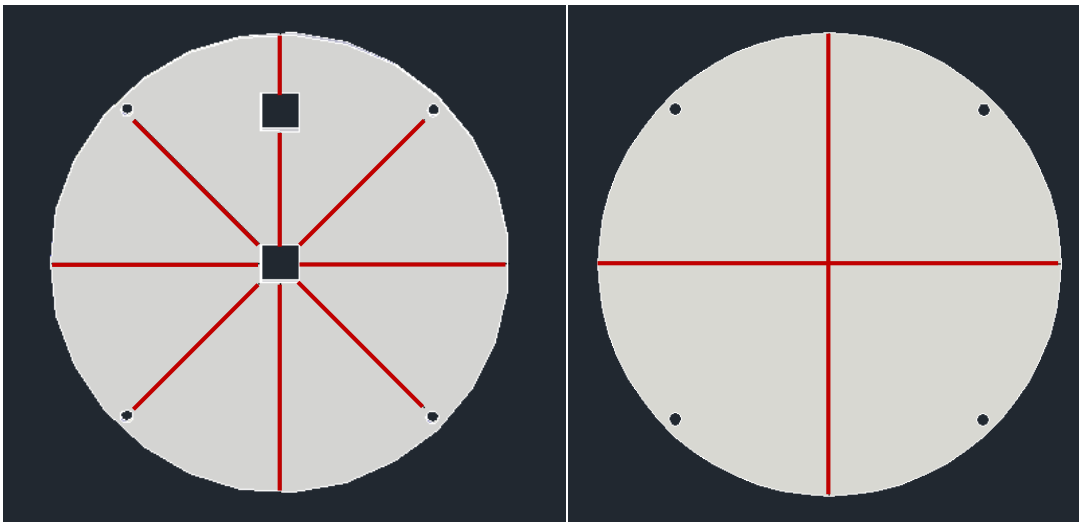
1cm

b)

0,2cm

Ø 20,00cm
18,00cm

Front internal lid (T_{I1})

Outside (a) and inside (b) views of the front internal lid (T_{I1})

Internal lids (T_{I1}, T_{I2})

- **References for localization:**
- Front internal lid (T_{I1}): a cross mark at 0° and other rotated at 45°, therefore it has a mark each 45°;
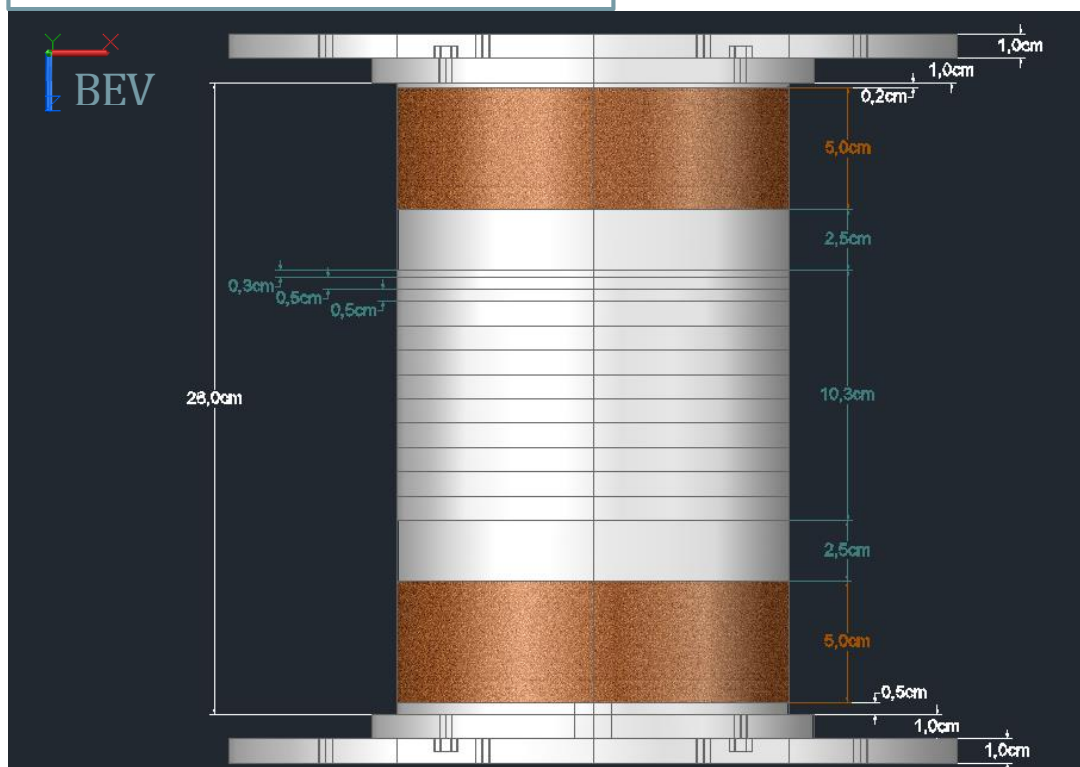- Back internal lid (T_{I1}): cross mark at 0°.

Representation of references (in red) of the two internal covers T_{I1} and T_{I2}
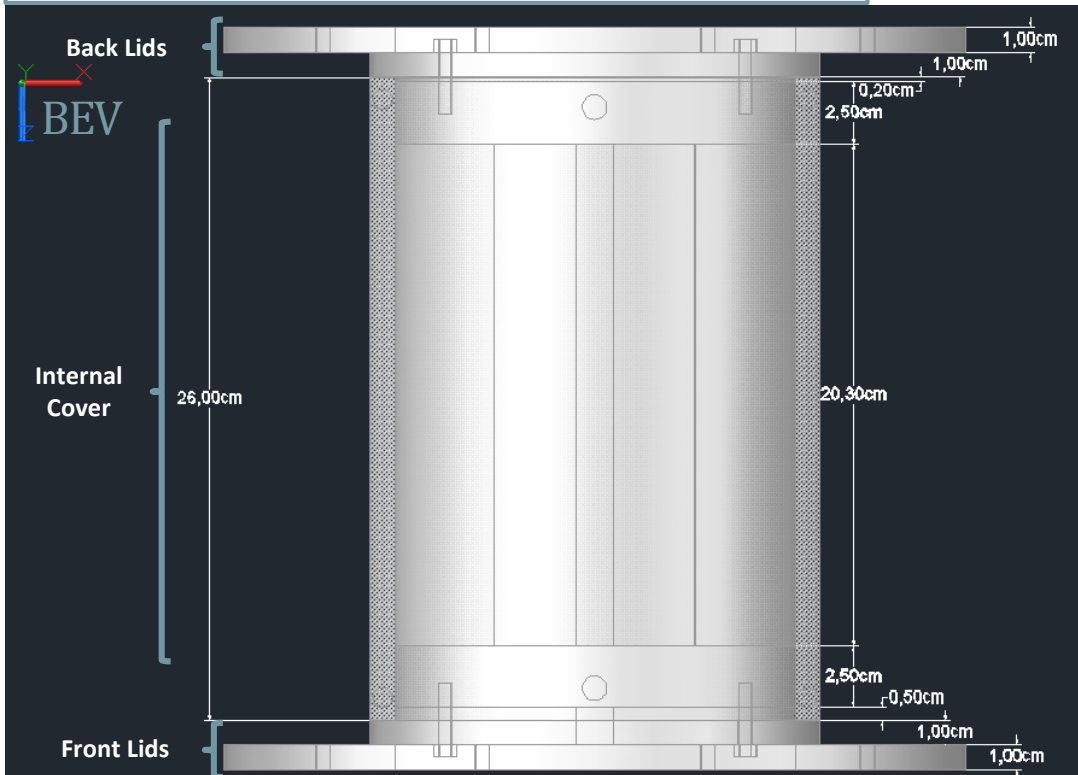
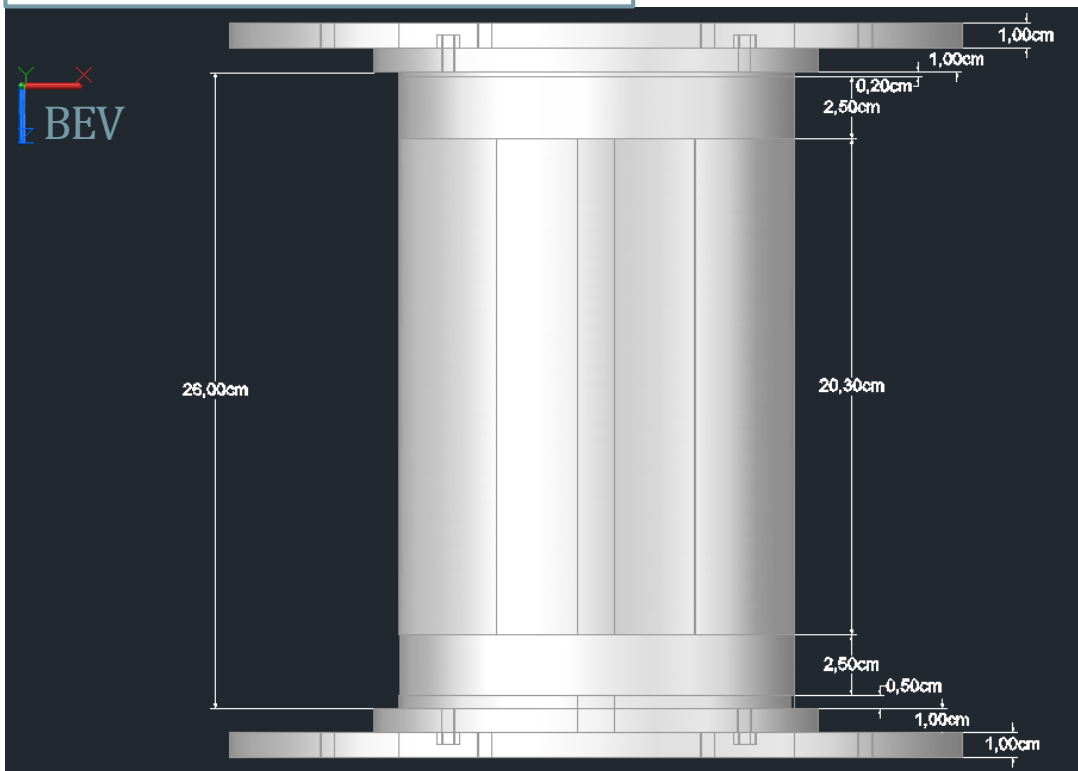Zenithal view with dimensions of the cork cylinders; plastic slices and lids.
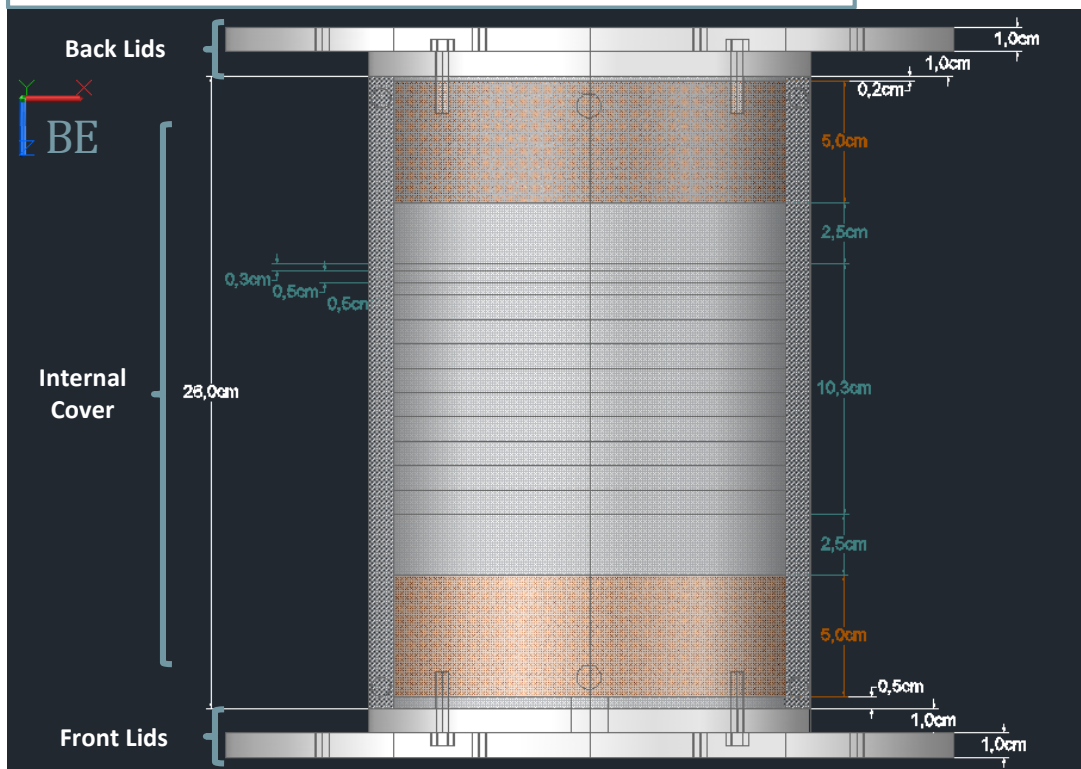
Zenithal view with dimensions of the cork cylinders; plastic slices and lids (without internal cover).

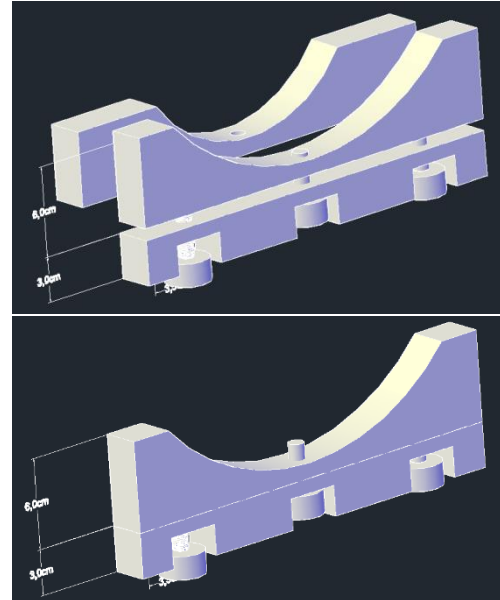Zenithal view with dimensions of the plastic cylinders; 2.5cm slices and lids.

Zenithal view with dimensions of the plastic cylinders; 2.5cm slices and lids (without internal cover)

Supports (S$_1$, S$_2$)

- The phantom will be placed on two identical supports, the front one and back one (S$_1$, S$_2$), as shown in the figure.
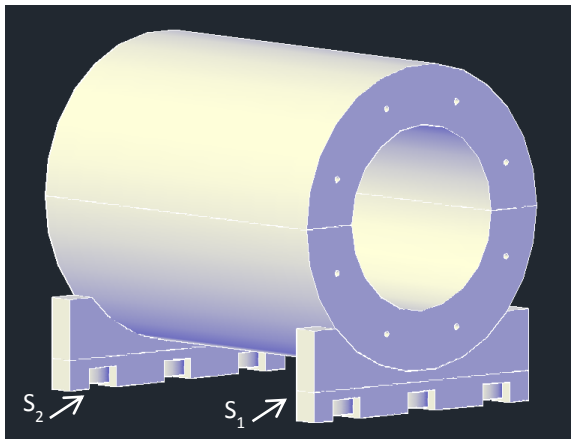
Supports (S$_1$, S$_2$)
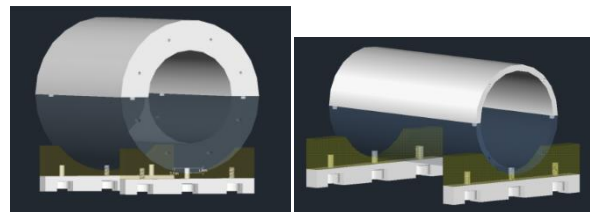
- Each support is formed by one **plinth** (blue) and two **bases** (yellow), which would be used alternately, depending on the intended setup type (big or small). Both plinths provide the possibility of leveling the phantom through 4 outermost screws, which in turn also allow to fix each one of the bases to the plinth. This plinth also has a central screw that overpasses the support as a pin, and screw the covers (external or internal), for their fixation.
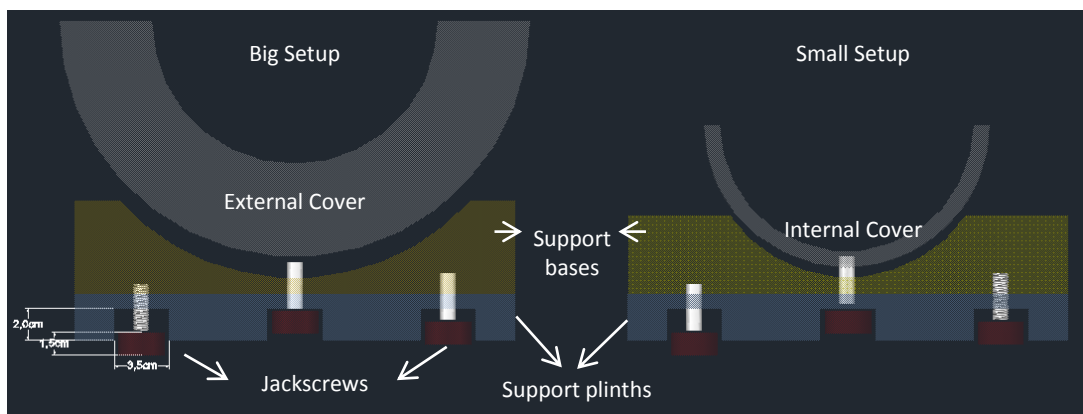
Supports (S₁, S₂) - plinths

Schemes of the plinths of S₁ and S₂:
- Both external holes with thread pitch of 0.1cm
- Central hole without thread pitch

14,00cm 4,25cm
4,25cm 28,00cm
Ø1,00cm 1,00cm
2,50cm 2,00cm
3,00cm 3,50cm 2,50cm
2,50cm 3,50cm 6,25cm 3,50cm 6,25cm Ø1,00cm

Scheme of one jackscrew:
- Amount (6)
- Thread pitch of 0.1cm

3,00cm
1,50cm Ø3,00cm
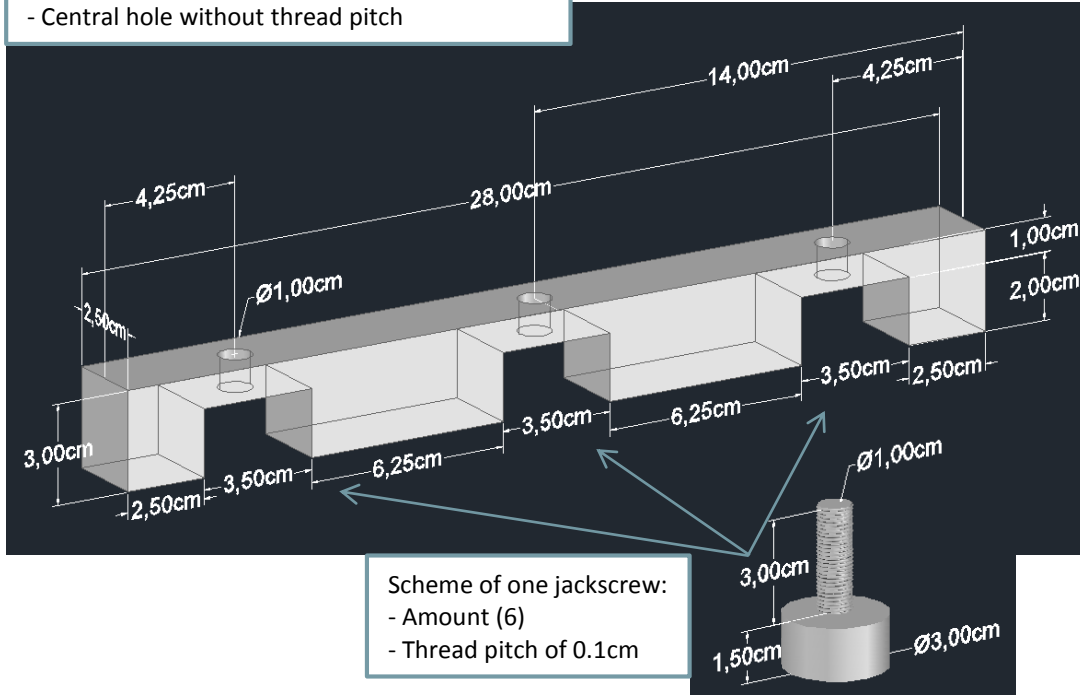
Supports (S₁, S₂) - bases

Ø30,00cm

28,00cm 2,80cm
22,40cm
2,80cm 1,25cm
6,00cm 2,00cm
2,00cm 1,00cm
2,50cm

For both bases:
- All holes of **1.00cm diameter**;
- The two outermost holes with **thread pitch of 0.1cm**;
- Central hole without thread pitch.

Scheme of the base for small setup, which is screwed to the internal cover.
- Amount (2)

Scheme of the base for big setup, which is screwed to the external cover.
- Amount (2)

28,00cm 5,50cm
5,50cm 17,00cm Ø20,00cm
1,25cm
5,00cm 2,00cm
2,00cm 1,00cm
2,50cm
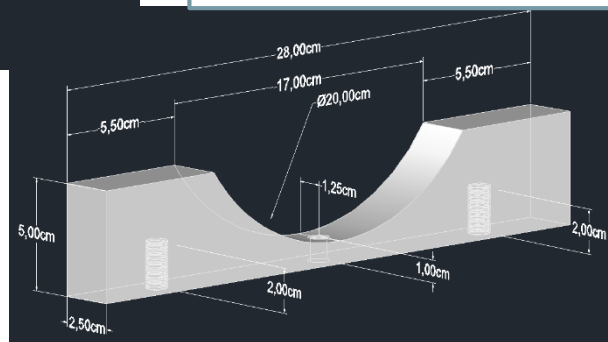
Inserts ($I_{1,2}$; $I_{3,4}$; I_{5-8} ; I_{9-11} ; I_{12-18})

- Six inserts to fill the cylinders in plastic and cork version ($I_{1,2}$, I_{5-8}). Three of them are cut longitudinally (hemi-prisms), which fill the small cylinders, allowing to place a coronal film in between.
- Two inserts to fill the 2.5cm slices ($I_{3,4}$).
- Three inserts for housing different types of ionization chamber (I_{9-11}) and the remaining seven of different length to be used with the chambers (I_{12-18}).

To center the chamber in the phantom a chamber insert is used along with the insert of 7.8cm, the chamber's tip thus stays located at the phantom's isocenter (touching the edge of the insert of 7.8cm). The table should be moved to place the chamber at its effective point.

Some of the considered chambers: **PTW Semiflex type 31010 (0,125cm^3) & PinPoint; Wellhofer CC13 (0,13cm^3), ...**

Insert of 7,8cm

Insert for chamber housing

Phantom's center reference

Chamber's tip
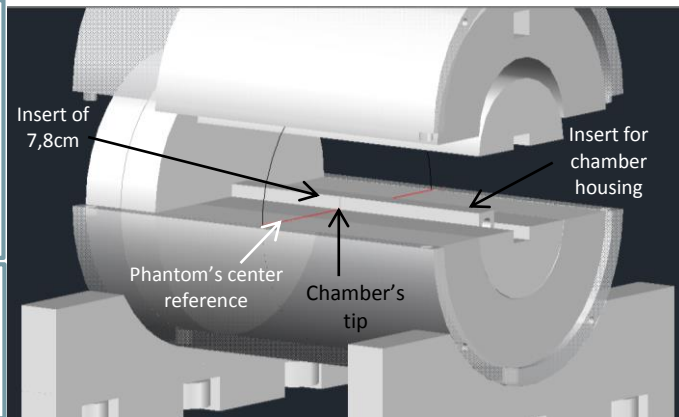
Inserts for slices and cylinders:

Inserts ($I_{1,2}$; $I_{3,4}$; I_{5-8})
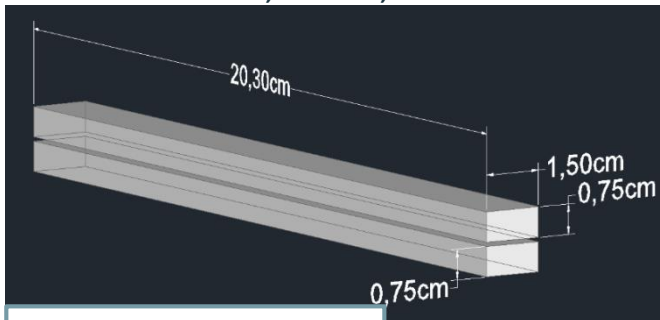
I_1 - Plastic prism longitudinally cut
- Amount (1)
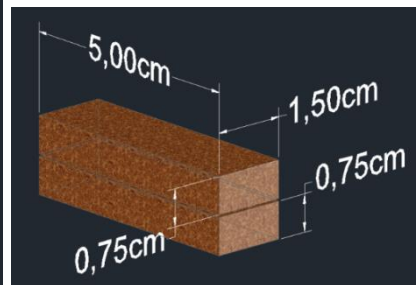
I_5 , I_6 – Cork prisms longitudinally cut
- Amount (2)

I_2 – Entire plastic prism
- Amount (1)

I_3 , I_4 – Entire plastic prisms
- Amount (2)

I_7 , I_8 - Entire cork prisms
- Amount (2)

Inserts for ionization chambers:

Inserts (I$_{9-11}$; I$_{12-18}$)

I$_9$ – **Semiflex I.C.**
Amount: (1)

I$_{10}$ –**PinPoint I.C.**
Amount: (1)

I$_{11}$ –**Wellhofer I.C.**
Amount: (1)

Inserts **I$_{12-18}$** of different lengths for chambers placement
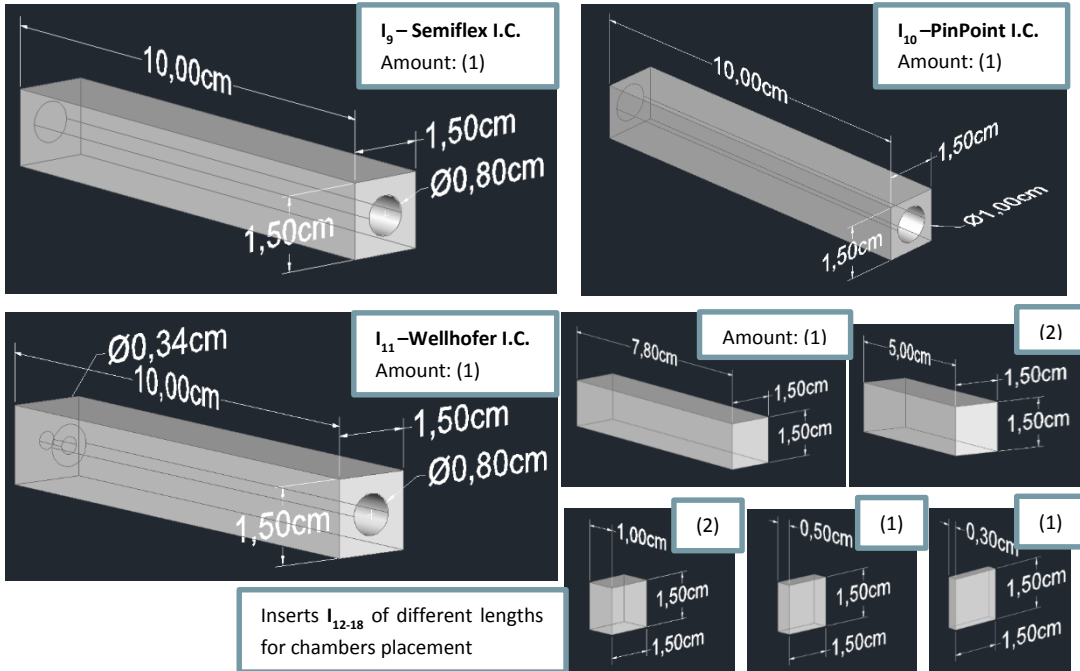
Inserts for ionization chambers:

Insert (I$_9$)

Transparency of the insert I$_9$ for **Semiflex I.C.**
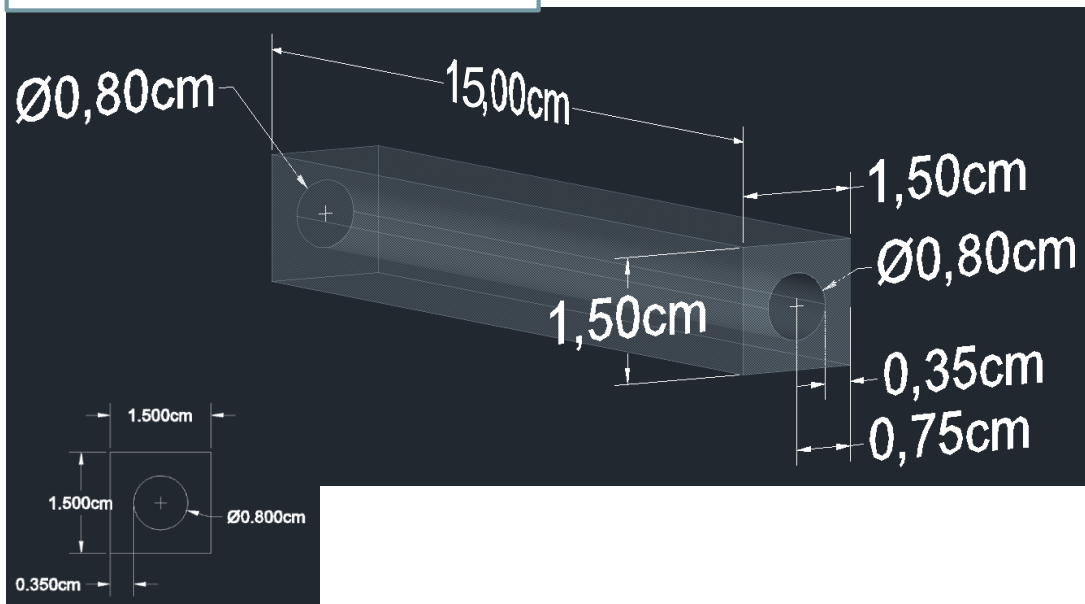
Inserts for ionization chambers:

Insert (I$_{10}$)

Transparency of the insert I$_{10}$ for **PinPoint I.C.**
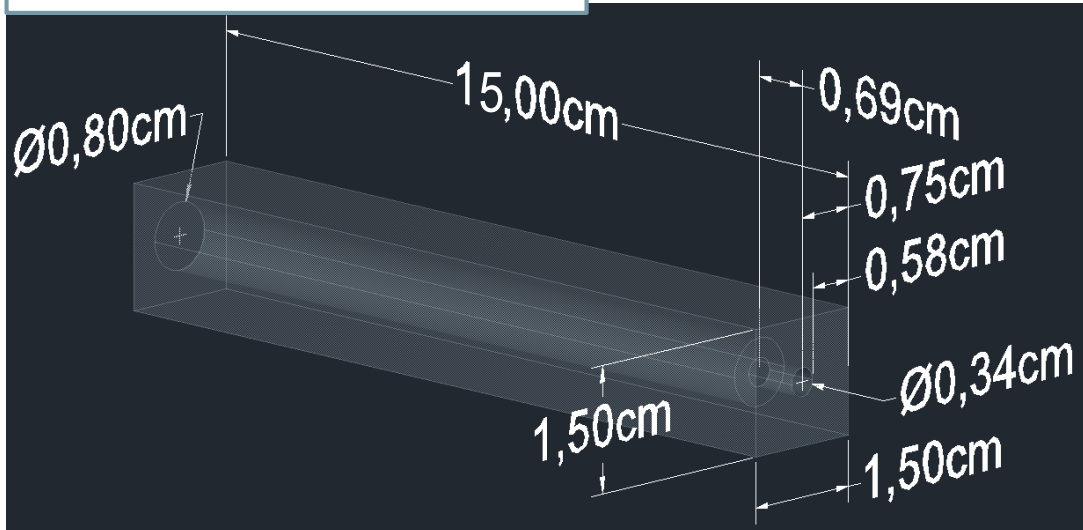
Inserts for ionization chambers:

Insert (I$_{11}$)

Transparency of the insert I$_{11}$ for **Wellhofer I.C**
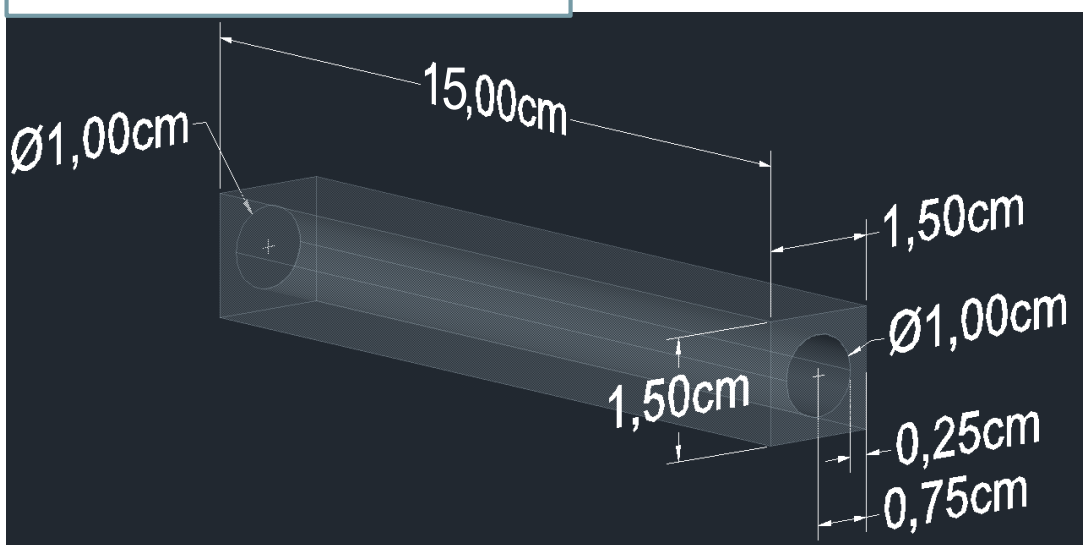
Bibliography

AAPM. Tissue inhomogeneity corrections for megavoltage photon beams. Madison, WI: Medical Physics Publishing: American Association of Physicists in Medicine, 2004 85.

Abo-Madyan Y, Aziz M H, Aly M M, Schneider F, Sperk E, Clausen S, Giordano F A, Herskind C, Steil V, Wenz F and Glatting G 2014 Second cancer risk after 3D-CRT, IMRT and VMAT for breast cancer *Radiother Oncol* **110** 471-6

Agnew A, Agnew C E, Grattan M W, Hounsell A R and McGarry C K 2014 Monitoring daily MLC positional errors using trajectory log files and EPID measurements for IMRT and VMAT deliveries *Phys Med Biol* **59** N49-63

Agnew C E, King R B, Hounsell A R and McGarry C K 2012 Implementation of phantom-less IMRT delivery verification using Varian DynaLog files and R/V output *Phys Med Biol* **57** 6761-77

Ahnesjo A 1989 Collapsed cone convolution of radiant energy for photon dose calculation in heterogeneous media *Med Phys* **16** 577-92

Aju-e-Taqaddas 2011 *Investigation of VMAT Algorithms and Dosimetry*: AuthorHouse UK)

Alfonso R, Andreo P, Capote R, Huq M S, Kilby W, Kjall P, Mackie T R, Palmans H, Rosser K, Seuntjens J, Ullrich W and Vatnitsky S 2008 A new formalism for reference dosimetry of small and nonstandard fields *Med Phys* **35** 5179-86

Almond P R, Biggs P J, Coursey B M, Hanson W F, Huq M S, Nath R and Rogers D W 1999 AAPM's TG-51 protocol for clinical reference dosimetry of high-energy photon and electron beams *Med Phys* **26** 1847-70

Alvarez-Moret J, Pohl F, Koelbl O and Dobler B 2010 Evaluation of volumetric modulated arc therapy (VMAT) with Oncentra MasterPlan(R) for the treatment of head and neck cancer *Radiat Oncol* **5** 110

Asuni G, van Beek T A, Venkataraman S, Popescu I A and McCurdy B M 2013 A Monte Carlo tool for evaluating VMAT and DIMRT treatment deliveries including planar detectors *Phys Med Biol* **58** 3535-50

Baeza J A, Ureba A, Jimenez-Ortega E, Barbeiro A R, Lagares J I and Plaza A L 2015 CARMEN: A MatLab-Based Research Platform for Monte Carlo Treatment Planning (MCTP) and Customized System for Planning Evaluation *Med. Phys.* **42** 3367-8

Bedford J L, Lee Y K, Wai P, South C P and Warrington A P 2009 Evaluation of the Delta4 phantom for IMRT and VMAT verification *Phys Med Biol* **54** N167-76

Bedford J L, Thomas M D and Smyth G 2013 Beam modeling and VMAT performance with the Agility 160-leaf multileaf collimator *J Appl Clin Med Phys* **14** 4136

Bedford J L and Warrington A P 2009 Commissioning of volumetric modulated arc therapy (VMAT) *Int J Radiat Oncol Biol Phys* **73** 537-45

Bertelsen A, Hansen C R, Johansen J and Brink C 2010 Single Arc Volumetric Modulated Arc Therapy of head and neck cancer *Radiother Oncol* **95** 142-8

Boggula R, Birkner M, Lohr F, Steil V, Wenz F and Wertz H 2011 Evaluation of a 2D detector array for patient-specific VMAT QA with different setups *Phys Med Biol* **56** 7163-77

Boggula R, Lorenz F, Mueller L, Birkner M, Wertz H, Stieler F, Steil V, Lohr F and Wenz F 2010 Experimental validation of a commercial 3D dose verification system for intensity-modulated arc therapies *Phys Med Biol* **55** 5619-33

Bortfeld T 2010 The number of beams in IMRT--theoretical investigations and implications for single-arc IMRT *Phys Med Biol* **55** 83-97

Bortfeld T and Webb S 2009 Single-Arc IMRT? *Phys Med Biol* **54** N9-20

Bouchard H, Lacroix F, Beaudoin G, Carrier J F and Kawrakow I 2009 On the characterization and uncertainty analysis of radiochromic film dosimetry *Med Phys* **36** 1931-46

Boylan C J, Aitkenhead A H, Rowbottom C G and Mackay R I 2013 Simulation of realistic linac motion improves the accuracy of a Monte Carlo based VMAT plan QA system *Radiother Oncol* **109** 377-83

Brahme A, Roos J E and Lax I 1982 Solution of an integral equation encountered in rotation therapy *Phys Med Biol* **27** 1221-9

Bzdusek K, Friberger H, Eriksson K, Hardemark B, Robinson D and Kaus M 2009 Development and evaluation of an efficient approach to volumetric arc therapy planning *Med Phys* **36** 2328-39

Capote R, Sanchez-Doblado F, Leal A, Lagares J I, Arrans R and Hartmann G H 2004 An EGSnrc Monte Carlo study of the microionization chamber for reference dosimetry of narrow irregular IMRT beamlets *Med Phys* **31** 2416-22

Cranmer-Sargison G, Beckham W A and Popescu I A 2004 Modelling an extreme water-lung interface using a single pencil beam algorithm and the Monte Carlo method *Phys Med Biol* **49** 1557-67

Crooks S M, Wu X, Takita C, Watzich M and Xing L 2003 Aperture modulated arc therapy *Phys Med Biol* **48** 1333-44

Chandraraj V, Stathakis S, Manickam R, Esquivel C, Supe S S and Papanikolaou N 2011 Comparison of four commercial devices for RapidArc and sliding window IMRT QA *J Appl Clin Med Phys* **12** 3367

Chen F, Rao M, Ye J S, Shepard D M and Cao D 2011 Impact of leaf motion constraints on IMAT plan quality, deliver accuracy, and efficiency *Med Phys* **38** 6106-18

Chetty I J, Curran B, Cygler J E, DeMarco J J, Ezzell G, Faddegon B A, Kawrakow I, Keall P J, Liu H, Ma C M, Rogers D W, Seuntjens J, Sheikh-Bagheri D and Siebers J V 2007 Report of the AAPM Task Group No. 105: Issues associated with clinical implementation of Monte Carlo-based photon and electron external beam treatment planning *Med Phys* **34** 4818-53

Delaney G, Jacob S, Featherstone C and Barton M 2005 The role of radiotherapy in cancer treatment: estimating optimal utilization from a review of evidence-based clinical guidelines *Cancer* **104** 1129-37

Dische S, Saunders M, Williams C, Hopkins A and Aird E 1993 Precision in reporting the dose given in a course of radiotherapy *Radiotherapy and Oncology* **29** 287-93

DonaldsonMarphil. [Web Page]. [cited 2016 09/29]. Available from: https://www.donaldsonmarphil.com/medical-physics/easycube/.

Donetti M, Garelli E, Marchetto F, Boriano A, Bourhaleb F, Cirio R, Cornelius I, Giordanengo S, La Rosa A, Nastasi U and Peroni C 2006 A method for the inter-calibration of a matrix of sensors *Phys Med Biol* **51** 485-95

Duthoy W, De Gersem W, Vergote K, Boterberg T, Derie C, Smeets P, De Wagter C and De Neve W 2004 Clinical implementation of intensity-

modulated arc therapy (IMAT) for rectal cancer *Int J Radiat Oncol Biol Phys* **60** 794-806

Earl M A, Shepard D M, Naqvi S, Li X A and Yu C X 2003 Inverse planning for intensity-modulated arc therapy using direct aperture optimization *Phys Med Biol* **48** 1075-89

Elekta. [Web Page]. [cited 2016 07/18]. Available from: https://www.elekta.com/radiotherapy/treatment-solutions/beam-shaping/mlci2/#mlci2-ar.

Ezzell G A, Burmeister J W, Dogan N, LoSasso T J, Mechalakos J G, Mihailidis D, Molineu A, Palta J R, Ramsey C R, Salter B J, Shi J, Xia P, Yue N J and Xiao Y 2009 IMRT commissioning: multiple institution planning and dosimetry comparisons, a report from AAPM Task Group 119 *Med Phys* **36** 5359-73

Fakir H, Gaede S, Mulligan M and Chen J Z 2012 Development of a novel ArcCHECK() insert for routine quality assurance of VMAT delivery including dose calculation with inhomogeneities *Med Phys* **39** 4203-8

Ferlay J, Soerjomataram I, Dikshit R, Eser S, Mathers C, Rebelo M, Parkin D M, Forman D and Bray F 2015 Cancer incidence and mortality worldwide: sources, methods and major patterns in GLOBOCAN 2012 *Int J Cancer* **136** E359-86

Feygelman V and Nelms B E 2011 Dose Verification in IMRT and VMAT *AIP Conference Proceedings* **1345** 145-64

Feygelman V, Zhang G and Stevens C 2010 Initial dosimetric evaluation of SmartArc - a novel VMAT treatment planning module implemented in a multi-vendor delivery chain *J Appl Clin Med Phys* **11** 3169

Guckenberger M, Richter A, Krieger T, Wilbert J, Baier K and Flentje M 2009 Is a single arc sufficient in volumetric-modulated arc therapy (VMAT) for complex-shaped target volumes? *Radiother Oncol* **93** 259-65

Haga A, Nakagawa K, Shiraishi K, Itoh S, Terahara A, Yamashita H, Ohtomo K, Saegusa S, Imae T, Yoda K and Pellegrini R 2009 Quality assurance of volumetric modulated arc therapy using Elekta Synergy *Acta Oncol* **48** 1193-7

Hall E J and Wuu C S 2003 Radiation-induced second cancers: the impact of 3D-CRT and IMRT *Int J Radiat Oncol Biol Phys* **56** 83-8

Hammond L, Brown K, Smith S and Lamb G 2011 VMAT versus IMRT — a Question of Modulation *Clinical Oncology* **23** S38

Han T, Mikell J K, Salehpour M and Mourtada F 2011 Dosimetric comparison of Acuros XB deterministic radiation transport method with Monte Carlo and model-based convolution methods in heterogeneous media *Med Phys* **38** 2651-64

Hartman Siantar C L, Walling R S, Daly, T.P., Faddegon B, Albright N, Bergstrom P, Bielajew A F, Chuang C, Garrett D, House R K, Knapp D, Wieczorek D J and Verhey L J 2001 Description and dosimetric verification of the PEREGRINE Monte Carlo dose calculation system for photon beams on a water phantom *Med. Phys.* **28** 1322–37.

Hauri P, Verlaan S, Graydon S, Ahnen L, Klock S and Lang S 2014 Clinical evaluation of an anatomy-based patient specific quality assurance system *J Appl Clin Med Phys* **15** 4647

Heath E and Seuntjens J 2003 Development and validation of a BEAMnrc component module for accurate Monte Carlo modelling of the Varian dynamic Millennium multileaf collimator *Phys Med Biol* **48** 4045-63

Hussein M, Rowshanfarzad P, Ebert M A, Nisbet A and Clark C H 2013 A comparison of the gamma index analysis in various commercial IMRT/VMAT QA systems *Radiother Oncol* **109** 370-6

IAEA. Absorbed Dose Determination in External Beam Radiotherapy: An International Code of Practice for Dosimetry Based on Standards of Absorbed Dose to Water. Vienna: 2001.

IBA. [Web Page]. [cited 2016 07/22]. Available from: http://www.iba-dosimetry.com/complete-solutions/compass-2-1.

ICRU 1976 Determination of absorbed dose in a patient irradiated by beams of x or gamma rays in radiotherapy procedures **24**

IMPAC 2012 *RTPConnect Interface Specification Manual* (Sunnyvale, CA, USA: IMPAC Medical Systems, Inc.)

IMRT Collaborative Working G 2001 Intensity-modulated radiotherapy: current status and issues of interest *Int J Radiat Oncol Biol Phys* **51** 880-914

Iori M, Cagni E, Paiusco M, Munro P and Nahum A E 2010 Dosimetric verification of IMAT delivery with a conventional EPID system and a commercial portal dose image prediction tool *Med Phys* **37** 377-90

Jin H, Keeling V P, Johnson D A and Ahmad S 2014 Interplay effect of angular dependence and calibration field size of MapCHECK 2 on RapidArc quality assurance *J Appl Clin Med Phys* **15** 4638

Jursinic P A, Sharma R and Reuter J 2010 MapCHECK used for rotational IMRT measurements: step-and-shoot, TomoTherapy, RapidArc *Med Phys* **37** 2837-46

Kawrakow I 2000a Accurate condensed history Monte Carlo simulation of electron transport. I. EGSnrc, the new EGS4 version *Med Phys* **27** 485-98

Kawrakow I 2000b VMC++, electron and photon Monte Carlo calculations optimized for radiation treatment planning in "Advanced Monte Carlo for Radiation Physics, particle transport simulation and applications" *Proceedings of the Monte Carlo 2000 Conference, Lisbon, October 2000* 229-36

Kawrakow I and Rogers D 2000 The EGSnrc code system *NRC Report PIRS-701, NRC, Ottawa*

Kerns J R, Childress N and Kry S F 2014 A multi-institution evaluation of MLC log files and performance in IMRT delivery *Radiat Oncol* **9** 176

Kjaer-Kristoffersen F, Ohlhues L, Medin J and Korreman S 2009 RapidArc volumetric modulated therapy planning for prostate cancer patients *Acta Oncol* **48** 227-32

Klein E E, Hanley J, Bayouth J, Yin F F, Simon W, Dresser S, Serago C, Aguirre F, Ma L, Arjomandy B, Liu C, Sandin C, Holmes T and Task Group A A o P i M 2009 Task Group 142 report: quality assurance of medical accelerators *Med Phys* **36** 4197-212

Knill C, Snyder M, Rakowski J T, Zhuang L, Matuszak M and Burmeister J 2016 Investigating ion recombination effects in a liquid-filled ionization chamber array used for IMRT QA measurements *Med. Phys.* **43** 2476-84

Knoos T, Ahnesjo A, Nilsson P and Weber L 1995 Limitations of a pencil beam approach to photon dose calculations in lung tissue *Phys Med Biol* **40** 1411-20

Kutcher G J, Coia L, Gillin M, Hanson W F, Leibel S, Morton R J, Palta J R, Purdy J A, Reinstein L E, Svensson G K and et al. 1994 Comprehensive QA for radiation oncology: report of AAPM Radiation Therapy Committee Task Group 40 *Med Phys* **21** 581-618

Leal A, Sanchez-Doblado F, Arrans R, Rosello J, Pavon E C and Lagares J I 2003 Routine IMRT verification by means of an automated Monte Carlo simulation system *Int J Radiat Oncol Biol Phys* **56** 58-68

Letourneau D, Publicover J, Kozelka J, Moseley D J and Jaffray D A 2009 Novel dosimetric phantom for quality assurance of volumetric modulated arc therapy *Med Phys* **36** 1813-21

Li J G, Yan G and Liu C 2009 Comparison of two commercial detector arrays for IMRT quality assurance *J Appl Clin Med Phys* **10** 2942

Ling C C, Zhang P, Archambault Y, Bocanek J, Tang G and Losasso T 2008 Commissioning and quality assurance of RapidArc radiotherapy delivery system *Int J Radiat Oncol Biol Phys* **72** 575-81

Lobo J and Popescu I A 2010 Two new DOSXYZnrc sources for 4D Monte Carlo simulations of continuously variable beam configurations, with applications to RapidArc, VMAT, TomoTherapy and CyberKnife *Phys Med Biol* **55** 4431-43

Low D A, Harms W B, Mutic S and Purdy J A 1998 A technique for the quantitative evaluation of dose distributions *Med Phys* **25** 656-61

Ma C M, Mok E, Kapur A, Pawlicki T, Findley D, Brain S, Forster K and Boyer A L 1999 Clinical implementation of a Monte Carlo treatment planning system *Med Phys* **26** 2133-43

Ma C M, Pawlicki T, Jiang S B, Li J S, Deng J, Mok E, Kapur A, Xing L, Ma L and Boyer A L 2000 Monte Carlo verification of IMRT dose distributions from a commercial treatment planning optimization system *Phys Med Biol* **45** 2483-95

Ma C M, Price R A, Jr., Li J S, Chen L, Wang L, Fourkal E, Qin L and Yang J 2004 Monitor unit calculation for Monte Carlo treatment planning *Phys Med Biol* **49** 1671-87

Mackie T R, Holmes T, Swerdloff S, Reckwerdt P, Deasy J O, Yang J, Paliwal B and Kinsella T 1993 Tomotherapy: a new concept for the delivery of dynamic conformal radiotherapy *Med Phys* **20** 1709-19

Manikandan A, Sarkar B, Holla R, Vivek T R and Sujatha N 2012 Quality assurance of dynamic parameters in volumetric modulated arc therapy *Br J Radiol* **85** 1002-10

Mans A, Remeijer P, Olaciregui-Ruiz I, Wendling M, Sonke J J, Mijnheer B, van Herk M and Stroom J C 2010 3D Dosimetric verification of volumetric-modulated arc therapy by portal dosimetry *Radiother Oncol* **94** 181-7

Matuszak M M, Yan D, Grills I and Martinez A 2010 Clinical applications of volumetric modulated arc therapy *Int J Radiat Oncol Biol Phys* **77** 608-16

Mehta M, Hoban P and Mackie T R 2009 Commissioning and quality assurance of RapidArc radiotherapy delivery system: in regard to Ling et al. (Int J Radiat Oncol Biol Phys 2008;72;575-581): Absence of data does not

constitute proof; the proof is in tasting the pudding *Int J Radiat Oncol Biol Phys* **75** 4-6; discussion 8-9

Meyer J 2011 *IMRT, IGRT, SBRT: advances in the treatment planning and delivery of radiotherapy* (Karger Medical and Scientific Publishers

Micke A, Lewis D F and Yu X 2011 Multichannel film dosimetry with nonuniformity correction *Med Phys* **38** 2523-34

Mijnheer B and Georg D 2008 *Physics for clinical radiotherapy - ESTRO Booklet no 9,* ed B Mijnheer and D Georg (Brussels: European Society for Therapeutic Radiology and Oncology)

Mijnheer B J, Battermann J J and Wambersie A 1987 What degree of accuracy is required and can be achieved in photon and neutron therapy? *Radiotherapy and Oncology* **8** 237-52

NCS. Code of Practice for the Quality Assurance and Control for Volumetric Modulated Arc Therapy. Delft, The Netherlands: 2015.

Neal B, Ahmed M, Kathuria K, Watkins T, Wijesooriya K and Siebers J 2016 A clinically observed discrepancy between image-based and log-based MLC positions *Med. Phys.* **43** 2933-5

Nelms B E, Zhen H and Tome W A 2011 Per-beam, planar IMRT QA passing rates do not predict clinically relevant patient dose errors *Med Phys* **38** 1037-44

Nelson W, Hirayama H and Rogers D W. The EGS4 Code System. Stanford Linear Accelerator Center report SLAC-265, 1985.

Ojala J J, Kapanen M K, Hyodynmaa S J, Wigren T K and Pitkanen M A 2014 Performance of dose calculation algorithms from three generations in lung SBRT: comparison with full Monte Carlo-based dose distributions *J Appl Clin Med Phys* **15** 4662

Oldham M, Thomas A, O'Daniel J, Juang T, Ibbott G, Adamovics J and Kirkpatrick J P 2012 A quality assurance method that utilizes 3D dosimetry and facilitates clinical interpretation *Int J Radiat Oncol Biol Phys* **84** 540-6

Oliver M, Ansbacher W and Beckham W A 2009 Comparing planning time, delivery time and plan quality for IMRT, RapidArc and Tomotherapy *J Appl Clin Med Phys* **10** 3068

Otto K 2008 Volumetric modulated arc therapy: IMRT in a single gantry arc *Med Phys* **35** 310-7

Otto K 2009 Letter to the Editor on 'Single-Arc IMRT?' *Phys Med Biol* **54** L37-41; author reply L3-4

Palma D, Vollans E, James K, Nakano S, Moiseenko V, Shaffer R, McKenzie M, Morris J and Otto K 2008 Volumetric modulated arc therapy for delivery of prostate radiotherapy: comparison with intensity-modulated radiotherapy and three-dimensional conformal radiotherapy *Int J Radiat Oncol Biol Phys* **72** 996-1001

Palma D A, Verbakel W F, Otto K and Senan S 2010 New developments in arc radiation therapy: a review *Cancer Treat Rev* **36** 393-9

Pardo Montero J and Fenwick J D 2011 The effect of different control point sampling sequences on convergence of VMAT inverse planning *Phys Med Biol* **56** 2569-83

Park J Y, Lee J W, Choi K S, Lee J S, Kim Y H, Hong S and Suh T S 2011 Development of a novel quality assurance system based on rolled-up and rolled-out radiochromic films in volumetric modulated arc therapy *Med Phys* **38** 6688-96

Pasler M, Kaas J, Perik T, Geuze J, Dreindl R, Kunzler T, Wittkamper F and Georg D 2015 Linking log files with dosimetric accuracy - A multi-institutional study on quality assurance of volumetric modulated arc therapy *Radiother Oncol* **117** 407-11

Poppe B, Blechschmidt A, Djouguela A, Kollhoff R, Rubach A, Willborn K C and Harder D 2006 Two-dimensional ionization chamber arrays for IMRT plan verification *Med Phys* **33** 1005-15

PTW. [Web Page]. [cited 2016 09/29]. Available from: http://www.ptw.de/.

Rao M, Yang W, Chen F, Sheng K, Ye J, Mehta V, Shepard D and Cao D 2010 Comparison of Elekta VMAT with helical tomotherapy and fixed field IMRT: plan quality, delivery efficiency and accuracy *Med Phys* **37** 1350-9

Reynaert N, Van der Marck S, Schaart D, Van der Zee W, Van Vliet-Vroegindeweij C, Tomsej M, Jansen J, Heijmen B, Coghe M and De Wagter C 2007 Monte Carlo treatment planning for photon and electron beams *Radiation Physics and Chemistry* **76** 643-86

Richardson S L, Tome W A, Orton N P, McNutt T R and Paliwal B R 2003 IMRT delivery verification using a spiral phantom *Med Phys* **30** 2553-8

Rogers D W, Walters B and Kawrakow I 2011 BEAMnrc Users Manual. In: *PIRS 509,* (Ottawa NRC (National Research Council of Canada)

Salguero Castaño F J. Modulación de haces de electrones para el tratamiento de tumores superficiales mediante planificación Monte Carlo. Sevilla, : Universidad de Sevilla; 2008.

Sanchez-Doblado F, Andreo P, Capote R, Leal A, Perucha M, Arrans R, Nunez L, Mainegra E, Lagares J I and Carrasco E 2003 Ionization chamber dosimetry of small photon fields: a Monte Carlo study on stopping-power ratios for radiosurgery and IMRT beams *Phys Med Biol* **48** 2081-99

Sanchez-Doblado F, Hartmann G H, Pena J, Capote R, Paiusco M, Rhein B, Leal A and Lagares J I 2007 Uncertainty estimation in intensity-modulated radiotherapy absolute dosimetry verification *Int J Radiat Oncol Biol Phys* **68** 301-10

Schreibmann E, Dhabaan A, Elder E and Fox T 2009 Patient-specific quality assurance method for VMAT treatment delivery *Med Phys* **36** 4530-5

Seco J, Clasie B and Partridge M 2014 Review on the characteristics of radiation detectors for dosimetry and imaging *Phys Med Biol* **59** R303-47

Shepard D M, Earl M A, Li X A, Naqvi S and Yu C 2002 Direct aperture optimization: a turnkey solution for step-and-shoot IMRT *Med Phys* **29** 1007-18

Song J H, Shin H J, Kay C S and Son S H 2015 Dosimetric verification by using the ArcCHECK system and 3DVH software for various target sizes *PLoS One* **10** e0119937

Spezi E and Lewis G 2008 An overview of Monte Carlo treatment planning for radiotherapy *Radiat Prot Dosimetry* **131** 123-9

Tang G, Earl M A, Luan S, Wang C, Cao D, Yu C X and Naqvi S A 2008 Stochastic versus deterministic kernel-based superposition approaches for dose calculation of intensity-modulated arcs *Phys Med Biol* **53** 4733-46

Teke T, Bergman A M, Kwa W, Gill B, Duzenli C and Popescu I A 2010 Monte Carlo based, patient-specific RapidArc QA using Linac log files *Med Phys* **37** 116-23

Teoh M, Clark C H, Wood K, Whitaker S and Nisbet A 2011 Volumetric modulated arc therapy: a review of current literature and clinical use in practice *Br J Radiol* **84** 967-96

Tillikainen L, Helminen H, Torsti T, Siljamaki S, Alakuijala J, Pyyry J and Ulmer W 2008 A 3D pencil-beam-based superposition algorithm for photon dose calculation in heterogeneous media *Phys Med Biol* **53** 3821-39

Tsai C L, Wu J K, Chao H L, Tsai Y C and Cheng J C 2011 Treatment and dosimetric advantages between VMAT, IMRT, and helical tomotherapy in prostate cancer *Med Dosim* **36** 264-71

Tyagi N, Yang K, Gersten D and Yan D 2012 A real time dose monitoring and dose reconstruction tool for patient specific VMAT QA and delivery *Med Phys* **39** 7194-204

Ulmer W, Pyyry J and Kaissl W 2005 A 3D photon superposition/convolution algorithm and its foundation on results of Monte Carlo calculations *Phys Med Biol* **50** 1767-90

Unkelbach J, Bortfeld T, Craft D, Alber M, Bangert M, Bokrantz R, Chen D, Li R, Xing L, Men C, Nill S, Papp D, Romeijn E and Salari E 2015 Optimization approaches to volumetric modulated arc therapy planning *Med Phys* **42** 1367-77

Ureba A. Planificación radioterápica de intensidad modulada en un modelo de simulación explícita del transporte de partículas mediante optimización por imagen médica. Sevilla: Universidad de Sevilla; 2015.

Ureba A, Salguero F J, Barbeiro A R, Jimenez-Ortega E, Baeza J A, Miras H, Linares R, Perucha M and Leal A 2014 MCTP system model based on linear programming optimization of apertures obtained from sequencing patient image data maps *Med. Phys.* **41** 081719

Van Esch A, Clermont C, Devillers M, Iori M and Huyskens D P 2007 On-line quality assurance of rotational radiotherapy treatment delivery by means of a 2D ion chamber array and the Octavius phantom *Med Phys* **34** 3825-37

Vassiliev O N, Wareing T A, McGhee J, Failla G, Salehpour M R and Mourtada F 2010 Validation of a new grid-based Boltzmann equation solver for dose calculation in radiotherapy with photon beams *Phys Med Biol* **55** 581-98

Venkataraman S, Malkoske K E, Jensen M, Nakonechny K D, Asuni G and McCurdy B M 2009 The influence of a novel transmission detector on 6 MV x-ray beam characteristics *Phys Med Biol* **54** 3173-83

Verbakel W F, Cuijpers J P, Hoffmans D, Bieker M, Slotman B J and Senan S 2009a Volumetric intensity-modulated arc therapy vs. conventional IMRT in head-and-neck cancer: a comparative planning and dosimetric study *Int J Radiat Oncol Biol Phys* **74** 252-9

Verbakel W F, Senan S, Lagerwaard F J, Cuijpers J P and Slotman B J 2009b Comments on 'Single-Arc IMRT?' *Phys Med Biol* **54** L31-4; author reply L5-6

Vikraman S, Manigandan D, Karrthick K P, Sambasivaselli R, Senniandavar V, Ramu M, Rajesh T, Lutz M, Muthukumaran M, Karthikeyan N and Tejinder K 2014 *Quantitative evaluation of 3D dosimetry for stereotactic volumetric-modulated arc delivery using COMPASS* vol 16

Walters B, Kawrakow I and Rogers D W 2009 DOSXYZnrc Users Manual. In: *PIRS 794,* (Ottawa NRC (National Research Council of Canada)

Wang C, Luan S, Tang G, Chen D Z, Earl M A and Yu C X 2008 Arc-modulated radiation therapy (AMRT): a single-arc form of intensity-modulated arc therapy *Phys Med Biol* **53** 6291-303

Webb S 2000 *Intensity-modulated radiation therapy* (Bristol: Institute of Physics Publishing)

Webb S and McQuaid D 2009 Some considerations concerning volume-modulated arc therapy: a stepping stone towards a general theory *Phys Med Biol* **54** 4345-60

WHO 1988 *Quality assurance in radiotherapy* (Geneva: World Health Organization)

Wong E, D'Souza D P, Chen J Z, Lock M, Rodrigues G, Coad T, Trenka K, Mulligan M and Bauman G S 2005 Intensity-modulated arc therapy for treatment of high-risk endometrial malignancies *Int J Radiat Oncol Biol Phys* **61** 830-41

Woodruff H C, Fuangrod T, Van Uytven E, McCurdy B M, van Beek T, Bhatia S and Greer P B 2015 First Experience With Real-Time EPID-Based Delivery Verification During IMRT and VMAT Sessions *Int J Radiat Oncol Biol Phys* **93** 516-22

Yu C X 1995 Intensity-modulated arc therapy with dynamic multileaf collimation: an alternative to tomotherapy *Phys Med Biol* **40** 1435-49

Yu C X, Li X A, Ma L, Chen D, Naqvi S, Shepard D, Sarfaraz M, Holmes T W, Suntharalingam M and Mansfield C M 2002 Clinical implementation of intensity-modulated arc therapy *Int J Radiat Oncol Biol Phys* **53** 453-63

Yu C X and Tang G 2011 Intensity-modulated arc therapy: principles, technologies and clinical implementation *Physics in Medicine and Biology* **56**

Zhang P, Happersett L, Hunt M, Jackson A, Zelefsky M and Mageras G 2010 Volumetric modulated arc therapy: planning and evaluation for prostate cancer cases *Int J Radiat Oncol Biol Phys* **76** 1456-62

Zhen H, Nelms B E and Tome W A 2011 Moving from gamma passing rates to patient DVH-based QA metrics in pretreatment dose QA *Med Phys* **38** 5477-89

Zhu J, Chen L, Jin G, Luo G, Cao W and Liu X 2013 A comparison of VMAT dosimetric verifications between fixed and rotating gantry positions *Phys Med Biol* **58** 1315-22

Zhuang M, Zhang T, Chen Z, Lin Z, Li D, Peng X, Qiu Q and Wu R 2013 Volumetric modulation arc radiotherapy with flattening filter-free beams compared with conventional beams for nasopharyngeal carcinoma: a feasibility study *Chin J Cancer* **32** 397-402